A NOVEL THERMAL STORAGE BASED REVERSE CYCLE DEFROSTING METHOD AND THE OPERATING PERFORMANCE EVALUATIONS FOR AN AIR SOURCE HEAT PUMP

QU MINGLU

Ph.D

The Hong Kong Polytechnic University

2012

The Hong Kong Polytechnic University
Department of Building Services Engineering

A Novel Thermal Storage Based Reverse Cycle Defrosting Method and the Operating Performance Evaluations for an Air Source Heat Pump

Qu Minglu

A thesis submitted in partial fulfillment of the requirements

for the Degree of Doctor of Philosophy

Jan 2012

Certificate of Originality

I hereby declare that this thesis is my own work and that, to the best of my knowledge and belief, it reproduces no material previously published or written, nor material that has been accepted for the award of any other degree or diploma, except where due acknowledgement has been made in the text.

Qu Minglu

Department of Building Services Engineering

The Hong Kong Polytechnic University

Hong Kong SAR, China

Jan, 2012

Abstract

Air source heat pumps (ASHPs) have been widely used worldwide as an energy efficient and environmental friendly means for indoor environmental control. However, when an ASHP unit operates in heating mode, frost may be accumulated on the surface of its outdoor coil. Frosting deteriorates its operational performance and energy efficiency, and therefore periodic defrosting becomes necessary.

Currently, the most widely used standard defrosting method for ASHPs is reverse cycle defrost. However, a fundamental problem for such a method is that there is insufficient heat available for defrosting, which leads to a number of associated operational problems including low-pressure cut-off or wet compression, a prolonged defrosting duration, the risk of having a lower air temperature inside a heated space without heating being provided during defrosting and longer transition from defrosting to heating-resumption, etc. On the other hand, for an outdoor coil used in an ASHP, on its refrigerant side, multiple parallel circuits are commonly used for minimized refrigerant pressure loss and enhanced heat transfer efficiency. On its airside, however, there is usually no segmentation corresponding to the number of refrigerant circuit. Consequently, uneven defrosting over the entire airside surface of the multi-circuit outdoor coil possibly caused by the downwards flowing of melted frost due to gravity is likely to occur. Therefore, it is necessary both to develop a novel thermal energy storage (TES) based reverse cycle defrosting method for

ASHPs so as to address the fundamental problem of inadequate heat available for defrosting through TES technology, and to study the defrosting performance on the airside surface of a multi-circuit outdoor coil.

This thesis begins with reporting the development of a novel TES-based reverse cycle defrosting method using phase change material (PCM). The operating performances of an experimental ASHP unit using the novel TES-based reverse cycle defrosting method have been experimentally studied. The measured operating performances on the refrigerant side of the experimental ASHP unit are firstly reported. Three operating modes at which extensive experiments were carried out for the experimental ASHP unit, namely, standard heating and reverse cycle defrosting, parallel TES-based heating and reverse cycle defrosting, and finally serial TES-based heating and reverse cycle defrosting, are detailed. The experimental results on the refrigerant side performances of the experimental ASHP unit suggested that the use of the novel TES-based reverse cycle defrosting method would result in a number of advantages, including a smoother transition from defrosting to space heating resumption, an enhanced operational reliability and reduced energy consumption.

Secondly, the thesis presents the operational performances on the airside of the experimental ASHP unit during the three operating modes, as well as the indoor thermal comfort characteristics during the use of the TES-based reverse cycle

defrosting method. The well-known Fanger's thermal comfort model is briefly introduced, with appropriate assumptions and simplifications. This is followed by reporting the measured indoor thermal parameters that were necessary for evaluating indoor thermal comfort under the standard reverse cycle defrosting method and the TES-based reverse cycle defrosting method. The experimental results on the airside performances of the ASHP unit and the evaluated indoor thermal comfort indexes (PMV and PPD) clearly suggested that the use of the novel TES-based reverse cycle defrosting method would lead to a shorter defrosting duration, a higher indoor air temperature and consequently, occupants' indoor thermal comfort can be significantly improved during a reverse cycle defrosting operation.

Thirdly, the thesis reports on a study on the airside defrosting performance of an on outdoor coil having four parallel circuits in the experimental ASHP unit, with a particular focus on studying the impact of allowing melted frost to flow downwards freely due to gravity along the coil surface on defrosting performance, using both experimental and modeling analysis approaches. The experimental part of the study is firstly reported. It was observed that defrosting was quicker on the airside of the upper circuits than that on the lower circuits in the four-circuit outdoor coil. The effects of downwards flowing of the melted frost along a multi-circuit outdoor coil surface in an ASHP unit on defrosting performance were discussed. The defrosting efficiency for the experimental ASHP unit was evaluated.

Then the modeling analysis part of the study is presented. A semi-empirical defrosting model for the four-circuit outdoor coil in the experimental ASHP unit, the first of its kind, was developed based on the fundamentals of mass and energy conservation, and using the experimental data. The model was validated by comparing the predicted defrosting duration and the temperature variation of the collected melted frost with the corresponding experimental results. Using the validated model, the negative effects of downwards flowing of the melted frost along the surface of a multi-circuit outdoor coil on defrosting performance were quantitatively analyzed and are reported. The model developed provided a useful tool for studying and understanding the effects of downwards flowing melted frost on the defrosting performance in the multi-circuit outdoor coil of an ASHP unit.

Finally, an experimental investigation on reverse cycle defrosting operation for the experimental ASHP unit when using an EEV as a refrigerant flow throttle regulator is reported. Comparative experiments under two control strategies for the EEV, i.e., the EEV being fully open and the EEV being regulated by a degree of refrigerant superheat (DS) controller during defrosting, were conducted. The experimental results revealed that when the EEV was regulated by the DS controller during defrosting, a higher defrosting efficiency and less heat wastage would be resulted in.

Publications Arising from the Thesis

I.   Journal Papers

- **Qu Minglu**, Deng Shiming and Jiang Yiqiang. An experimental study on the defrosting performance of a PCM based reverse-cycle defrosting method for air source heat pumps. *International Journal of Air-Conditioning and Refrigeration*, 18 (2010) 327-337 (Based on Chapter 5).

- **Qu Minglu**, Xia Liang, Deng Shiming and Jiang Yiqiang. Improved indoor thermal comfort during defrost with a novel reverse-cycle defrosting method for air source heat pumps. *Building and Environment*, 45 (2010) 2354-2361 (Based on Chapter 6).

- **Qu Minglu**, Xia Liang, Deng Shiming and Jiang Yiqiang. A study of the reverse cycle defrosting performance on a multi-circuit outdoor coil unit in an air source heat pump-Part I: experiments. *Applied Energy*, 91 (2012) 122-129 (Based on Chapter 7).

- **Qu Minglu**, Pan Dongmei, Xia Liang, Deng Shiming and Jiang Yiqiang. A study of the reverse cycle defrosting performance on a multi-circuit outdoor

coil unit in an air source heat pump-Part: II modeling analysis. *Applied Energy*, 91 (2012) 274-280 (Based on Chapter 8).

- **Qu Minglu,** Xia Liang, Deng Shiming and Jiang Yiqiang. An experimental investigation on reverse-cycle defrosting performance for an air source heat pump using an electronic expansion valve. *Applied Energy, in press* (Based on Chapter 9).

II.   Conference papers

- **Qu Minglu**, Deng Shiming and Jiang Yiqiang. An experimental study on the defrosting performance of a PCM-based reverse-cycle defrosting method for air source heat pumps. *International Refrigeration and Air Conditioning Conference* , Purdue University, USA, July 12-15, 2010

- **Qu Minglu**, Xia Liang, Deng Shiming and Jiang Yiqiang. An experimental investigation on the defrosting performance of an air source heat pump during reverse-cycle defrost using EEV as a throttle regulator. *International Conference on Applied Energy*, Perugia, Italy, May 16-19, 2011

Acknowledgements

I must express my grateful thanks to my Chief Supervisor, Prof. Deng Shiming, Professor and Associate Head, and my Co-Supervisor, Dr. M.Y. Chan, Assistant Professor, both from the Department of Building Services Engineering (BSE), The Hong Kong Polytechnic University, and Co-Supervisor, Prof. Y.Q. Jiang, Professor, Institute of Heat Pump and Air Conditioning Technology, Harbin Institute of Technology, for their readily available supervision, valuable suggestions, patient guidance, continuous help and encouragement throughout the course of the work.

My special thanks go to The Hong Kong Research Grant Council (RGC) and The Hong Kong Polytechnic University for financially supporting my study. I would also like to thank Dr. Qi Qi, Dr. Liang Xia, Dr. Xiangguo Xu, Dr. Wenju Hu and Mr. Jiankai Dong, for their assistance in my simulation and experimental work. In addition, I wish to express my gratitude to the technicians in the Heating Ventilation and Air Conditioning Laboratory of the BSE Department for their supports during my experimental work.

Finally, I would like to express my deepest appreciation to my family members: Yuan Yao - my husband, my parents, my parents-in-law. I could not have finished my work without their encouragement, supports and understandings.

Table of Contents

List of Figures

List of Tables

Nomenclature

Variable	Description	Unit
A_o	equivalent airside surface area of a refrigerant circuit in a multi-circuit outdoor coil	m^2
$AAHP$	Air-air heat pump	
A/C	air conditioning	
$A_{dr\text{-}a}$	effective dry airside surface area of a refrigerant circuit in a multi-circuit outdoor coil (used in the third stage of defrosting process)	m^2
$A_{f\text{-}a}$	effective airside surface area covered by only the melted frost of a refrigerant circuit in a multi-circuit outdoor coil (used in the second stage of defrosting process)	m^2
A_i	inside surface area of a refrigerant circuit in a multi-circuit outdoor coil	m^2
$ANSI/$ $ASHRAE$	American National Standard/American Society of Heating, Refrigerating and Air-conditioning Engineers	
A_{pw}	surface area of the melted frost in contact with the ambient air in a water collecting pan	m^2
$ASHP$	Air source heat pump	
$A_{w\text{-}a}$	effective wetted airside surface area of a refrigerant circuit in a multi-circuit outdoor coil (used in the third stage of defrosting process)	m^2
c_p	specific heat of water	kJ/ (kg °C)
COP	coefficient of performance	ND
D	globe diameter	m

DAS	data acquisition system	
DC	direct current	
DS	degree of superheat	
DX	direct expansion	
EEV	electronic expansion valve	
f_{cl}	clothing area factor	ND
FDC	fan-defrost contribution	
g	gravity acceleration	m/s^2
Gr	Grashof Number	ND
h_c	convective heat transfer coefficient	W /(m^2 °C)
h_n	coefficient of natural convective heat transfer	W /(m^2 °C)
h_D	coefficient of convective mass transfer	m/s
h_L	heat transfer coefficient of liquid refrigerant	W /(m^2 °C)
h_r	enthalpy of refrigerant	kJ/kg
HTF	heat transfer fluid	
h_{tp}	heat transfer coefficient of refrigerant in the two-phase region	W /(m^2 °C)
h_w	average coefficient of convective heat transfer caused by water flow	W /(m^2 °C)
$h_{w,x}$	coefficient of local convective heat transfer caused by water flow	W /(m^2 °C)
H	height of a control volume	m
HVAC	heating, ventilation and air conditioning	
I_{cl}	clothing insulation value	clo
ISO	International Organization for Standardization	
L	thermal load on a human body	met (W/m^2)
Le	Lewis number	ND
LGU	load generating unit	
L_{sf}	latent heat of frost melting, 334 kJ/kg	kJ/kg

L_v	latent heat of water vaporization, 2443 kJ/kg	kJ/kg
m	mass flow rate or frost-melting rate	kg/s
$m_{w,j}$	mass flow rate of the melted frost falling from Circuit j (j=1-4)	kg/s
M	rate of metabolic heat production (for Chapter 6)	met (W/m^2)
M	mass (for Chapter 7)	kg
M_f	total mass of the frost formed on an outdoor coil surface	kg
M_{pw}	mass of the retained melted frost in a water collecting pan	kg
M_w	mass of the retained melted frost on an outdoor coil surface	kg
MRT	mean radiant temperature	°C
Nu	Nusselt Number	ND
p_{asw}	saturated water vapor pressure	kPa
p_{av}	water vapor pressure	kPa
p_r	reduced pressure	ND
P	input power	W
P_c	critical pressure of refrigerant	MPa
PCM	phase change material	
PCM-HE	PCM based heat exchanger	
PID	proportional-integral-derivative	
P_{sat}	saturated pressure of the refrigerant	MPa
PMV	Predicted Mean Vote	ND
PPD	Predicted Percentage Dissatisfied	%
Pr	Prandtl Number	ND
PWM	pulse-width-modulation	
q	defrosting heating capacity	kW
Q	heat provided	kJ

R	thermal resistance	$(m^2 \,°C)/W$
Re	Reynold Number	ND
RTD	Resistance Temperature Device	
SSR	Solid State Relay	
t	time	s
t_{adb}	air dry-bulb temperature	°C
t_{cl}	clothing temperature	°C
t_d	defrosting duration	s
t_g	globe temperature	°C
$\bar{t}_r$	mean radiant temperature	°C
T	temperature	°C
T_{adb}	air dry-bulb absolute temperature	K
TES	thermal energy storage	
TEV	thermostatic expansion valve	
$T_{w,j}$	temperature of the melted frost falling from Circuit j (j=1-4)	°C
w	air moisture content	g/kg dry air
W	rate of mechanical work accomplished	met(W/m^2)
W_d	energy consumption during defrosting	kJ
v	velocity	m/s
v_w	average velocity of water layer flowing downwards	m/s
VFD	variable-frequency drives	

Greek symbols

β	volumetric thermal expansion coefficient	1/°C
ε	globe emissivity (for Chapter 7)	ND

η_d	defrosting efficiency	%
λ	thermal conductivity	W/(m °C)
v	kinematic viscosity	m^2/s
ρ_a	density of ambient air	kg/m^3
ρ_{va}	density of water vapor within ambient air	kg/m^3
ρ_{vs}	density of water vapor at the interface (saturated density)	kg/m^3
φ	relative humidity	%

Note: ND = No Dimensions

Subscripts

a	air
cl	clothing
d	defrost
dr	dry
db	dry-bulb
e	exit
f	frost
i	inlet
ICW	interface between the coil surface and the water layer
j	control volume j ($j = 1$-4)
m	melting
max	maximum
pw	melted frost in the water collecting pan
r	refrigerant
tp	triple point
w	water or melted frost layer
v	vaporization

Chapter 1

Introduction

The development of air conditioning and heat pump technology is a natural consequence to both pursuing high quality living and working environment, and at the same time addressing the issue of sustainability. Air source heat pumps (ASHPs) have been widely used for space cooling in summer and space heating in winter for many years, due to their distinguished advantages of energy saving and environmental protection. However, when an ASHP is used for space heating, frost may be formed on its outdoor unit's coil surface. Frosting deteriorates its operational performance and energy efficiency, and reduces its output heating capacity, therefore periodic defrosting is necessary. Defrosting may be realized by a number of methods including compressor shut-down, electric heating, hot gas by-pass and reverse cycle.

Currently, the most widely used standard defrosting method is reverse cycle defrost. When a space heating ASHP is operated at a reverse cycle defrost mode, its outdoor coil acts as a condenser and its indoor coil as an evaporator. Hence during defrosting, a space heating ASHP unit may actually cool a space, degrading indoor thermal comfort while consuming electrical energy for melting frost. Therefore, a defrosting period should be controlled to as short as possible. Also, during defrosting, the indoor air fan in an ASHP unit is normally switched off to avoid blowing cold air directly to a heated indoor space, affecting thermal comfort of occupants. In this case, the energy to melt frost mainly comes from the input work to compressor and is thus not sufficient for quick defrosting. Insufficient heat available during defrosting is currently a fundamental problem as far as reverse cycle defrost is concerned, with

which a number of operational problems during defrosting for ASHPs are associated. These includes: low-pressure cut-off or wet compression, a prolonged defrosting duration, the risk of having a lower air temperature inside a heated space without heating being provided during defrosting and longer transition from defrosting to heating-resumption, etc. Furthermore, during defrosting, while most melted frost drains off from a finned outdoor coil surface, the surface may however retain residual water which must be removed to prevent it from becoming ice when the ASHP returns to heating mode. Therefore a complete defrosting process covers both melting frost and drying coil surface. On the other hand, for an outdoor coil used in an ASHP, on its refrigerant side, multiple parallel circuits are commonly used for minimized refrigerant pressure loss and enhanced heat transfer efficiency. On its airside, however, there is usually no segmentation corresponding to the number of refrigerant circuit. Consequently, uneven defrosting over the entire airside of the multi-circuit outdoor coil possibly caused by the downwards flowing of melted frost due to gravity is likely to occur.

In order to improve reverse cycle defrosting performance, thus minimize or even eliminate the operational problems mentioned above, and with the wide-spread applications of TES in building HVAC systems, it is necessary to develop a novel thermal energy storage (TES) based reverse cycle defrosting method for an experimental ASHP unit to address the fundamental problem of inadequate heat available for defrosting through TES technology, and study the defrosting performance on the surface of multi-circuit outdoor coil.

The thesis begins with an extensive literature review on the operating performance of

ASHPs under both frosting and defrosting conditions. A review of the previous related studies on defrosting performance of ASHPs is reported, covering defrosting methods and their control, with a particular emphasis on reverse cycle defrosting. This is followed by reviewing the previous related studies on improving the operational performance for ASHPs during both frosting and defrosting operations. A brief review of the previous work related to applying TES to heat pump systems is also included. A number of important issues where further extensive research work in achieving a better defrosting performance for ASHPs have been identified and are summarized. These issues are the expected targets of the investigation reported in this thesis.

The research proposal covering the aims and objectives, the project title and the methodologies adopted in this project is presented in Chapter 3.

Chapter 4 describes an ASHP experimental setup to facilitate carrying out the research work reported in this thesis. Detailed descriptions of the experimental setup and its major components are firstly given. This is followed by reporting the computerized measuring devices and a data acquisition system (DAS). The control for the refrigerant degree of superheat at compressor suction is also explained. The availability of the ASHP experimental setup is expected to be very essential in successfully carrying out the research work proposed in Chapter 3.

In order to solve the fundamental problem of insufficient heat available during reverse cycle defrosting, a novel TES-based reverse cycle defrosting method using phase change material (PCM) has been developed for ASHPs, and the operating

performances of the experimental ASHP unit using the novel TES-based reverse cycle defrosting method have been experimentally studied. Chapter 5 presents the measured operating performances on the refrigerant side of the experimental ASHP unit. Three operating modes, at which extensive experiments were carried out, for the experimental ASHP unit, namely, standard heating and reverse cycle defrosting, parallel TES-based heating and reverse cycle defrosting, and finally serial TES-based heating and reverse cycle defrosting, are detailed. The experimental results on the refrigerant side performances of the experimental ASHP unit suggested that the use of the novel TES-based reverse cycle defrosting method would lead to a number of advantages, including a smoother transition from defrosting to space heating resumption, an enhanced operational reliablity and reduced energy consumption.

Chapter 6 reports on the operational performances on the airside of the experimental ASHP unit during the three operating modes, as well as the indoor thermal comfort characteristics during the use of the TES-based reverse cycle defrosting method. The well-known Fanger's thermal comfort model is briefly introduced, with appropriate assumptions and simplifications. This is followed by reporting the measured indoor thermal parameters that were necessary for evaluating indoor thermal comfort under the standard reverse cycle defrosting method and the TES-based reverse cycle defrosting method. The experimental results of the airside performances of the ASHP unit and the evaluated indoor thermal comfort indexes (PMV and PPD) clearly suggested that the use of the novel TES-based reverse cycle defrosting method would lead to a shorter defrosting duration, a higher indoor air temperature and consequently, occupants' indoor thermal comfort can be significantly improved during a reverse cycle defrosting operation.

A study on the defrosting performance of the four-circuit outdoor coil in the experimental ASHP unit, with a particular focus on studying the impact of allowing melted frost to flow downwards freely due to gravity along the coil surface on defrosting performance, has been carried out, using both experimental and modeling analysis approaches. The study is reported in Chapter 7 and Chapter 8. Chapter 7 presents the experimental part of the study. It was observed that defrosting was quicker on the airside of the upper circuits than that on the lower circuits in the four-parallel circuit outdoor coil. The effects of downwards flowing of the melted frost along a multi-circuit outdoor coil surface in an ASHP unit on defrosting performance were discussed. The defrosting efficiency for the experimental ASHP unit was evaluated.

Chapter 8 reports on the modeling analysis part of the study. A semi-empirical defrosting model for the four-circuit outdoor coil of the experimental ASHP unit, the first of its kind, was developed based on the fundamentals of mass and energy conservation, and using the experimental data reported in Chapter 7. The model was validated by comparing the predicted defrosting duration and the temperature variation of the collected melted frost with the corresponding experimental results reported in Chapter 7. Using the validated model, the negative effects of downwards flowing of the melted frost along the surface of a multi-circuit outdoor coil on defrosting performance were quantitatively analyzed and are reported. The model developed provided a useful tool for studying and understanding the effects of downwards flowing melted frost on the defrosting performance in the multi-circuit outdoor coil of an ASHP unit.

Chapter 9 presents an experimental investigation on reverse cycle defrosting operation for the experimental ASHP unit using an EEV as a refrigerant flow throttle regulator. Comparative experiments under two control strategies for the EEV, i.e., the EEV being fully open and the EEV being regulated by a degree of refrigerant superheat (DS) controller during defrosting, were conducted. The experimental results revealed that when the EEV was regulated by the DS controller during defrosting, a higher defrosting efficiency and less heat wastage would be resulted in.

The conclusions of the thesis and the proposed future work are presented in the final Chapter.

Chapter 2

Literature Review

2.1 Introduction

A heat pump unit is an environmentally friendly and reliable means to maintain thermal comfort level in an indoor space, and can be used for both heating and cooling. During a cooling season, it transfers heat from the indoor space to a heat sink, in the same way as an air conditioner dose. During a heating season, it extracts heat from a heat source such as ambient air, waste water, etc, and delivers the extracted heat energy to the indoor conditioned space. With the rising cost of energy being at the forefront of world attention, there has been a growing interest in heat pump technology as a means to save energy, as it offers one of the most practicable solutions to the mitigation of greenhouse emissions. Studies have shown the potential of using heat pumps to drastically reduce greenhouse gases emissions for space heating and for heat generation. From a global point of view, over 90% of the world population resides in the regions where heat pumps can be suitably used for indoor environmental control. Almost for the whole Pacific region including the highly urbanized areas in both China and Japan except during extremely cold winter [Nishimura 2002], the use of heat pumps for space heating in winter is appropriate.

A number of heat sources are available for heat pumps, such as air, and geothermal

sources, including underground water and soil, etc. On the other hand, air and water are the common mediums used for space heating. Therefore, air-air heat pumps (AAHPs), air-water heat pumps, water-air heat pumps, water-water heat pumps, ground-air heat pumps, and ground-water heat pumps are commonly seen in building heating, ventilation and air conditioning (HVAC) applications.

Air source heat pumps (ASHPs) are relatively easy and inexpensive to install and have therefore historically been the most widely used heat pump type. In 1970's the National Bureau of Standards in the US conducted extensive tests on residential heat pumps. Their tests revealed two effects that significantly degraded heat pump performance: (1) the 'cycling effect' resulting from the need to establish a dynamic equilibrium during the off-cycle, and (2) the 'frosting effect' on outdoor coils, which increased both the heat conduction resistance and the air flow passage resistance during heating operation [Kelly and Bean 1977]. Since then, extensive experimental and theoretical investigations have been carried out on ASHPs to study their operating performances under frosting and/or defrosting conditions.

In this Chapter, a comprehensive literature review on the operating performances of ASHPs under both frosting and defrosting conditions and other related issues is presented. Firstly, a review on the performance degradation due to frost formation on the outdoor coil of ASHPs, covering both experimental and numerical studies, is reported. Secondly, a review of the previous studies on defrosting performance of

ASHPs is presented, including defrosting methods and their control, with a particular emphasis on reverse cycle defrosting. Thirdly, a review of the previous related studies on the improvements for ASHPs with respect to frosting and defrosting is presented. This is followed by reporting the review of the previous work related to applying thermal energy storage (TES) to heat pump technology. Finally, a number of important issues where further extensive research work is required have been identified and are summarized. It is expected that successfully studying these issues will help to solve some fundamental problems related to the defrosting methods for ASHPs currently used, so as to contribute to the development of heat pump technology.

2.2 The operating performance of ASHPs under frosting condition

Frost formation on the outdoor coil of a space heating ASHP unit deteriorates its operating performance and energy efficiency, which has attracted a lot of research interest over the past many years. A large number of experimental and theoretical investigations on the subject have been reported.

2.2.1 Experimental studies on frost formation process and its effects of on the performance of ASHPs

2.2.1.1 Mechanisms of frost formation

The mechanism for frost growth is the diffusion of water onto cold surfaces due to the difference between the water vapor concentration of an air stream and that of the surface of a frost layer [Sanders 1974]. The water mass that is transferred to the frost surface creates two distinct effects in the frost layer. A portion of the water vapor is deposited onto the frost layer, thereby contributing to the further frost growth while the remainder of the water vapor diffuses into the frost layer where it changes phase and increases the density of the frost.

The early experimental studies on frosting concentrated on frost properties, mechanism of frost growth and heat transfer in different types of heat exchanger were carried out, covering: flat plate [Yonko et al. 1967, Jones and Parker 1975, Mao et al. 1999, Cheng and Shiu 2002, Kwon et al. 2006], vertical plate [Fossa and Tanda 2002, Lee and Ro 2002], vertical channel [Tanda and Fossa 2006], parallel plates [Lüer and Beer 2000], horizontal cylinder [Lee and Ro 2001, Mago and Sherif 2003]. A typical frost growth process was described by Hayashi et al. [1977]. An initial one-dimensional crystal growth period was followed by a frost layer growth period. Finally, a so-called frost layer full-growth period concluded a frost growth process.

Each growth period was characterized by specific values of frost density which in turn affected the other frost properties, such as thickness, thermal conductivity, etc.

Many researchers have also studied the influences of ambient conditions and the surface temperature of a heat exchanger on frost growth. Nowadays, it is commonly acknowledged that frost formation on the surface of a heat exchanger is associated with the following factors:

- Heat exchanger:

    1) The structure: rim effects, fin pitch, surface roughness, tube arrangement;

    2) The surface temperature of a heat exchanger.

- Air flow: temperature, humidity and flow rate.

- Frosting duration.

2.2.1.2 Frost formation process on the surface of a heat exchanger

Frost formation on the surface of a heat exchanger is a complex process because of the continuous changes in frost properties and the air-frost interface temperature, with respects to both time and position, during the growth of a frost layer.

The drops in both overall heat transfer coefficient and airside pressure are the two

major concerns, because not only they are the two important factors used in evaluating the performance of a heat exchanger, but also frost growth may be quantitatively evaluated by airside pressure drop across the heat exchanger. As reported by Emery and Siegel [1990], 50–75% decrease in heat transfer and a substantial increase in pressure drop were caused by frost formation on a compact heat exchanger. Moreover, the effects of ambient air and the geometrical parameters of a heat exchanger on frost growth have been studied comprehensively. Kondepudi and O'Neal [1989] experimentally studied the effects of frost growth on the performance of louvered finned-tube heat exchangers. It was reported that frost growth, pressure drop and heat transfer coefficient increased with air humidity, air velocity and fin density. Thereafter, Kondepudi and O'Neal [1990] compared the performance of finned-tube heat exchangers with that of other heat exchangers having different fin configurations. It was found that the heat exchangers with louvered fins had the best thermal performance under frosting conditions, followed by those with wavy fins and flat fins. Rite and Crawford [1991a, 1991b] investigated the effects of different ambient and operational parameters on frost formation of the finned-tube evaporator used in a domestic refrigerator-freezer. They concluded that frosting rate increased at a higher air humidity, or a higher air temperature, or a higher air flow rate and a lower refrigerant evaporating temperature. The overall heat transfer coefficient, or UA value, and the airside pressure drop also increased with the growth of frost on the evaporator coil surface at a constant air flow rate. Yan et al. [2003] experimentally investigated the performances of a flat plate finned-tube heat exchanger operated under frosting

conditions. Air flow rate remained unchanged during each test. It was shown that frost

formation was faster at a lower air flow rate (which contradicted to what Kondepudi

and O'Neal [1989], and Rite and Crawford [1991a, 1991b] reported). The results also

showed that an increase in air temperature at different ranges of ambient temperature

would have different effects on frost growth as evaluated by the pressure drop across

the heat exchanger. When the ambient air temperature was increased from 2.5 to 5 $^{\circ}$C,

the amount of frost was increased. However, on the contrary, when it was increased

from 5 to 7.5 $^{\circ}$C, the amount of frost was actually decreased. The performance of a

heat exchanger was not significantly affected when its fin pitch was increased. Yan et

al. [2005] studied the operating performance of frosted finned-tube heat exchangers

with three different types of fins, namely, flat plate fins, one-sided louver fins and

re-direction louver fins. The effects of air flow rate, inlet air relative humidity,

refrigerant evaporating temperature and different types of fins on the thermofluid

characteristics of the heat exchangers were discussed. It was also pointed out that the

amount of frost formation was the highest when re-directional louver fins was used.

Xia et al. [2006] studied the airside thermal-hydraulic performances of a

louvered-finned flat-tube heat exchanger under frosting, defrosting and refrosting

conditions. The overall heat transfer coefficient, pressure drop, j and f factors were

compared with those of a fold-louvered-fin, micro-channel heat exchanger.

Comparison results showed a decrease in the overall heat transfer coefficient and an

increase in pressure drop during a frosting process. Both the reduction in airside flow

rate and the bridging of louver gaps by frost significantly reduced the airside heat

transfer coefficient as frost accumulated. For heat exchangers with a large fin length, their averaged UA value per unit volume of heat exchanger was much lower. The study results also suggested that the pressure drop across a heat exchanger during refrosting was largely affected by the water retained on the surface of the heat exchanger.

The previous experimental studies reviewed above described the impacts of ambient parameters, such as air temperature, relative humidity, air velocity and geometrical parameters of a finned-tube heat exchanger, such as fin spacing, fin and tube arrangements on frost growth and the operating thermal performance of the finned-tube heat exchanger.

It appeared that there were different results from previous studies related to frosting. This may well be due to the strong dependence of frost thermal properties on individual experimental conditions. Albeit the differences, almost all of the previous experimental studies gave the similar conclusions regarding the effect of inlet air relative humidity and fin spacing on the performance of a finned-tube heat exchanger under frosting conditions. These results may be summarized as follows:

- Higher inlet air relative humidity led to a faster frost formation on, and thus a greater pressure drop, across a heat exchanger.
- The effect of frost growth on the operating performance of a finned-tube heat

exchanger decreased significantly as its fin pitch increased.

2.2.1.3 Frost formation on the outdoor coil surfaces in ASHPs

As discussed above, frost formation on the surfaces of a heat exchanger would deteriorate its operating performance. In an ASHP unit, frost formation and accumulation on its outdoor coil or evaporator surface would affect its operating parameters, such as evaporating and condensing temperatures, which would in turn affect frost formation. It has been commonly acknowledged that frost formation and accumulation on evaporator surfaces have two main consequences for ASHPs. Firstly, the accumulation of large amounts of frost would deteriorate the heat transfer performance of an evaporator by fouling its outside surface since the frost itself had a low thermal conductivity [Stoecker 1957, Machielsen and Kerschbaumer 1989]. With a deteriorated heat transfer performance, the evaporator's capacity would decrease. To meet the specified heating requirement, its evaporating temperature must be decreased which further reduced system efficiency. Secondly, frost impeded airflow through an outdoor coil, leading to an increased fan energy consumption and a reduced air flow rate through the evaporator [Stoecker 1957, Barrow 1985, Seker et al. 2004b, Yao et al. 2004].

From the open literature available, much research work has been carried out to

investigate the operating performance of ASHPs under frosting conditions. Domingorena and Ball [1980] investigated the performance of a 3-ton AAHP in heating mode. They concluded that under frosting conditions, airflow through the outdoor coil of the AAHP decreased substantially, with a concurrent rapid decreases in compressor discharge and suction pressures, and refrigerant flow rate. However, He et al. [2003], Ding et al. [2004] and Wang et al. [2011] reported that the discharge temperature/pressures were increased during frosting, which may be caused by different expansion devices used in experiments. Ameen [1993] pointed out that the decreased refrigerant evaporating temperature and the decreased refrigerant density at compressor suction during frosting would lead to a reduction in both refrigerant flow rate and compressor power input. Huang et al. [2007] tested the dynamic characteristics of an air-to-water heat pump with a multi-circuit evaporator controlled by a thermostatic expansion valve (TEV) under the frosting/defrosting conditions. The experimental results showed that airflow maldistribution over the outdoor coil would result in intermittent or unceased hunting during frosting. Guo et al. [2008] considered that frost growth on an outdoor coil surface of an experimental ASHP unit may be divided into three stages. In the first stage, the performance of the ASHP unit was improved due to the rough surface formed by an initial frost layer, similar to those reported by Stoecker [1957], Hosoda and Uzuhashi [1967], Huang et al. [2008]. The initial increase in heat transfer was attributed to an increase in air velocity and frost surface roughness, both of which led to an increase in the airside heat transfer coefficient, as well as an increase in heat transfer area since the nuclei of frost crystals

acted like small fins. In the second stage, column-shaped ice crystals on frost surface grew in its radial rather than longitudinal direction. Therefore, the rate of increase in frost thickness was reduced or remained unchanged as frosting went on. The heating capacity and coefficient of performance (COP) of the test ASHP unit were only slightly affected by frosting on outdoor coils due to a slow growth in frost thickness. During the third stage, column-shaped ice crystals on frost surface grew in its longitudinal rather than in its radial direction, thus acerose-shaped ice crystals on frost layer were formed, and the growth rate of frost thickness increased rapidly to about 2.7- 4.5 times of that in the second stage. Therefore, the performance of the ASHP unit deteriorated rapidly, and the decreasing rates of both heating capacity and COP could reach up to a level of several times of these in the second stage. The experimental results suggested that the rapid performance degradation was mainly caused by the morphological variation of frost layer in the third stage.

Many researchers have studied the degree of performance losses under frosting conditions. Miller [1984] studied the effects of frosting on COP and heating capacity of ASHPs under the frosting conditions of 4.4 ^{o}C (40 ^{o}F) to -6.7 ^{o}C (20 ^{o}F) with air relative humidity ranging between 60% and 90% using a 3-ton residential ASHP unit, where a single row spiny fin outdoor coil was used. Performance losses due to frosting were the largest when tests were conducted at between 1.7 ^{o}C and -1.1 ^{o}C (35 ^{o}F and 30 ^{o}F), with air relative humidity being greater than 70%. Approximately 10% reduction in COP and 15% reduction in heating capacity were reported under an

operating condition of 80% and 90% humidity after a 60 minutes-long frosting operation. Based on the experimental study conducted by Votsis [1989], the reductions in the steady state COP varied between 10% and 27%, depending on the ambient conditions and the frosting duration.

2.2.2 Numerical studies on frost formation and its effects on the operating performance of ASHPs

Some numerical studies in this respect are reported. It is commonly acknowledged that to analyze a frosting process is rather difficult because it is a composite unsteady heat and mass transfer problem, due to the variation in roughness of frost surface in relation to time, a very large number of variables involved, the complex surface geometry of heat exchangers and the thermodynamic properties of humid air and frost. Nonetheless, to better understand the operating characteristics of ASHPs under frosting conditions, researchers have attempted to model mathematically a frosting process.

Martinez-Frias and Aceves [1999] reported a transient frost formation model, and its integration into an existing heat pump model for predicting heat pump operating conditions and COP as a function of environmental conditions. Verma et al. [2002] developed a quasi-steady, finite-volume model for frosting on plain-fin-round-tube

heat exchangers. Seker et al. [2004a, 2004b] investigated experimentally and numerically the heat and mass transfer characteristics in finned-tube heat exchangers during frosting. Xia et al. [2004] carried out an empirical study on the effects of frost accumulation on louvered-fin micro-channel heat exchangers. One of the outcomes was that bridging louver gaps by frost was a major reason for decreased airside heat transfer and therefore a capacity reduction of an outdoor coil. Yao et al. [2004] reported a detailed distributed model for the outdoor unit under frosting condition in an ASHP water heater/chiller. The model consisted of a frosting sub-model and a heat exchanger sub-mode. Frost formation and its distribution on the surface of the outdoor unit and their impacts on the operational performance of the ASHP water heater/chiller were evaluated. Yang et al. [2006] proposed a mathematical model using correlations for heat transfer coefficients and a water-vapor diffusion equation to predict the thermal performance of a finned-tube heat exchanger under frosting conditions. Tso et al. [2006a, 2006b] developed a general distributed model for two-phase flow of refrigerant coupled with a frosting model for studying the dynamic behaviors of an evaporator. The model could be used to predict liquid dry-out position, evaporator coil wall temperature distribution, air temperature flowing onto each row and frost height on each row, etc.

2.3 The performance of ASHPs during defrosting

As discussed above, frost formed on tube surface of the outdoor coil in an ASHP would deteriorate its operating and energy efficiency, reliability and life span. Therefore, periodic defrosting becomes necessary for guaranteeing the ASHP's satisfactory operation.

2.3.1 Defrosting methods for ASHPs

Defrosting can be realized by a number of methods including: (1) compressor shut-down defrost; (2) electric heating defrost; (3) hot gas by-pass defrost; and (4) reverse cycle defrost.

Compressor shut-down defrost is normally used in applications where the ambient air temperature is not lower than 1^oC. When the ambient air temperature requirement is satisfied, the compressor is shut down and an outdoor coil air fan continues to run and the frost on the coil is melted. Therefore under certain ambient conditions in winter when ambient air temperature is lower than 1^oC, the compressor shut-down defrosting method is not suitable.

Electric heating defrost usually involves electrically heating up the surface of an outdoor coil to melt off frost. Usually heat is applied externally to the coil as

opposed to applying internal heat in hot gas by-pass defrost or reverse cycle defrost. Such a defrosting method requires a longer defrosting period than the reverse cycle defrosting method, usually 1-1/2 times. Furthermore, it is a costly operation since energy is required to melt frost and an ASHP is out of operation during defrosting.

Hot gas by-pass defrost is largely used for industrial ASHPs. The superheated refrigerant vapor discharged from compressor is directed into an evaporator, or outdoor coil, by-passing condenser and expansion device. Most likely latent heat of condensation of refrigerant vapor is used as the heat source; however, sensible heat of highly superheated refrigerant vapor may also be used. Most hot gas by-pass systems introduce the hot gas at the discharge connection through a relief valve into the suction line downstream of a suction solenoid valve which closes during defrosting.

For reverse cycle defrost, the operation cycle during heating is reversed by using a four way valve, and so is the refrigerant flow direction. During defrosting, hot gas is pumped into the outdoor coil to melt the frost off. When the frost is melted and drained away from the coil, an ASHP switches back to resume heating operation.

Defrosting helps an ASHP return to its rated performance, although a defrosting process itself can cause a number of problems. Firstly, defrosting reduces an ASHP's COP because energy is required to melt off the frost. Secondly, the operation of the ASHP would be interrupted during defrosting, so that normal space heating in an

indoor space served by the ASHP would be suspended, degrading the indoor thermal comfort of occupants. Finally, defrosting increases equipment cost due to the addition of auxiliary heating elements and reduces equipment reliability.

2.3.2 Reverse cycle defrost

Currently, the most widely used standard defrosting method is reverse cycle defrost [Ding et al. 2004, Byun et al. 2006]. Therefore, in this Chapter, more discussions on reverse cycle defrost are given.

It is noted that the research related to reverse cycle defrosting operation for ASHPs is relatively less seen comparing with that related to frosting [Yao et al. 2004]. This is because that reverse cycle defrost is a complex process involving spatial and time variations of the temperatures of refrigerant, metal and air, as well as many other indeterminate factors resulted from transient cycling which may last for only a few minutes [Krakow et al. 1993a]. Also, an energy balance on the airside of an outdoor coil is complex due to the fact that the energy extracted from hot refrigerant gas is utilized in several different ways, e.g., heating up the evaporator coil metal surfaces, melting the frost, re-evaporating the melted frost and direct transfer to ambient by natural convection.

2.3.2.1 Experimental studies for ASHPs during defrosting

When a space heating ASHP unit is operated at a reverse cycle defrosting mode, its outdoor coil acts as a condenser and its indoor coil as an evaporator. Also, during defrosting, the indoor air fan in an ASHP unit is normally switched off to avoid blowing cold air directly to a heated indoor space, affecting thermal comfort of occupants. Hence, the energy available from the indoor coil is basically that stored in coil metal but there is an insignificant amount of energy available from indoor air because of a negligibly small airside convective heat coefficient resulted from de-energized indoor air fan during defrosting. When there is no more heat to be absorbed from coil metal (i.e., when coil temperature drops to a sufficiently low level), evaporating temperature, as well as the evaporating pressure, will significantly drop. Consequently, low-pressure cut-off or wet compression may take place, which may cause the ASHP unit to shut down [Miller 1987, Kondepudi and O'Neal 1990, 1991] and possibly damage the compressor. In this case, the energy to melt frost mainly comes from that stored in indoor coil metal and the input work to compressor but is not sufficient for quick defrosting. Insufficient heat available during defrosting is currently a fundamental problem as far as reverse cycle defrost is concerned, with which a number of operational problems during defrosting for ASHPs are associated. These include a prolonged defrosting time and the risk of having a lower air temperature inside a heated space without heating being provided during defrosting, etc.

O'Neal et al. [1989] experimentally investigated the transient defrosting performance of a nominal 3-ton residential ASHP unit using a TEV. It was found that the accumulator of the ASHP unit and the TEV impacted significantly on the system's dynamic responses. The liquid levels in the accumulator varied during defrosting. The TEV appeared to work well as a defrost expansion device because of its ability to vary orifice size in response to changing system operating conditions. On the other hand, the cycle performances during defrosting for ASHPs with either a scroll or a reciprocating compressor were experimentally studied and compared, in accordance with American National Standard/American Society of Heating, Refrigerating and Air-conditioning Engineers (ANSI/ASHRAE) Standard 116-1983 [Payne and O'Neal 1995]. The results suggested that an ASHP unit using scroll compressor achieved a slightly higher integrated cyclic COP and a lower compressor discharge temperature during frosting and defrosting. Based on the tests on an air-to-water heat pump, Huang et al. [2007] pointed out that a 'critical point' existed during a defrosting cycle, after which operational parameters such as refrigerant temperature at the outdoor coil outlet, evaporating temperature and degree of superheat increased quickly. This was because the modes of heat transfer on the airside of the outdoor coil changed from phase-change of frost melting to air natural convection. Chen et al. [2009] investigated the effects of outdoor air parameters on reverse cycle defrosting characteristics for an ASHP unit. The experimental results showed that with an increase in outdoor air relative humidity at a constant air temperature and a constant air velocity, the total power consumption, defrosting duration and the heat taken away from an indoor space

during defrosting decreased linearly.

On the other hand, for an outdoor coil used in an ASHP, on its refrigerant side, multiple parallel circuits are commonly used for minimized refrigerant pressure loss and enhanced heat transfer efficiency. On its airside, however, there is usually no segmentation corresponding to the number of refrigerant circuit. In the open literature, not many reported studies on defrosting characteristics over the surface of multi-circuit outdoor coils may be identified. The outdoor coil in the experimental residential ASHP unit, as reported by O'Neal et al. [1989], had four parallel refrigerant circuits. Noticeable differences in the surface temperatures at the exit of the four circuits were reported. The rates of increase in the surface temperatures at the exits of the up circuit(s) were much quicker than that of the down circuit(s). Termination of defrost was triggered when the surface temperature at the exit of the lowest circuit reached 18.3 ℃ (65 ℉). However at the same time, the surface temperature at the exit of the top circuit already reached about 37.7 ℃ (100 ℉). Similar results can also be seen in the experimental study on an outdoor coil having six rows and fourteen circuits during hot gas by-pass defrosting conducted by Stoecker et al. [1983]. Furthermore, in the study reported by Wang et al. [2008], it was shown that at six minutes into defrosting, the surfaces of down refrigerant circuit(s) in a multi-circuit outdoor coil were still covered by frost while that of up circuits were already free of frost.

Uneven defrosting over the surface of a multi-circuit outdoor coil, as discussed above, may well be resulted from uneven frosting. It however may also be caused by the downwards-flowing of melted frost due to gravity. However, the research work related to accounting the effect of downwards flowing of melted frost along the surface of a multi-circuit outdoor coil on defrosting performance can be hardly identified in open literature.

2.3.2.2 Modeling of defrosting

One key feature with modeling a defrosting process is that it is at least somewhat stochastic; during defrosting, the frost on an outdoor coil will not necessarily be melted uniformly throughout the coil. The frost over some parts of the coil remains attached to the coil surfaces until it is completely melted and sublimated while the frost at other locations may be partially melted, and then detaches from the coil surface, falling down to the coil surface at a lower level or to a drainage pan.

From the open literature available, modeling of a defrosting process has attracted lots of research attention. Early research work focused mainly on outdoor units of simple geometry, such as finite slabs [Goodman and Shea 1960], horizontal flat plate [Abdel-Wahed et al. 1983], or flat plate cooler [Sherif and Sherif 1992]. Thereafter, a number of studies on modeling a defrosting process in ASHP units were carried out.

Krakow et al. [1992a, 1992b] developed a reverse cycle defrosting model for an outdoor coil. In this model, the process of frost melting on an outdoor coil surface was idealized by subdividing it into four stages: preheating, melting, vaporizing and dry heating. A number of heat and mass transfer parameters required for simulating defrosting performance, e.g., the maximum mass of surface water, free-convection air film conductance, air/water film conductance and surface water vaporization coefficient, were however experimentally determined. Afterwards, Krakow et al. [1993a, 1993b] presented an idealized reverse cycle defrosting model for an ASHP unit with a receiver. On the basis of the above mentioned model, a validated defrosting model for an ASHP unit using capillary tube was developed by Liu et al. [2003]. Distributed modeling was used for both evaporator and condenser because of their importances during reverse cycle defrosting. Sherif and Hertz [1998] presented a semi-empirical model for electric defrosting of a cylindrical coil cooler. In this model, it was assumed that the heat provided by an electric-heater was taken away by both the frost layer and the refrigerant vapor, but the ratio between the two was arbitrarily chosen. Al-Mutawa and Sherif [1998a, 1998b] developed an analytical model of a cylindrical coil cooler to predict the evaporation, sublimation and melting rates during hot gas by-pass defrosting. In this model, a moving boundary technique was used and the defrosting process was divided into two stages, pre-melting and melting. Alebrahim and Sherif [2002] reported an electric defrosting model for a finned-tube outdoor coil using the enthalpy method to predict defrosting duration and frost surface temperature profiles. Hoffenbecker et al. [2005] reported the

27

development of a transient model for predicting the heat and mass transfer during a hot gas by-pass defrosting process on an industrial air-cooling evaporator. The model focused on both the energy distribution during defrosting and the optimization of hot gas temperature. Dopazo et al. [2010] developed a detailed transient simulation model of hot gas by-pass defrosting in an air-cooled evaporator. In this model, a defrosting process was subdivided into six stages: preheating, tube frost melting, fin frost melting, air presence, retained water vaporizing and dry-heating.

Although the above mentioned defrosting models were developed and used in studying defrosting performance, none of them in fact considered the effects of downwards flowing of the melted frost due to gravity along an outdoor coil surface on the defrosting performance, by either assuming a stable water layer or no water retention on coil surface. However, the experimental study on a nominal 3-ton residential ASHP unit reported by Payne and O'Neal [1995] suggested that after ~1 hour frosting process under the condition of 1.7 ℃ dry-bulb temperature and 80% relative humidity, and ~7 min defrosting process, over 1.6 liter of melted frost was collected. This amount of water flowing downwards due to gravity over the entire outdoor coil surface would affect the defrosting process as an additional thermal resistance layer was introduced [Cheng and Seki 1991].

2.3.2.3 End-uses of defrosting heat

The energy balance on the airside of an outdoor unit during defrosting is complex because energy is used for different purposes, including heating the outdoor coil metal surfaces, melting the frost, vaporizing melted frost retained on coil surface and direct transfer to ambient air by natural convection. Consequently, related experimental or numerical studies on end-uses of defrosting heat during a defrosting process have been carried out, focusing however on hot gas by-pass defrost for industrial air coolers or freezers.

Niederer [1976] firstly attempted to determine the amount of thermal energy required for defrosting by measuring the amount of hot gas that condensed during a hot gas by-pass defrost cycle and the power input during an electric defrost cycle. It was pointed out that only 15 to 25% of the total heat available to a defrosting process was actually used to melt the frost, with the remaining going to surrounding environment and coil/cabinet surfaces. Kerschbaumer [1971] defined defrosting efficiency as a ratio of the total energy required to melt the accumulated frost only (including sensible warming) to the total amount of defrosting energy input (including any refrigeration load effects). Stoecker et al. [1983] experimentally investigated the end use of defrosting heat in hot gas by-pass defrosting for industrial cooling coils. It was pointed out that the losses during defrosting mainly came from the heat transferred from warm coil surface to a refrigerated space. Coley [1983] suggested that during a defrost cycle

for a freezer, at least 15% of the frost sublimed into the surrounding refrigerated air space, which represented an additional load on the freezer. Approximately 24 to 28% (depending on coil material used) of the heat input was required to warm the evaporator coil sufficiently to melt frost. After that, Cole [1989] validated Coley's estimation using the data presented by Stoecker et al. [1983]. The study results showed that the largest portion, typically at more than 80%, of the heat required to defrost an evaporator in a freezer went back to the freezer as an added load, thus resulting in a defrosting efficiency of less than 20%. According to the simulation results on reverse cycle defrosting from Krakow et al. [1993a, 1993b], the defrosting efficiency, defined as a ratio of the actual amount of heat required to melt the accumulated frost and vaporize the retained water to the total amount of heat provided to the outdoor coil during a defrosting period, was between 40.4% and 58% on an ASHP unit with a single circuit outdoor coil.

On the other hand, studies about examining the energy loss caused by defrosting have also been performed. Baxter and Moyers [1984] tested an ASHP unit with a heating capacity of 10 kW for two years to characterize the dynamic losses in capacity and efficiency due to cycling, frosting and reverse cycle defrosting. It was concluded that defrosting losses were responsible for 10.1% of the total energy consumption (excluding supplemental electric resistance heating). A seasonal analysis conducted by Miller [1984] suggested that the frosting/defrosting degradation was primarily due to defrosting of an outdoor heat exchanger. The defrosting losses were almost three

times as much as those associated with frosting. Also, using auxiliary heat during defrosting can cause a significant cumulative reduction in COP. Al-Mutawa and Sherif [1998c, 1998d, 1998e] used a special test apparatus to determine the actual defrosting load associated with frosted industrial freezer coils using hot gas by-pass defrosting method. It was found that fan-defrost contribution (FDC), defined as the theoretical contribution of the fan and defrost heat loads to the net refrigeration load, exceeded 15% of the net refrigeration load.

2.3.2.4 Thermal comfort in a heated space served by an ASHP during defrosting

Indoor thermal environment is important as it affects the health and productivity of building occupants. A person's sense of thermal comfort is primarily the result of body' heat exchange with environment, which is influenced by two personal and four environmental parameters: metabolic rate, clothing insulation, and air temperature, mean radiant temperature (MRT), air velocity and humidity [ASHRAE 2010].

Two indexes proposed by Fanger [1970, 1982] have been extensively used and accepted in assessing indoor thermal comfort [Yang and Su 1997, Kumar and Mahdavi 2001, Chowdhury et al. 2008, Kuchen and Fisch 2009, Hwang and Shu 2011]. The first one is Predicted Mean Vote (PMV) [Fanger 1970] that expresses the quality of a thermal environment as a mean value of votes of a large group of people

according to the thermal sensation scale approved in the ANSI/ASHRAE Standard 55 [2010]. The other is the Predicted Percentage Dissatisfied (PPD) [Fanger 1982] which expresses the thermal comfort level as a percentage of thermally dissatisfied people, and is directly determinable by PMV. Standards for maintaining comfortable indoor thermal environments have been developed by ASHRAE and International Organization for Standardization (ISO). ASHRAE [2010] has defined the recommended PPD and PMV ranges for typical applications. The acceptable thermal environment for general comfort is PPD < 10% or - 0.5 < PMV < 0.5, which may be applied to a space where occupants have activity levels with metabolic rates between 1.0 and 1.3 met, and where clothing is worn providing between 0.5 and 1.0 clo of thermal insulation.

Fig. 2.1 shows the summer and winter comfort zones based on 90% acceptance of thermal conditions or 10% PPD, which may be applied to a space where clothing is worn providing between 0.5 clo and 1.0 clo of thermal insulation. As seen, the ASHRAE winter comfort zone was confined to an area on a psychrometric chart between 19.5 $^{\circ}$C and 26.5 $^{\circ}$C dry-bulb operative temperature.
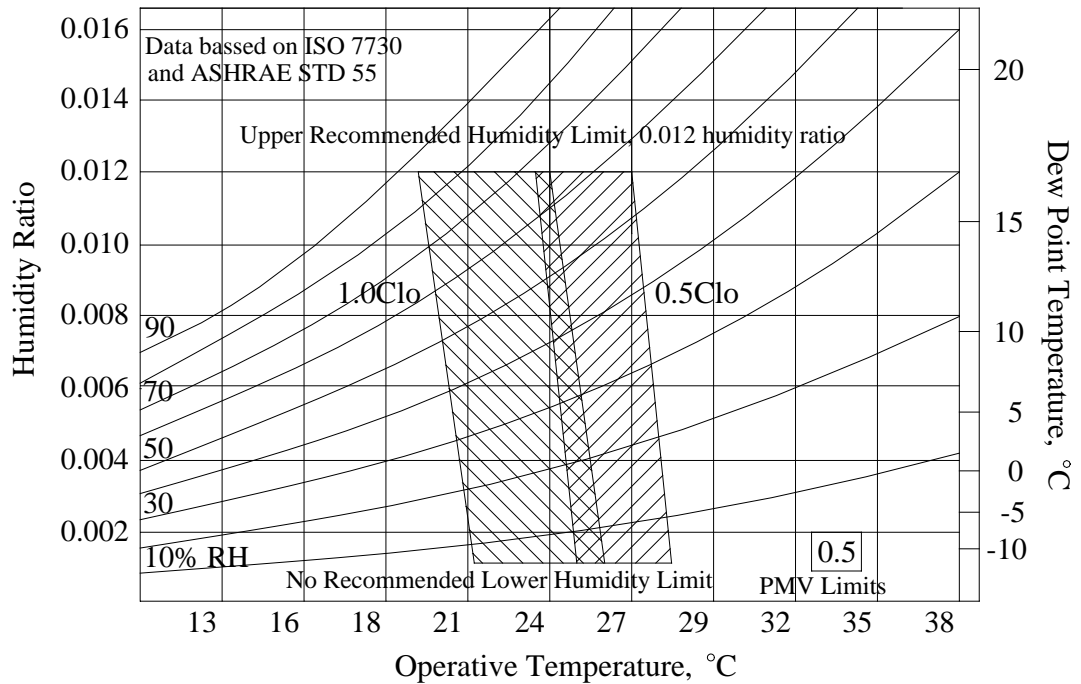
Fig. 2.1 ASHRAE summer and winter comfort zones (ASHRAE 2009)

[Acceptable ranges of operative temperature and humidity with air speed ≤ 0.2 m/s for

people wearing 1.0 and 0.5 clo clothing during primarily sedentary activity(≤ 1.1 met)]

When an ASHP unit is undergoing a reverse cycle defrosting operation, its outdoor

coil acts as a condenser and its indoor coil as an evaporator. Hence there is no space

heating provided during defrosting, thus degrading indoor thermal comfort while

consuming electrical energy for melting frost. As mentioned earlier, when an ASHP

unit starts its reverse cycle defrosting, its indoor air fan and outdoor air fan are all

switched off. The reason to turn off indoor air fan is to avoid blowing cold air out

from the indoor coil which works as an evaporator during defrosting, so that

occupants will not feel cold draft. Thus, a small airside convective heat coefficient

resulted from de-energized indoor air fan during defrosting makes a defrosting

33

duration longer. Furthermore, because an indoor coil is at a very low temperature immediately after the completion of defrosting, it would take a longer time to heat up the coil first before space heating can become available. This further lengthens the time period without heat supply. Therefore, it could be understood that during a reverse cycle defrosting process, indoor air temperature, relative humidity (RH), air velocity and mean radiant temperature (MRT) would be directly and/or indirectly affected, consequently deteriorating indoor thermal comfort. However, few research work where the effects of a reverse cycle defrosting operation of an ASHP on indoor thermal comfort for building occupancy in a heated space served by the ASHP were studied may be identified.

2.3.2.5 Effects of a throttle regulator on defrosting operation in an ASHP

For a heat pump/refrigeration system, a throttle regulator is a key component for refrigerant mass flow control to maintain the refrigerant in a superheated state before entering compressor. With a faster response to load variation, a wider range of flow rate regulation and a higher control precision, an electronic expansion valve (EEV) has a robust adaptability to all refrigerants in use under different operating conditions, and therefore can be used to replace other types of expansion devices or throttle regulators, such as a TEV or a capillary tube. In fact, the ranges of EEV applications have expanded gradually and successfully from small-scale to

large-scale systems, especially in inverter driven variable speed compressor systems and/or multi-evaporator systems [He et al. 1997, Aprea and Mastrullo 2002, Choi and Kim 2002, Li et al. 2004, Chen et al. 2005, Chen et al. 2008, Jiang et al. 2011].

From the open literature available, the reported studies on the effects of using various throttle regulators on defrosting performance in ASHPs are available but limited. O'Neal et al. [1991] carried out defrosting experiments aiming at shortening defrosting duration and reducing energy losses using short-tube orifice as a throttle regulator. The results suggested that increasing orifice diameter of the short-tube would lead to a shorter defrosting duration. For an air-to-water heat pump using a TEV, Ding et al. [2004] suggested using a solenoid valve to by-pass the TEV during defrosting to improve defrosting performance, with a smooth resumption of heating operation after the termination of defrosting. However, no reported studies on the effects of various control strategies for an EEV on reverse cycle defrosting performance for space heating ASHPs may be identified.

2.3.3 Control methods to start and end a defrosting operation

Since proper defrosting initiation and termination can lead to a higher energy efficiency and system reliability [Votsis et al. 1989, Hewitt and Huang 2006], relevant research work on selecting suitable control parameters for defrost initiation and

termination has therefore been carried out and reported.

2.3.3.1 Initiation of defrost

For the reasons of simplicity and low-cost, many of the earlier ASHPs employed a simple timer to control a defrost cycle. Usually, for every 60 to 90 minutes of frosting-time, a defrosting operation would be initiated. Performances of these earlier ASHPs could well suffer from some unnecessary defrosting operations, resulting in a degraded operational efficiency. On the other hand, demand defrost control, firstly proposed by Eckman [1987], has been applied to initiating defrost cycle in ASHP for decades. With this control method, an ASHP unit started defrosting only when an adequate frost buildup was detected. Demand defrost techniques included measuring air pressure differential across an outdoor coil; sensing the temperature difference between air and the outdoor coil surface; sensing fan power. Zakrzewski [1984] established a defrost cycle model for an air cooler to optimize defrost cycle by using an index called cooler efficiency. Modeling results showed that heat transfer coefficient of cooler surface, surface frosting intensity and defrost initiation time would all affect cooler efficiency. It was pointed out that the selection of an optimal defrost cycle required the simultaneous consideration of air cooler capacity, the type of frost accumulated on cooler surface and defrosting mechanism. Huang et al. [2008] conducted a numerical study concerning the effect of frost thickness on the heat transfer of a four rows plate finned-tube exchanger. The study results revealed that

the heat exchanger should go through defrosting when half of a single flow channel area was blocked by frost.

Recent defrosting methods developed included defrost initiation by measuring the ice thickness through using holographic interferometry technique [Hao et al. 2002], measuring the frost surface temperature by infrared thermometer [Iragorry and Tao 2005], sensing refrigerant flow instability [Lawrence and Evans 2008], using photo-coupler [Byun et al. 2006, Xiao et al. 2010] or fiber optic sensors [Paone and Rossi 1991] as a frost sensing device, applying neural networks to modeling the amount of frost on coil surface [Datta and Tassou 1997, 2002].

None of the above recent methods has however gained acceptance in industrial application in general due to excessive capital cost and reliability problems associated with complex and unreliable sensing methods.

2.3.3.2 Termination of defrost

With respects to defrost termination, related research is much less seen. It should be noted that a complete defrosting process covers both melting frost and drying coil surface. Otherwise, once an ASHP unit is switched back to heating operation, retained melted frost on outdoor coil surface would become ice. This may change the

structure of a frost layer, increase the density and enhance thermal conductivity of the frost layer [Lee and Ro 2001].

In practical applications, a defrosting operation can be terminated based on surface temperature of an outdoor coil, pressure difference across an outdoor coil, or time. Terminating a defrosting operation based on the surface temperature of an outdoor coil is currently the most popular method. A temperature sensor is usually placed on the lowest liquid-line circuit of an outdoor coil. A defrosting operation will be terminated once a preset temperature is reached. However, different temperature settings have been used and reported, such as 12 ^{o}C [Ding et al. 2004], 22 ^{o}C [Huang et al.2004], 24 ^{o}C [Huang et al. 2007], 26.7 ^{o}C [Payne and O'Neal 1995].

2.4 Frosting mitigation measures and performance improvement for reverse cycle defrosting for ASHPs

As discussed in earlier sections, both frosting and defrosting for an ASHP are disadvantageous to energy efficiency and operating performance. Therefore, for a higher energy efficiency and a better indoor thermal environment control using an ASHP, various methods of both preventing frosting and improving reverse cycle defrosting performance have been investigated.

2.4.1 Measures for preventing frosting for ASHPs

A number of different methods to prevent or delay frosting for ASHPs have been investigated so as to alleviate the negative impact of frosting on their operating performances. These methods focused on the following three respective aspects:

- Environmental variables

Kondepudi et al. [1995] compared frosting performance of an ASHP, with and without solid desiccant placed in air stream, and found that the use of desiccant significantly reduced frosting formation rate on outdoor coil surfaces. Wang and Liu [2005] also proposed a method using solid desiccant to dehumidify the air before it entered an outdoor coil. It was found that air humidity was reduced and air temperature increased, so that less frost was formed within a given frosting duration. Kwak and Bai [2010] added an electric heater at the entrance of an outdoor unit of a window-type ASHP to increase both the heating capacity and COP of the ASHP during frosting operating.

- ASHPs' structure

Mei et al. [2002] reported that the heating capacity of an ASHP can be increased, and the frost accumulation on its outdoor coil retarded by heating up the liquid refrigerant in the accumulator. Byun et al. [2008] presented a method to delay frost formation in

an ASHP unit by injecting a portion of high temperature refrigerant from compressor discharge into evaporator inlet. The results showed that COP and heating capacity were improved at an average of 8.5% and 5.7%, respectively. Li et al. [2011] developed a novel frost-free ASHP unit by integrating a multi-stage regeneration solution endothermic subsystem.

- Structure and surface treatment for an outdoor coil

The use of an outdoor coil having a wider fin spacing was recommended to slow down frost growth thus reducing the number of defrost cycles by Young [1980] and Watters et al. [2002]. On the other hand, there were reported studies on the influence of surface treatment of outdoor coil on frosting and defrosting performance. Kuwahara et al. [1986] applied a surface-active agent to the fin surface of an outdoor coil to reduce water retention as the contact angle between water and coil surface became small. Wu and Webb [2001] and Jhee et al. [2002] found that a heat exchanger with a hydrophobic surface treatment was more effective during defrosting in terms of the efficiency and duration, than that with a hydrophilic surface. Liu et al. [2006] reported that the use of surface hydrophilic polymer paint could retard frost formation up to 3 hours and reduce frost thickness by at least 40%. In addition, the frost layer formed on the coated surface was loose and could be easily removed. Wang et al. [2012] investigated the possibility and the effect of frost release from a finned-tube evaporator covered with hydrophilic coatings by using ultrasonic

vibrations during the whole frosting process. The experimental results showed that the basic ice layer on the fins could not be removed with ultrasonic vibrations, but frost crystals and frost branches on the ice layer could be fractured and removed effectively.

Although various methods including those mentioned earlier have been studied for the purpose of preventing or delaying frosting on outdoor coil in ASHPs, not many actual applications were seen partly due to their costs of implementation were too high. Furthermore, these methods were not capable of eliminating frosting, but only reducing the extent of frosting.

2.4.2 Performance improvements for reverse cycle defrosting of ASHPs

As discussed previously, defrosting an ASHP consumes energy and causes undesirable fluctuations of indoor air temperature and other operational problems, such as low-pressure cut-off or wet compression. Therefore, extensive research work has been carried out to improve the performance for reverse cycle defrosting of ASHPs. Young [1980] suggested that high refrigerant mass flow could be maintained by a properly sized separate defrost expansion bypass device for shorter defrosting duration. It was further found that an outdoor unit having a 45° slanted coil could drain off 50% more melted frost than that having a horizontal coil while still permitting a snow sheltered

design and an upward directed exhaust. Fans pre-start with reverse cycle defrosting on both air to air and air to water heat pumps were found to be effective in protecting the unit from being turned off owing to discharge pressure protection [Anand et al.1989, Huang et al. 2004]. Nutter et al. [1996] studied the effects of an accumulator in suction line on frosting/defrosting performance of an ASHP unit utilizing an orifice expansion device in heating (frosting) mode and TEV in cooling (defrosting) mode. The results showed that the removal of the accumulator produced a 10% reduction in defrosting duration time and a 25% reduction in the integrated cyclic COP. Wang et al. [2008] developed a new heat pump defrosting method using a refrigerant charge compensator instead of an accumulator. The test results showed an increase in refrigerant flow rate and larger suction and discharge pressures of compressor during defrosting. Liang et al. [2010] proposed a sensible heat defrosting method with self-organizing fuzzy control system. The results of comparative tests showed that the sensible heat defrosting method could avoid adverse shock and 'oil rush', which were commonly seen in conventional reverse cycle defrosting operations. Choi et al. [2011] reported a dual hot gas by-pass defrosting method for AAHPs using an additional hot gas by-pass line connecting the compressor discharge and the accumulator inlet. This defrosting method would help reduce the defrosting time by 36%, as compared to the conventional hot gas by-pass defrosting method.

However, the fundamental problem for the reverse cycle defrosting method was that there was insufficient heat available for ASHPs during defrosting. None of the above

mentioned methods can help solve this fundamental problem, and the other associated operational problems. These would consequently lead to a poorer cyclic operating performance, reduced indoor thermal comfort for occupants and a poorer system reliability for ASHP.

2.5 Applying phase change materials (PCMs) based thermal energy storage (TES) technology to buildings

Thermal energy storage (TES) technology has played an important role in energy management, and has been used extensively in building heating, ventilation, and air conditioning (HVAC) systems. When compared to sensible heat energy storage, latent heat energy storage requires a smaller amount of mass of storage medium for a given amount of energy to be stored. A further advantage of latent heat storage is that heat storage and delivery normally occur over a fairly narrow temperature range (the transition zone) which corresponds to the phase transition temperature of a phase change material (PCM). The operating temperature span of latent heat storage systems can, therefore, be quite narrow [Paris et al. 1993]. Based on these advantages, the technology of latent heat thermal energy storage has been developed rapidly over recent decades.

In general, PCMs can be classified into organic type such as paraffin, and inorganic

type such as hydrated salts and binary mixture. Inorganic PCMs have been widely used currently because of their high thermal conductivity and excellent chemical stability. The selection criteria of PCMs are listed as follows [Sharma and Sagara 2005, Pasupathy et al. 2008]:

Thermodynamic properties:

- Melting temperature in the desired operating temperature range;
- High latent heat of fusion per unit volume so that the required volume of container to store a given amount of energy is smaller;
- High specific heat to provide additional significant sensible heat storage;
- High thermal conductivity in both solid and liquid phases to assist energy charging and discharging;
- Small volume changes on phase transformation and small vapor pressure at operating temperatures to reduce the containment problem;
- Congruent melting of the PCM for a constant storage capacity of the material with each freezing/melting cycle.

Kinetic properties:

- High nucleation rate to avoid super cooling of the liquid phase ;
- High rate of crystal growth, so that it can meet demands of heat recovery from a

storage system.

Chemical properties:

- Chemical stability;

- Complete reversible freeze/melt cycle;

- No degradation after a large number of freeze/melt cycles;

- Non-corrosiveness, non-toxic, non-flammable and non-explosive materials.

Economic properties:

- Low cost;

- Large-scale availability.

2.5.1 TES for HVAC applications

The compactness of a PCM storage system allows a greater flexibility in choosing a location for a storage system. TES for HVAC applications can involve storage at various temperatures associated with heating and cooling processes [ASHRAE 2007]. For example, high temperature storage is typically associated with the use of solar energy collectors [Rabin et al. 1995, Esen and Ayhan 1996, Bajnoczy et al. 1999],

waste heat utilization [Gu et al. 2004], heat pump applications, and low temperature storage with the use of ice storage system [Masoero 1984, Matsuki et al. 1999, Ismail and Jesus 2001] and free cooling [Vakilaltojjar and Saman 2001, Arkar et al. 2007], etc.

TES for heat pump applications mainly focused on solar-assistant heat pump systems and on waste heat recovery. Rabin et al. [1995] studied a solar collector with storage for water heating using salt hydrate as a PCM. The results of parametric studies on the effects of both the transition temperature and the thickness layer of the salt-hydrate PCM on the thermal performance of charging processes were presented. Esen and Ayhan [1996] developed a model for a solar assisted cylindrical energy storage tank. Results showed that the PCM, cylinder radius of storage tank, the mass flow rate and inlet temperature of the high temperature heat transfer fluid (HTF) should be chosen carefully to optimize the performance of the storage tank. Bajnoczy et al. [1999] studied a two-grade heat storage system (60-30 $^{\mathrm{o}}$C and 30–20 $^{\mathrm{o}}$C) using $CaCl_2 \cdot 6H_2O$ and $CaCl_2 \cdot 4H_2O$ for a domestic water-heating system with solar energy storage. Gu et al. [2004] used latent heat thermal energy storage systems to recover the rejected (sensible and latent) heat from air conditioning. The results showed that the use of latent heat thermal energy storage systems would help reduce both the consumption of primary energy for domestic hot water heating and the heat dissipation to the surroundings. Long and Zhu [2008] designed an ASHP water heater with PCM for thermal storage to take the advantage of low-cost

off-peak electrical energy. Qi et al. [2008] proposed a solar heat pump heating system with seasonal latent heat thermal storage, and investigated its operating performances using a specifically developed model. However, adopting latent heat storage in ASHPs and using the stored heat as the source for defrosting have not been found in the open literature.

2.5.2 Heat transfer enhancement for TES systems

Most PCMs have an unacceptably low thermal conductivity, leading to slow charging and discharging rates. Hence heat transfer enhancement techniques are required for most latent heat thermal energy storage applications. There are several methods to enhance the heat transfer in a latent heat thermal storage system, including optimized design of a suitable heat exchanger. Herrick [1982] and Santamouris and Leafs [1988] designed a rolling cylinder heat exchanger consisted of a collection of smaller sub-units of cylinder shape, in which actual energy storage took place. Farid and Kanzawa [1989] studied the performance of a heat storage unit consisted of cylindrical capsules filled with PCM, with air flowing across them for heat exchange. Watanabe et al. [1993] described a heat storage unit consisted of an encapsulated PCM in horizontal cylindrical tubes. On the other hand, the use of finned-tubes with different configurations was proposed [Velraj et al. 1997 and 1999, Ismail et al. 2001]. A storage unit composed of spherical capsules filled with PCM

placed inside a cylindrical tank was investigated both numerically and experimentally by Ismail and Henriquez [2002]. Zukowski [2007] analyzed a TES unit consisted of a Plexiglas casing, light steel nets and PCM enclosed in polyethylene film bags. Solidification and melting characteristics of PCM encapsulated inside cylindrical enclosures were experimentally and analytically studied by Kalaiselvam et al. [2008].

In addition, other heat transfer enhancement techniques in PCMs have been also reported, including for example, using PCMs dispersed with high conductivity particles [Siegel 1977], embedding PCMs in a metal matrix structure [Hoogendoorn and Bart 1992, Tong et al. 1996], adding carbon fiber brushes [Fukai et al. 2000 and 2002, Hamada and Fukai 2005], employing bubble agitation [Velraj et al. 1997], applying thin aluminum plates filled with PCMs [Bauer and Wirtz 2000] or embedding aluminum powder [Mettawee and Assassa 2007], inserting copper plates in spherical capsules for noctadecane PCMs [Koizumi 2004], using metal screens/spheres placed inside the PCMs [Ettouney et al. 2004] and applying microencapsulated PCMs [Brown et al. 1998, Hawlader et al. 2003, Griffiths and Eames 2007], etc.

2.6 Conclusions

The development of air conditioning and heat pump technology is a natural consequence to both pursuing high quality living and working environments, and at the same time, addressing the issue of sustainability. ASHPs have been widely used for space cooling in summer and space heating in winter for many years, due to their distinguished advantages of energy saving and environmental protection. However, when an ASHP unit operates in space heating mode, frost can be accumulated on the surface of its outdoor coil when its temperature is below 0 ℃ and lower than the dew point of ambient air. Frosting deteriorates the operation and energy efficiency, and reduces the output heating capacity of the ASHP unit. Therefore periodic defrosting becomes necessary. Currently, the most widely used standard defrosting method for ASHPs is reverse cycle defrost. Defrosting helps an ASHP return to its rated performance, although the process itself consumes energy, causing undesirable fluctuations of indoor air temperature and other operational problems.

Extensive related studies on the performance of ASHPs under frosting or defrosting condition have been undertaken. From the open literature available, the research work related to reverse cycle defrosting performance of ASHPs is relatively less seen comparing with that related to frosting. This is because that reverse cycle defrosting is a complex process involving spatial and time variations as well as many other indeterminate factors resulted from transient cycling which may last for only a few

minutes. Both experimental and theoretical approaches were adopted in these studies, to investigate the operating performances of ASHPs under both frosting and defrosting conditions. Various measures to address the problems associated with the frosting and defrosting operations of ASHPs have been considered. However, there are still a number of issues where further extensive research work is required, as follows:

- As presented in Section 2.4, for reverse cycle defrosting operations for ASHPs, the energy to melt frost comes mainly from that stored in indoor coil metal and the input work to compressor, which are not sufficient for quick defrosting. Insufficient heat available during defrosting is currently a fundamental problem as far as reverse cycle defrost is concerned, with which a number of operational problems during defrosting for ASHPs are associated. However, no previous studies on solving this fundamental problem may be identified.

- Secondly, during a reverse cycle defrosting process, the indoor coil of an ASHP unit actually acts as an evaporator. Therefore, no space heating is provided and hence indoor air temperature in a heated space can drop, during defrosting. Also, since indoor coil metal was at a low temperature, a longer period of time is needed before space heating can become available immediately after the completion of defrosting. This further lengthens the time period without effective heating. Consequently, occupants' thermal

comfort may be adversely affected, as discussed in Section 2.3.2.4. However, relevant research work on assessing indoor thermal comfort of building occupants during a reverse cycle defrosting process for ASHPs has been seldom seen in open literature.

- Furthermore, as presented in Section 2.3.2.1, although previous experimental and modeling studies on understanding the operating performance during a reverse cycle defrosting of a multi-circuit outdoor coil in ASHPs have been conducted and reported, the research work on accounting the effect of downwards flowing of the melted frost due to gravity along the surface of a multi-circuit outdoor coil on defrosting performance cannot be identified. It was further noted that none of the previous defrosting models considered the effects of the melted frost flowing down on defrosting performance, as reported in Section 2.3.2.2, by assuming either a stable water layer or no water retention on coil surfaces. However, as reported in the previous experimental studies, quite an amount of melted frost flowed downwards due to gravity along the surfaces of multi-circuit outdoor coils. This amount of water flowing downwards on the entire outdoor coil surface would disturb defrosting as additional thermal resistance was introduced.

- Finally, with respect to the investigation on the effects of using different types of throttle regulators, or expansion devices, on the performance of reverse cycle defrosting, it is shown in Section 2.3.2.5 that no reported

51

studies on the effects of various control strategies for an EEV on the reverse

cycle defrosting performance for space heating ASHPs may be identified.

The literature review presented in this Chapter has identified a number of important

areas where further in-depth research work is required. These are the expected

targets of the investigation reported in this thesis.

Chapter 3

Proposition

3.1 Background

It is evident from the literature review presented in Chapter 2 that ASHPs have been widely used worldwide as an energy efficient and environmental friendly means for building environmental control. However, when an ASHP unit operates in heating mode, frost can be accumulated on the surface of its outdoor coil. Frosting deteriorates its operation and energy efficiency, and therefore periodic defrosting becomes necessary. Currently, the most widely used standard defrosting method for ASHPs is reverse cycle defrost. Defrosting helps an ASHP return to its rated performance, although the process itself consumes energy, causing undesirable fluctuations of indoor air temperature and other operational problems.

The previous limited related studies available in the open literature concentrated on studying the operating performances of ASHPs under both frosting and defrosting conditions, and various possible measures to address the problems associated with the frosting and defrosting operations of ASHPs. For ASHPs, during reverse cycle defrosting, the energy to melt frost mainly comes from that stored in indoor coil metal and the input work to compressor, which are not sufficient for quick defrosting. Insufficient heat available during reverse cycle defrosting is currently a fundamental

problem for ASHPs. However, no previous studies on solving this fundamental problem may be identified. With the wide-spread applications of TES in HVAC systems, it is possible to develop a novel TES-based reverse cycle defrosting method so that adequate heat could be made available for reverse cycle defrosting.

Furthermore, the research work related to accounting the effects of downwards flowing of the melted frost due to gravity along the surface of a multi-circuit outdoor coil in an ASHP unit on defrosting performance has been rarely seen. In defrosting mathematical models currently available, either a stable water layer or no water retention on coil surfaces was assumed. This strongly suggests a need to investigate the effects of downwards flowing of the melted frost along the surface of a multi-circuit outdoor coil on defrosting performance, using both experimental and modeling approaches. In addition, although EEVs have been widely used in ASHPs, no reported studies on the effects of various control strategies for an EEV on the reverse cycle defrosting performance for space heating ASHPs may be identified.

3.2 Project title

The thesis focuses on the following major issues related to reverse cycle defrosting for ASHP units: (1) developing a novel TES-based reverse cycle defrosting method

for ASHPs to provide adequate heat during defrosting; (2) assessing indoor thermal comfort level for occupants when using the novel TES-based reverse cycle defrosting method; (3) studying the effects of downwards flowing of melted frost due to gravity over a multi-circuit outdoor coil surface during reverse cycle defrosting on defrosting performance; and (4) investigating the effects of an EEV under different control strategies on defrosting performance. The research project reported in this thesis is therefore entitled "A novel thermal storage based reverse cycle defrosting method and the operating performance evaluations for an air source heat pump".

3.3 Aims and objectives

The objectives of the research work reported in this thesis are as follows:

1) To develop a novel TES-based reverse cycle defrosting method for an experimental ASHP unit so as to make adequate heat available for melting frost during defrosting, and thus minimize or even eliminate a number of the operational problems associated with conventional reverse cycle defrost. The operational performances of the experimental ASHP unit using the novel

TES-based reverse cycle defrosting method developed will be experimentally examined;

2) To assess thermal comfort level when using the novel TES-based reverse cycle defrosting method developed for the experimental ASHP unit;

3) To experimentally and numerically study the effects of downwards flowing of melted frost along a multi-circuit outdoor coil surface on defrosting performance using the experimental ASHP unit. A semi-empirical mathematical model will be developed; and,

4) To investigate the effects of an EEV under different control strategies on reverse cycle defrosting performance of the experimental ASHP unit.

3.4 Research methodologies

Both experimental and numerical approaches will be adopted in the project. A specially developed experimental ASHP setup will be constructed, consisting of the experimental ASHP unit having a four-circuit outdoor coil, an environmental chamber including one simulated heated indoor space and one simulated frosting outdoor space. The experimental ASHP unit will be built by incorporating a PCM based heat exchanger (PCM-HE) into a commercially available standard ASHP unit. The experimental ASHP unit may be operated at following three different modes: (1)

standard heating and defrosting, (2) parallel TES-based heating and reverse cycle defrosting, (3) serial TES-based heating and reverse cycle defrosting. The three modes will be detailed in Chapter 5.

Experimental investigations on the operational performances and indoor thermal comfort under both standard reverse cycle defrosting method and the novel TES-based reverse cycle defrosting method will be carried out using the experimental setup. The experimental results and the thermal comfort indexes obtained/evaluated under standard heating and the defrosting conditions would provide a base for comparison. For comparison purpose, the same frosting outdoor condition, the amount of frost formation on outdoor coil surface and indoor thermal conditions using both standard reverse cycle defrosting and the novel TES-based reverse cycle defrosting method will be maintained.

Experimental studies on the effects of allowing melted frost to freely flow downwards over the four-circuit outdoor coil surface of the experimental ASHP unit will also be undertaken. The development of the semi-empirical mathematical model to quantitatively analyze the effects of downwards flowing of melted frost along the entire outdoor coil surface on defrosting performance will be primarily based on the fundamentals of mass and energy conservation, and partially supported by the experimental data obtained.

The effects of the EEV under different control strategies on defrosting performance will be experimentally studied using the experimental ASHP unit. Two control strategies for the EEV on defrosting performance will be considered: the EEV being fully open, and the EEV being regulated by the degree of superheat (DS) controller with a DS setting of 5 ℃.

The experimental ASHP setup will be built up in the HVAC Laboratory in the Department of Building Services Engineering, The Hong Kong Polytechnic University.

Chapter 4

The Experimental Setup

4.1 Introduction

The experimental setup was constructed in the HVAC Laboratory of Department of Building Services Engineering, The Hong Kong Polytechnic University. The primary purpose of having the experimental setup was to facilitate carrying out the research work related to novel TES-based reverse cycle defrosting method and operating performance evaluations for ASHP systems.

The ASHP experimental setup consisted of an experimental ASHP unit, an environmental chamber including one simulated heated indoor space and one simulated frosting outdoor space. A computerized data measuring, logging and control system was built into the experimental setup. A PCM based heat exchanger (PCM-HE), which was a key component to the successful development of the TES-based reverse cycle defrosting method, was incorporated into the experimental ASHP unit.

This Chapter firstly describes the experimental setup and its major components in detail. This is followed by reporting the computerized measuring devices and data acquisition system. Lastly, the control for the refrigerant degree of superheat at compressor suction is explained.

4.2 Detailed descriptions of the experimental setup and its major components

Fig. 4.1 shows the schematic diagram of the experimental setup. The experimental ASHP unit was modified from a commercially available standard ASHP unit and was installed inside the existing environmental chamber. The environmental chamber was divided into a heated indoor space and a frosting outdoor space, which simulated both the indoor and outdoor conditions (temperature and humidity) necessary for testing the performance of the experimental ASHP unit. The indoor coil of the experimental ASHP unit was installed inside the heated indoor space and the four-circuit outdoor coil of the experimental ASHP unit inside the frosting outdoor space. As seen from Fig. 4.1, inside the indoor space, there were the indoor coil, the PCM-HE and a receiver. And inside the outdoor space, there were the compressor, an accumulator, the outdoor coil, four way reverse valve and outdoor air flow ductwork.

4.2.1 The experimental ASHP unit

4.2.1.1 Heat pump unit

A nominal 6.5 kW heating capacity split-system residential ASHP unit was retrofitted. The major components in the ASHP unit included a variable-speed rotor compressor, an EEV, a four-circuit outdoor coil and an indoor coil. Its specifications are listed in
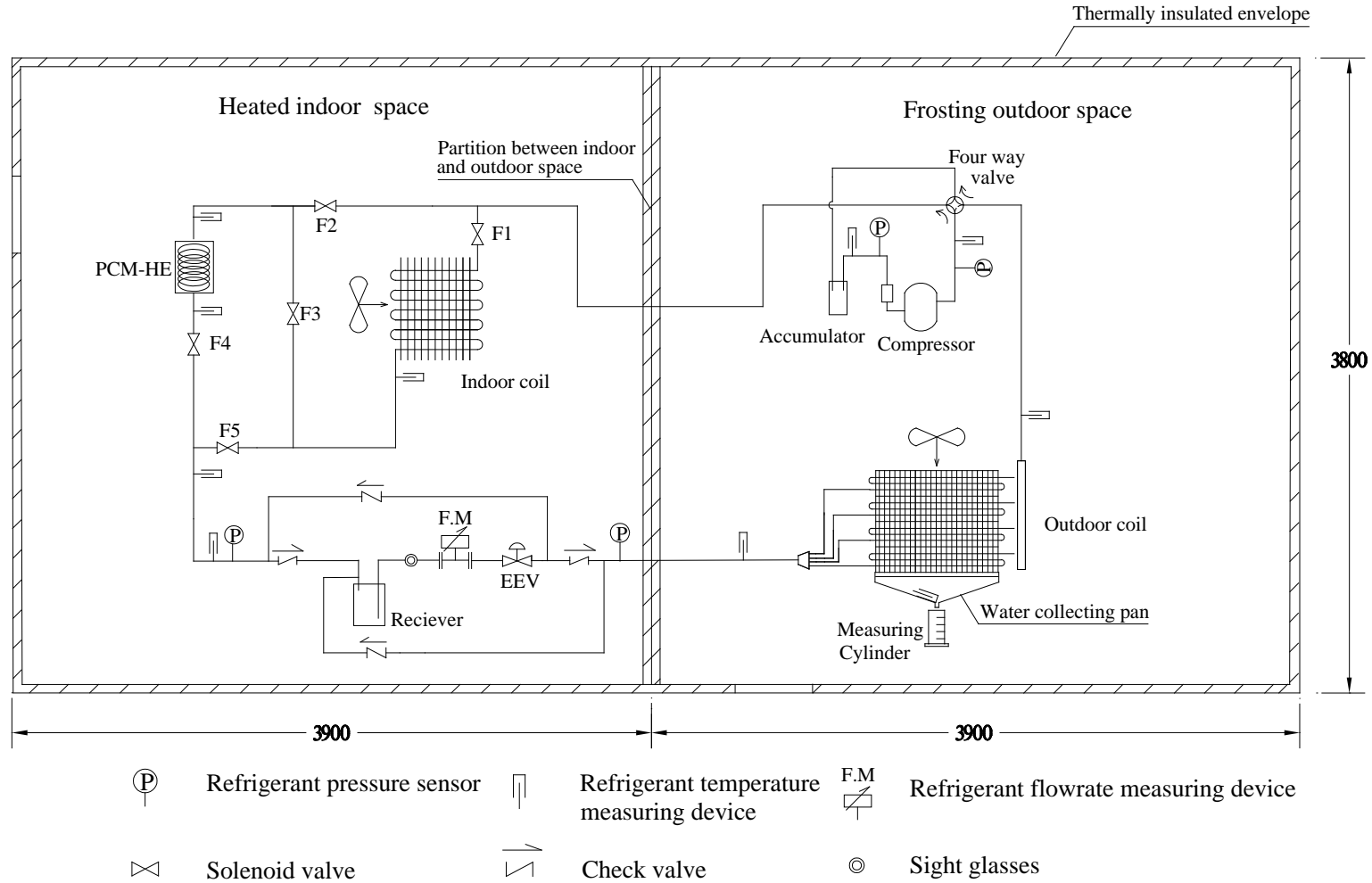
Fig. 4.1 The schematic diagram of the experimental setup

Table 4.1. The compressor was of swing type and equipped with a suction line accumulator to minimize liquid flow to the compressor during start up and transient operation periods. The refrigerant used was R22. Other necessary accessories and control devices, such as a refrigerant receiver, a sight glass, a filter and safety devices, were provided to ensure the normal and safe operation of the ASHP unit.

The outdoor coil, where frosting and defrosting took place, had four parallel single-row refrigerant circuits, as shown in Fig. 4.2. The airside surface areas corresponding to the four circuits were equal. The indoor coil had four parallel two-row refrigerant circuits. The fins were made of aluminum and tubes made of copper for both outdoor coil and indoor coil. A water collecting pan was placed directly under the outdoor coil.

The EEV used in the experimental ASHP unit was driven by a four-phase pulse motor, with a total of 500-steps of valve opening positioning. It was used to maintain a desired degree of refrigerant superheat at the evaporator exit. The port diameter of the EEV was 1.6 mm. The opening of the EEV was regulated by a proportional-integral-derivative (PID) degree of superheat (DS) controller to maintain a fixed DS during actual operation.

Table 4.1 Specifications of the experimental ASHP unit

Parameters	Values/ details	
Compressor		
Compressor type	Swing	
Rated heating capacity (kW)	6.5	
Rated input power (kW)	1.84	
Refrigerant	R22	
EEV		
Port diameter(mm)	1.6	
Coil	*Indoor*	*Outdoor*
Tube length (mm)	875	920
Tube external diameter (mm)	7.9	7.9
Tube spacing (mm)	12	12
Fin thickness (mm)	0.16	0.16
Fin pitch (mm)	1.2	1.1
Number of tube rows	2	1
Number of circuits	4	4
Air flow rate (m^3/h)	1050	2560
Tube material	Copper	Copper
Fin material	Aluminum	Aluminum
Fin type	Louver	Plate
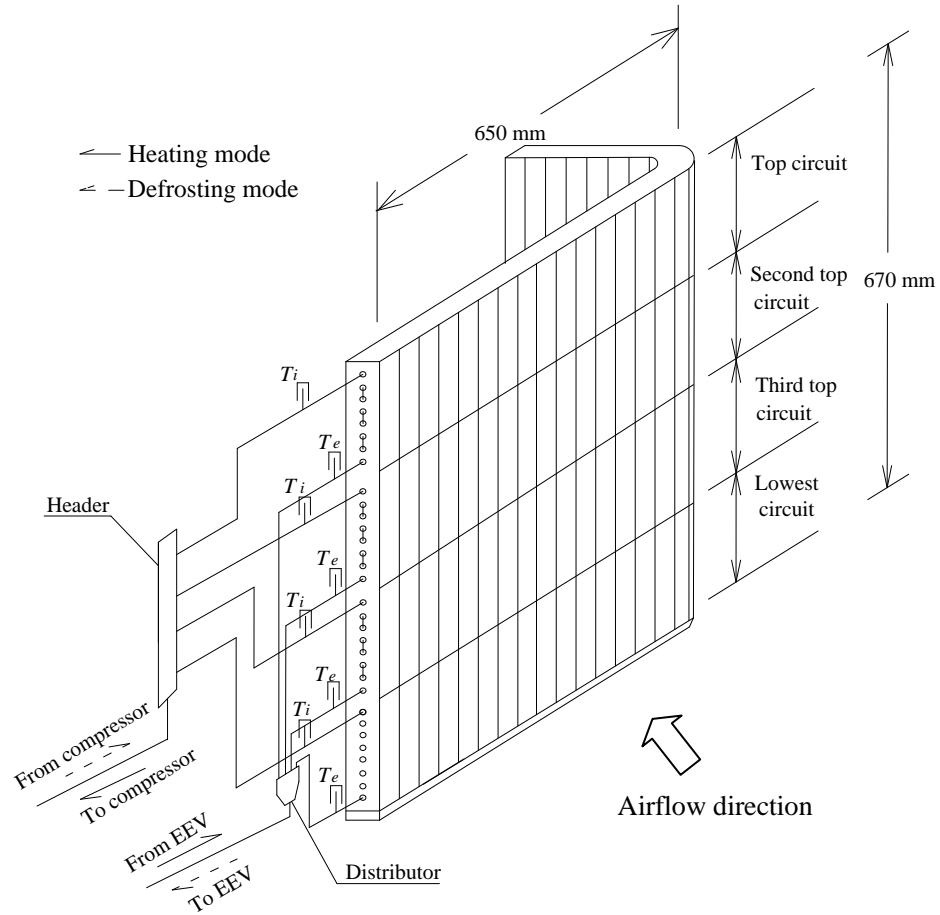
Fig. 4.2 Details of the single-row four parallel refrigerant circuit outdoor coil and

locations of temperatures sensors

4.2.1.2 PCM based heat exchanger

The PCM-HE was designed as a thermally insulated shell-and-tube storage unit with

the PCM on the shell side and the refrigerant being circulated inside the tubes, to

maximize the heat transfer between refrigerant and PCM. Fig. 4.3 shows its detailed

structure. As seen, there were an outer shell and an inner shell, both made of acrylic.

The diameter of outer shell was 250 mm and that of the inner shell at 160 mm, both

at a height of 225 mm. Between the two shells, spiral refrigerant tubes, were placed, with the clearances between tubes and shells filled up with PCM.

Part A (Enlarged)
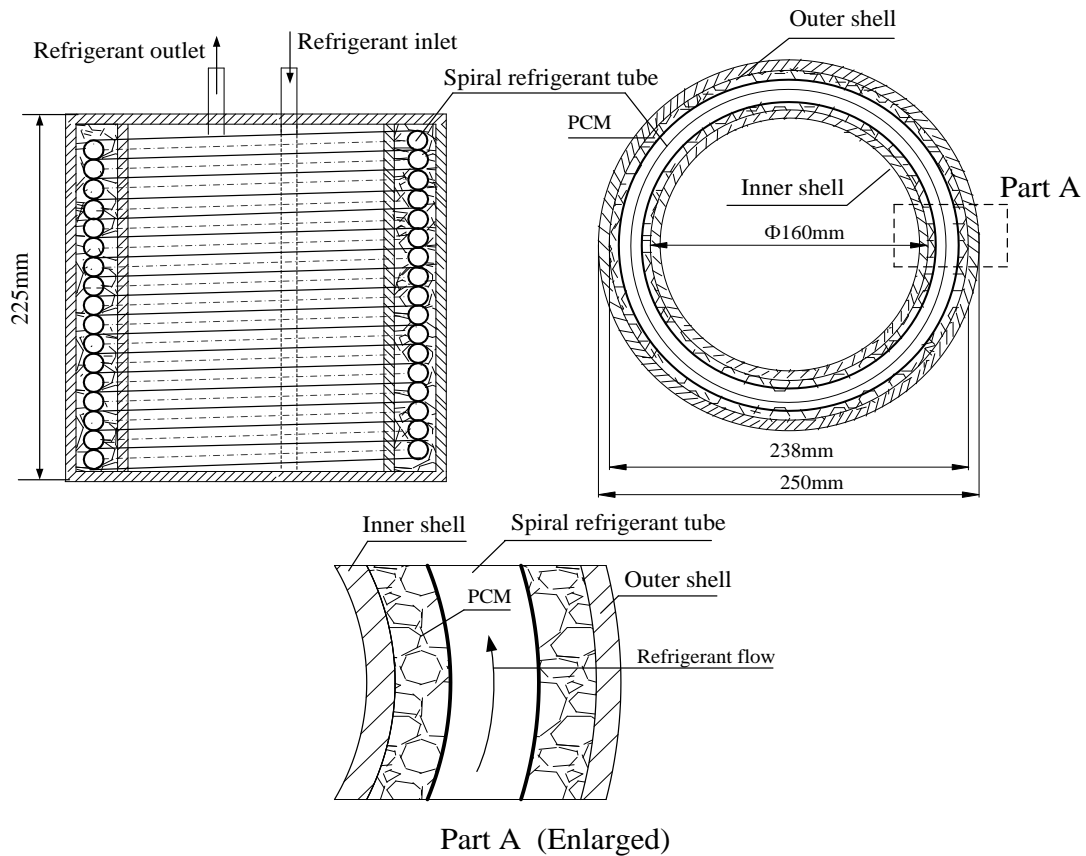
Fig. 4.3 Detailed structure of the PCM based heat exchanger used in the experimental

ASHP unit

With the control of the five solenoid valves (F1 to F5 in Fig. 4.1), different operating modes, such as those mentioned in Section 3.4, could be realized. When the PCM was storing heat, high temperature and high pressure refrigerant flowed through the spiral tube from bottom to top, heating the PCM. While the PCM was discharging heat, the flow direction of low temperature and low pressure refrigerant was reversed.

In selecting the appropriate PCM to be used in the PCM-HE, its melting point was carefully considered. It should be between the operating condensing temperature and the operating evaporating temperature of an ASHP unit, but not close to both temperatures to allow an adequate temperature difference for heat exchange. Its ideal melting point was approximately 10 $^{\circ}$C lower than condensing temperature, so as to facilitate efficient heat releasing from a PCM during defrosting. In addition, if the melting point of a PCM was close to condensing temperature, a slower heat storage process during heating/heat storing was resulted in. Furthermore, a higher suction temperature during defrosting would also be resulted in, leading to compressor overheating.

Therefore, according to the operating temperatures of the experimental ASHP unit, the melting point of the PCM to be used would ideally be between 20 $^{\circ}$C and 30 $^{\circ}$C. Table A1 in Appendix A shows the properties of various PCMs whose melting point is between 20 $^{\circ}$C and 30 $^{\circ}$C [Zalba et al. 2003]. In general, PCMs can be classified into organic type, inorganic type and binary mixture, among which inorganic PCM has been widely used currently because of its high thermal conductivity and excellent chemical stability.

Table 4.2 The physical and thermal properties of $CaCl_2 \cdot 6H_2O$

Properties	Value	Unit
Melting point	29	^{o}C
Heat of fusion	190.8	kJ/kg
Specific heat		
(I) Solid	1.46	kJ/kg ^{o}C
(II) Liquid	2.13	kJ/kg ^{o}C
Thermal conductivity		
(I) Solid at 23 ^{o}C	1.088	W/m ^{o}C
(II) Liquid at 38.7 ^{o}C	0.540	W/m ^{o}C
Density		
(I) Solid at 23 ^{o}C	1802	kg/m^3
(II) Liquid at 38.7 ^{o}C	1562	kg/m^3

In the current study, $CaCl_2 \cdot 6H_2O$, an inorganic PCM whose physical and thermal properties are shown in Table 4.2, was chosen because of its following excellent characteristics:

- high heat of fusion (190.8 kJ/kg)

- suitable melting point (29 ^{o}C)

- higher thermal conductivity and excellent chemical stability

- high density in both solid and liquid phases, suitable for small-sized PCM

based heat exchanger

- low price

- non-corrosive to plastic and copper, and non flammable and explosive

To obtain the highest possible defrosting performance, firstly, the storage capacity of the PCM should be determined based on the frequency of defrost cycle, outdoor air temperature and humidity and the capacity of an ASHP unit, etc. Otherwise, insufficient energy would be available at the later part of a defrosting cycle, slowing down an entire defrosting process. Secondly, the PCM-HE should be able to release the stored energy quickly to ensure that the energy stored could be used efficiently for defrosting. On the other hand, although a large PCM-HE may speed up a defrosting process, it could also lead to energy waste due to increased surface area. Therefore, it was very important to size the PCM-HE appropriately to facilitate the development of the novel TES-based reverse cycle defrosting method. Based on the evaluated amount of heat necessary for effective defrosting, 1.8 kg of $CaCl_2 \cdot 6H_2O$ was used in the PCM-HE, so that ~343 kJ of latent heat could be stored in the PCM-HE for defrosting.

4.2.2 Environmental chamber

The experimental ASHP unit was installed in an existing environmental chamber

having a simulated heated indoor space and a simulated frosting outdoor space. The

two spaces were separated by a thermally insulated partition. The sizes of both indoor

and outdoor spaces were each measured at 3.9 m (L) × 3.8 m (W) × 2.8 m (H). The

existing chamber in the experimental setup had a separate air conditioning (A/C)

system and sensible and latent load generating units (LGUs), so that suitable testing

conditions in both indoor and outdoor spaces may be maintained, as illustrated in Fig.

4.4.
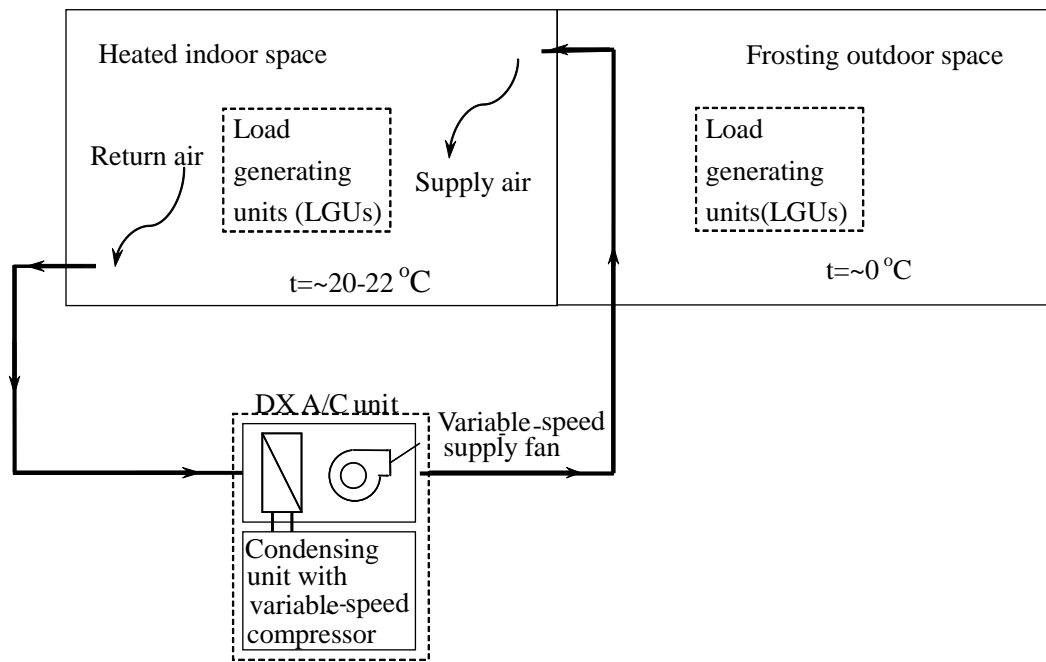
Fig. 4.4 The schematic diagram of the environmental chamber

The A/C unit mainly included a variable-speed rotor compressor, an EEV, an air

cooled tube-plate-finned condenser and a high-efficiency louver-fin-and-tube direct

expansion (DX) evaporator, a supply fan, etc. The nominal output cooling capacity

from the DX A/C system was 9.9 kW, but the actual output cooling capacity could

however be modulated from 15% to 110% of the nominal capacity. Both supply air fan and compressor were driven by variable-frequency drives (VFD). The working fluid of the plant was refrigerant R22. The sensible and latent heating capacities of the LGUs were 12 kW and 4.8 kW, respectively. The heat and moisture generation rate regulated by Solid State Relay (SSR) may be varied manually or automatically with a pre-set pattern through operator's programming. Test conditions in both the indoor space and the outdoor space were monitored with air temperature and humidity measuring sensors located in the rooms. During normal heating (or frosting) operation, the frosting environment in the outdoor space was maintained by running the experimental ASHP unit and LGUs together while the heated environment in the indoor space jointly by the experimental ASHP unit, the A/C system and LGUs.

4.3 Computerized instrumentation and data acquisition system (DAS)

The computerized instrumentation for the experimental setup is also shown in both Fig. 4.1 and Fig. 4.2. The experimental setup was fully instrumented for measuring all of its operating parameters, which may be classified into three types, temperature, pressure and flow rate. Since all measurements were computerized, all sensors and measuring devices are able to output direct current (DC) signal of 4-20 mA or 1-5 V, which were transferred to a DAS for logging and recording.

4.3.1 Sensors/measuring devices for temperatures, pressures and flow rates

Pre-calibrated K-type thermocouples were used for measuring the temperatures of tube/coil surfaces of the outdoor coil. Eight of them were for measuring the refrigerant tube surface temperatures at both the inlets and exits of the four refrigerant circuits of the outdoor unit. Furthermore, a thermocouple was placed at the outlet of the water collecting pan to measure the temperature of the melted frost. The temperature sensors for air were of platinum Resistance Temperature Device (RTD) type (PT100, Class A) with a pre-calibrated accuracy of ± 0.1 ºC. Five RTDs were fixed evenly at outlet of the indoor unit to measure dry bulb temperature of the supply air.

On the other hand, in the experimental ASHP unit, refrigerant pressures were measured using pressure transmitters with an accuracy of ± 0.3% of full scale reading and refrigerant mass flow rate by a variable area flow meter with a reported accuracy of ± 1.6% of full scale reading.

Fig. 4.5 shows the airside details of outdoor unit of the experimental ASHP unit installed in the frosting outdoor space of the experimental setup. An air sampling device with 28 sampling points was placed upstream of the outdoor unit, and then the sampled air was mixed and its temperature and humidity were measured by a temperature sensor (PT100, Class A) and a humidity transmitter (of ± 3.0% accuracy). On the other hand, air temperature and humidity downstream of the outdoor coil were measured by a hygrosensor (± 0.2 ºC and ± 1.0% RH accuracy,

respectively) located inside an air duct 900 mm downstream of the outdoor unit outlet. To ensure the best possible measuring accuracy, the humidity transmitter positioned upstream of the outdoor coil was calibrated by using the hydrosensor. Furthermore, the air flow rate passing through the outdoor coil was measured by using a flow hood (of ± 3% accuracy) with a 16-point velocity grid located downstream of a 600 × 600 mm air duct of 900 mm long.
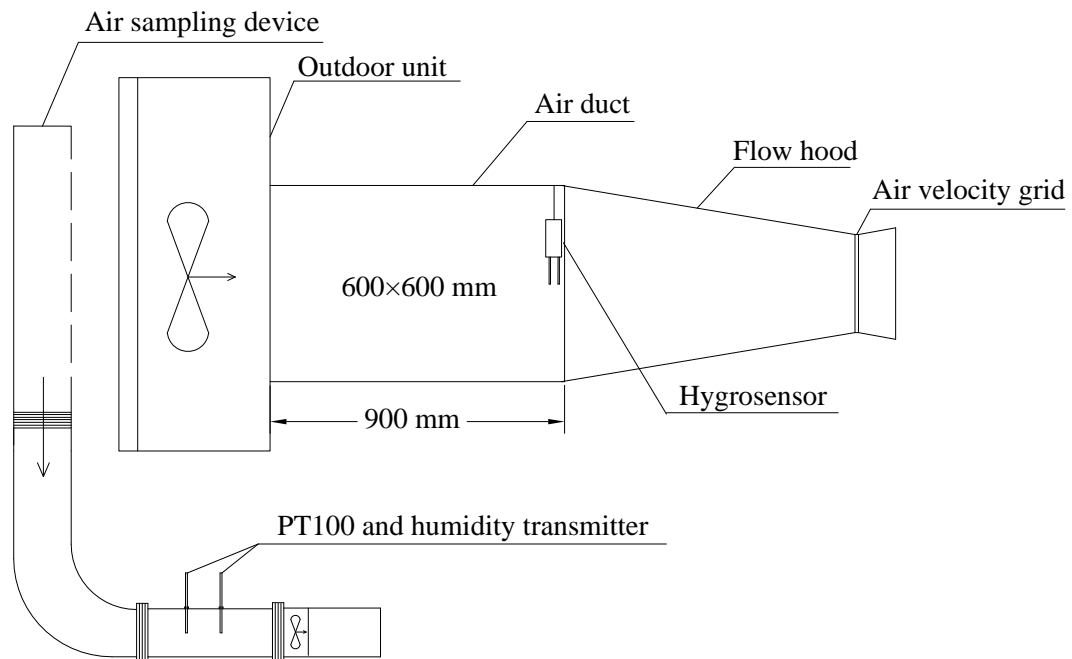
Fig. 4.5 The airside details of outdoor unit of the experimental ASHP unit installed in the frosting outdoor space of the experimental setup

The airflow rate of the indoor unit was obtained from averaging velocity at five evenly distributed points multiplied by area of air outlet. Air velocity was measured using air velocity transducer (of accuracy ± 1.0%) at the five points.

On the other hand, a measuring cylinder was located under the water collecting pan for measuring the amount of the melting water. The power consumption of the compressor was measured using a pulse-width-modulation (PWM) digital power meter with a reported uncertainty of ± 2% of reading.

4.3.2 The DAS and calculation

A data acquisition unit was used in this experimental setup. It provided up to 66 channels for measuring/monitoring various operating parameters of the setup. The DC signal from various measuring devices/sensors could be scaled into their real physical values of the measured parameters using a data logging & control supervisory program. The data sampling interval during experimentation was 5 s.

4.3.3 Evaluating the mass of accumulated frost on outdoor coil surface

With the availability of the above instrumentation on the airside of the outdoor coil, the air parameters up- and down-stream of the outdoor coil, such as air temperatures and moisture contents may be real time measured and the mass of frost accumulated during the period of Δt can be evaluated by Equation (4.1) [Guo et al. 2008]:

$$\Delta M_f = \frac{m_a \Delta t}{1 + w_i}(w_i - w_e)$$

(4.1)

where m_a is the mass flow rate of the air across the outdoor coil, w_i and w_e are the air moisture contents at the inlet and the exit of the outdoor coil, respectively, which can be obtained by:

$$w = \frac{622 \varphi p_{asw}}{(101.325 - \varphi p_{asw})}$$

(4.2)

where φ is the measured air relative humidity, and p_{asw} is the saturated water vapor pressure as a function of measured dry-bulb temperature, t_{adb}. p_{asw} can be estimated by the following equations:

when t_{adb} is between -100 and 0 ℃:

$$p_{asw} = \frac{e^{-5.67 \times 10^3 T_{adb}^{-1} + 6.39 - 9.68 \times 10^{-3} T_{adb} + 6.22 \times 10^{-7} T_{adb}^2 + 2.07 \times 10^{-9} T_{adb}^3 - 9.48 \times 10^{-13} T_{adb}^4 + 4.16 \times \ln(T_{adb})}}{1000}$$

(4.3a)

when t_{adb} is between 0 and 200 ℃:

$$p_{asw} = \frac{e^{-5.800 \times 10^3 T_{adb}^{-1} + 1.391 - 0.0486 T_{adb} + 0.418 \times 10^{-4} T_{adb}^2 - 0.145 \times 10^{-7} T_{adb}^3 + 6.546 \times \ln(T_{adb})}}{1000}$$

(4.3b)

where T_{adb} is the absolute air temperature, to be evaluated by:

$$T_{adb} = 273 + t_{adb} \tag{4.4}$$

In this study reported in this thesis, Δt was set at 5 s, same as the time interval used for data logging. Hence, the actual total amount of frost formed on the outdoor coil surface, M_f, could be real time evaluated by summing up ΔM_f, displayed and recorded using the data logging supervisory program.

4.4 The control of refrigerant superheating

To facilitate carrying out the investigation of effects of an EEV under different control strategies on reverse cycle defrosting performance, the original control loop for the EEV of commercially available ASHP unit before retrofit was disabled, and a new control loop to maintain a certain refrigerant degree of superheating at the compressor suction using PID controller was developed. The PID controller's proportional band, integral times, and set points were all allowed to be reset.

The PID control loop worked as follows: when enabled, the PID controller monitored both pressure and temperature at compressor suction. The pressure was used to determine the saturated evaporating temperature, and then difference between the suction temperature and the saturated evaporating temperature was the operating degree of superheat (DS). Then the controller compared the operating DS with its set point. A deviation was processed in the controller according to a pre-set PID control algorithm and a digital control signal was produced and sent by the PID controller to a driver for EEV motor to regulate its opening.

4.5 Conclusions

To facilitate the intended research work reported in this thesis, an experimental ASHP setup was constructed. The experimental setup mainly included the experimental ASHP unit, the existing environmental chamber and the instrumentation and DAS.

The experimental ASHP setup was fully instrumented using high quality sensors/measuring devices. Totally thirty-nine operating parameters in the setup could be real-time measured, monitored, recorded and processed by a data logging & control supervisory programs.

The availability of such an experimental setup was expected to be extremely useful in investigating the operating performance of novel TES-based reverse cycle defrosting method to be developed, as well as operating performance evaluations for ASHP systems.

Photos showing the details of the experimental ASHP setup are in Appendix B, and the list of the measured parameters is in Appendix C.

Chapter 5

Operational Performances of an Experimental ASHP Unit Using a Novel TES-Based Reverse Cycle Defrosting Method – Refrigerant Side

5.1 Introduction

As mentioned in Chapter 2, for an ASHP unit, during a standard reverse cycle defrosting process, its indoor air fan is normally switched off. In this case, the energy to melt frost mainly comes from that stored in indoor coil metal and the input work to compressor, which is not sufficient for quick defrosting. Insufficient heat available during defrosting is currently a fundamental problem as far as reverse cycle defrost is concerned, with which a number of operational problems during defrosting for ASHPs are associated. These include a prolonged defrosting time when a lower indoor air temperature inside a heated space can be resulted in since no heating is provided during defrosting, so that the thermal comfort of occupants can be adversely affected. Furthermore, because an indoor coil is at a very low temperature immediately after the completion of defrosting, it would take a longer time to heat up the coil first before space heating can become available. This further lengthens the time period without effective heating. Although previous related studies on improving reverse cycle defrosting performance for ASHPs are available in the open literature [Young 1980, Nutter et al. 1996, Wang et al. 2008, Liang et al. 2010, Choi

et al. 2011], the fundamental problem of insufficient heat available during reverse cycle defrosting remains unaddressed.

In order to solve this fundamental problem, a novel thermal energy storage (TES) based reverse cycle defrosting method using PCM has been developed for ASHPs, and the operating performances of the experimental ASHP unit, as part of the experimental setup reported in Chapter 4, using the novel TES-based reverse cycle defrosting method have been experimentally studied. This Chapter reports the operating performances on the refrigerant side of the experimental ASHP unit. Firstly, three operating modes of the experimental ASHP unit, namely, standard heating and reverse cycle defrosting, parallel TES-based heating and reverse cycle defrosting, and serial TES-based heating and reverse cycle defrosting, are presented. Then, the experimental results of the operating performances on the refrigerant side during heating or TES-based heating process, defrosting process and heating resumption process at the three modes are presented and analyzed. On the other hand, the airside performances of the experimental ASHP unit and indoor thermal comfort characteristics using the TES-based reverse cycle defrosting method will be reported in Chapter 6.

5.2 Experimental conditions

All experimental work reported in this Chapter was carried out using the experimental ASHP setup whose schematic diagram is shown in Fig. 4.1 in Chapter 4.

5.2.1 Comparative experiments: mode and procedures

Three operating modes can be realized with the experimental ASHP unit, namely, standard heating and reverse cycle defrosting (Mode A), parallel TES-based heating and reverse cycle defrosting (Mode B), and serial TES-based heating and reverse cycle defrosting (Mode C). Figs. 5.1 to 5.5 show the refrigerant flow direction at each of the three operating modes.

Comparative experiments were carried out at the following three operating modes:

Mode A: Standard heating and reverse cycle defrosting operating mode (Fig. 5.1 and Fig. 5.2, baseline mode)
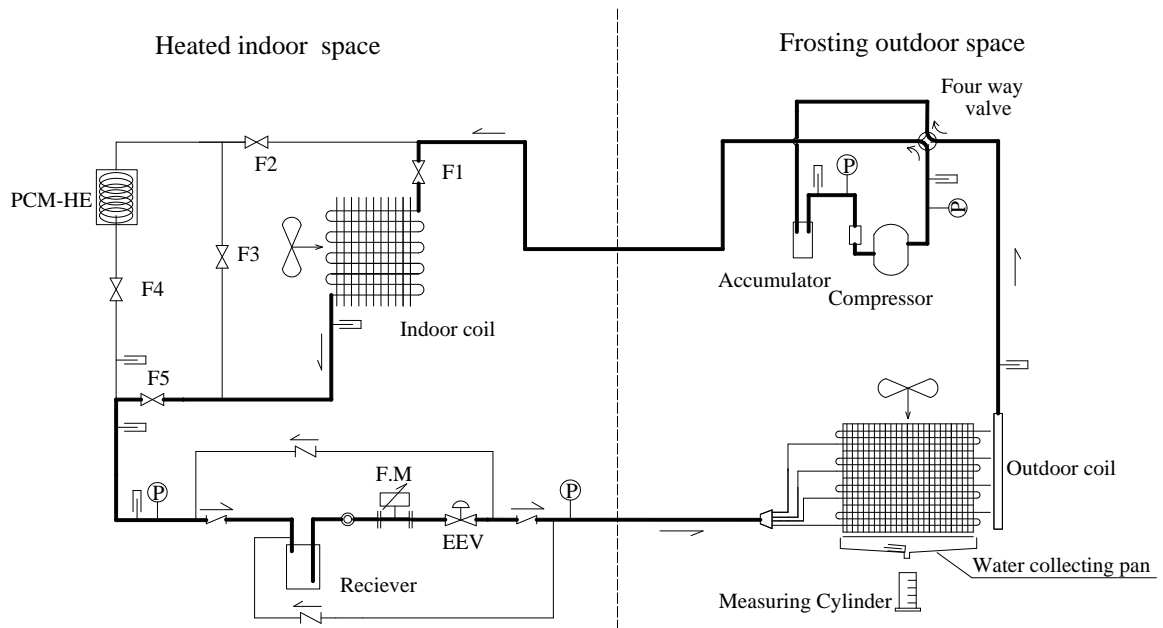
Fig. 5.1 Mode A: Standard heating
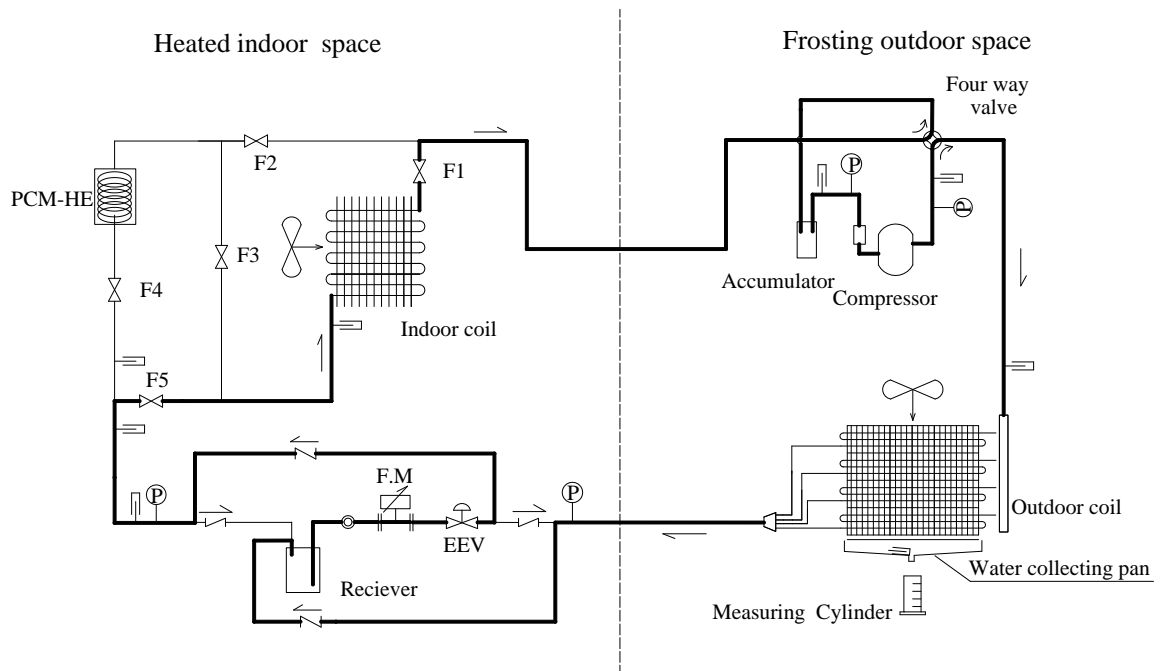
Fig. 5.2 Mode A: Standard reverse cycle defrosting

Heated indoor space   Frosting outdoor space

Fig. 5.3 Mode B: Parallel TES-based heating
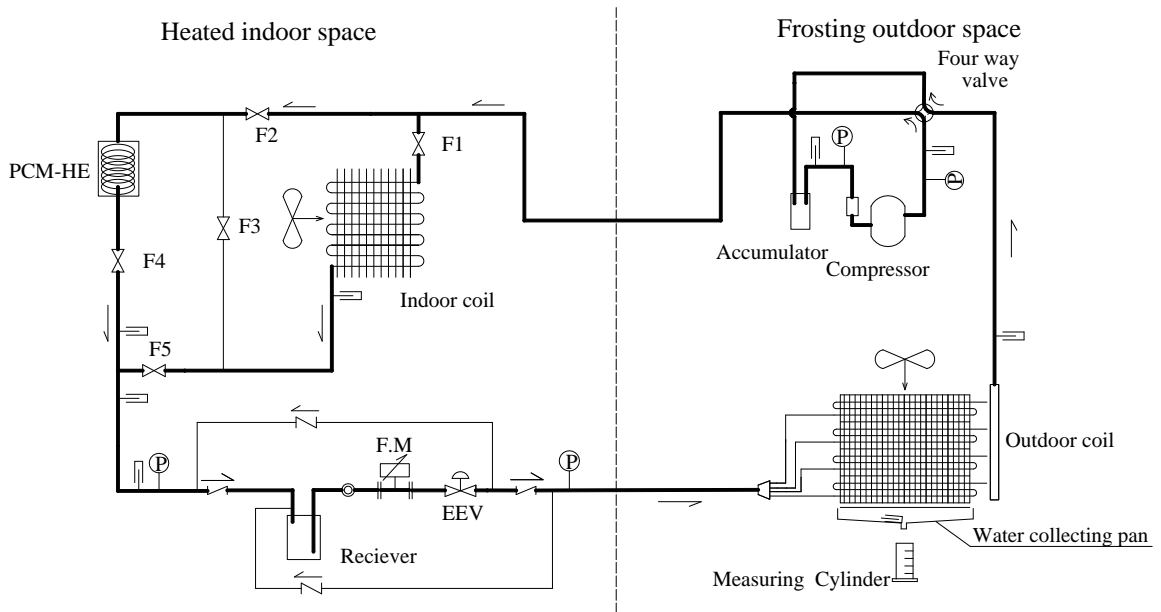
Heated indoor space   Frosting outdoor space
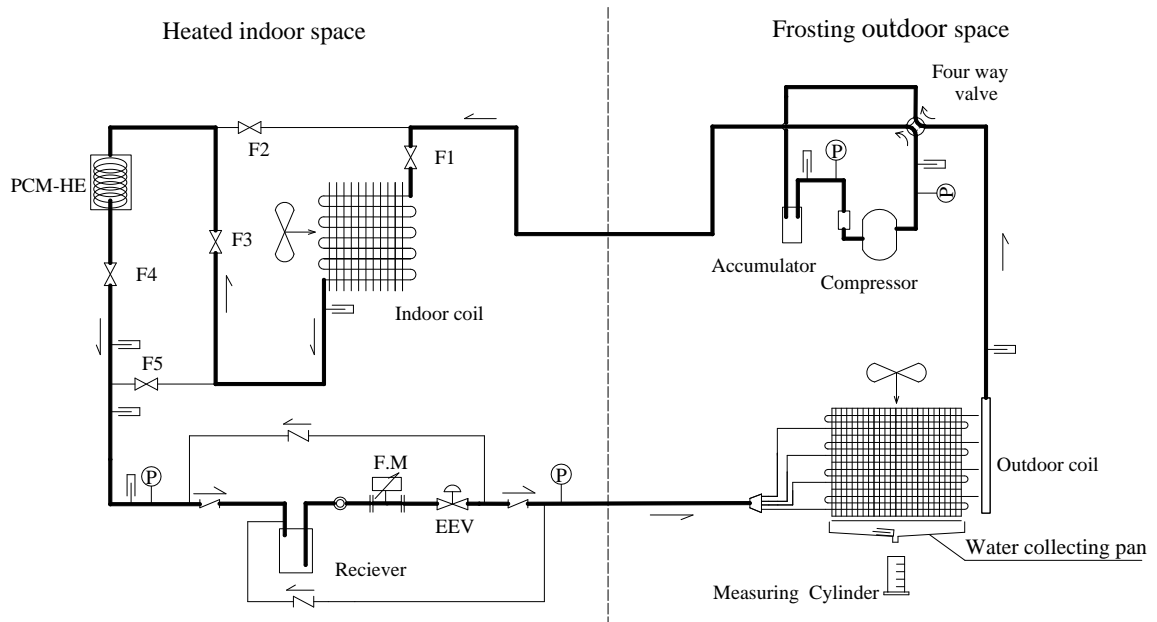
Fig. 5.4 Mode C: Serial TES-based heating
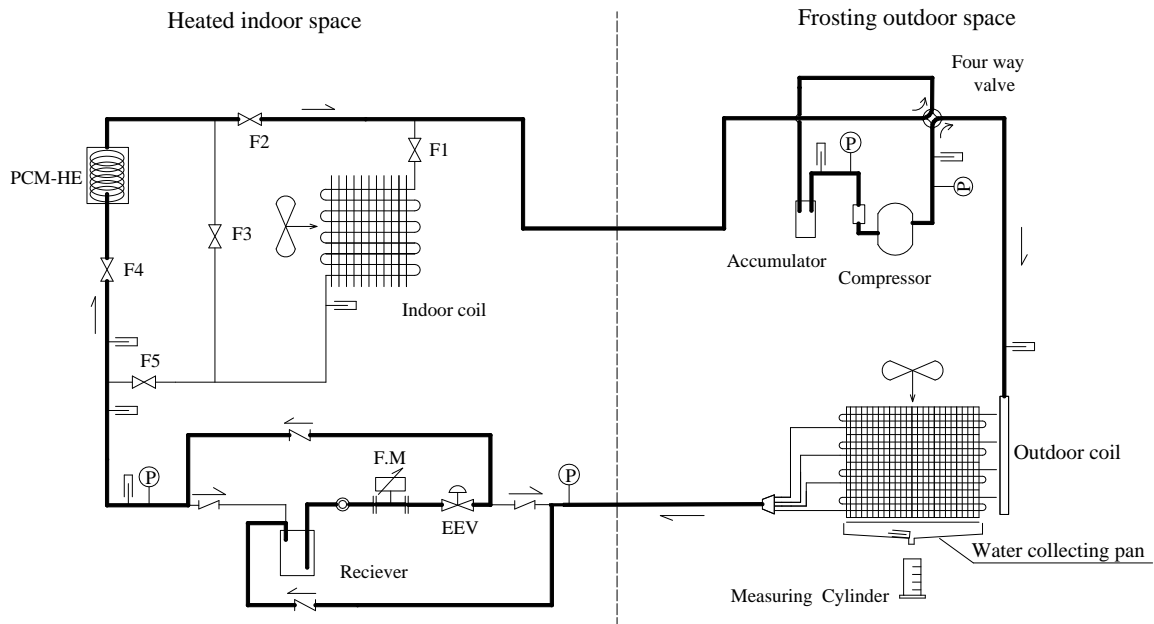
Fig. 5.5 Mode B and Mode C: TES-based reverse cycle defrosting

During a standard heating operation, air temperature and RH inside the heated indoor space were maintained at 22 ℃ and 50%, respectively, jointly by the use of the experimental ASHP unit, the existing A/C system and LGUs. The experimental ASHP unit was then operated in the heating (or frosting) mode for 1.5 hours with both Valves F1 and F5 in open position, and F2, F3 and F4 in closed position. During the 1.5 hours heating (or frosting) period, the amount of frost accumulation on outdoor coil surface of the experimental ASHP unit was real time evaluated using Equations (4.1) to (4.4). After defrosting was initiated, the four way valve was reversed, as shown in Figs. 5.1 and 5.2. The experimental results obtained at this operating mode would provide a base for comparison.

When adopting TES-based heating in both Mode B and Mode C, the ASHP unit was firstly operated in standard heating mode for 10 minutes, in order to maintain a stable operation and provide a baseline for comparison.

Mode B: Parallel TES-based heating and reverse cycle defrosting operating mode (Fig. 5.3 and Fig. 5.5)

At this operating mode, air temperature and RH inside the heated space were also maintained at 22 ℃ and 50%, respectively, jointly by the use of the experimental ASHP unit, the existing A/C system and LGUs. The outputs from both A/C system and the LGUs were however slightly different from that at operating Mode A in order to simulate a smaller heating load, so that there was surplus heat available for storage in the PCM-HE. After 10 min of standard heating operation, with the Valves F1, F2, F4 and F5 in open position, and F3 in closed position, the hot refrigerant gas flowed through both the indoor coil and the PCM-HE, as shown in Fig. 5.3. To facilitate carrying out of the intended comparative experiments, the amount of frost formed on the surface of outdoor coil must be the same as that formed at Mode A after the 1.5 hours frosting (heating) operation. To this end, the actual amount of the frost formed was also real-time evaluated and a defrosting operation was not enabled until the same amount of frost formed as that at Mode A operation arrived.

During TES-based reverse cycle defrosting, Valves F2 and F4 were in open position,

and F1, F3 and F5 in closed position, as shown in Fig. 5.5. The PCM-HE actually acted as an evaporator, and the energy stored in PCM was discharged and used to melt the frost on outdoor coil surface.

Mode C: Serial TES-based heating and reverse cycle defrosting operating mode (Fig. 5.4 and Fig. 5.5)

At this operating mode, air temperature and RH inside the heated space were the same as that at Mode A and Mode B, i.e., 22 ℃ and 50%, respectively, jointly by the use of the experimental ASHP unit, the existing A/C system and LGUs. After 10 min of standard heating operation, Valves F1, F3 and F4 were in open position, and F2 and F5 in closed position, as illustrated in Fig. 5.4, and hot refrigerant gas flowed through the indoor coil and the PCM-HE successively. The sensible heat of refrigerant was then absorbed by and stored in PCM through melting. Therefore, at this operating mode, the PCM-HE acted both as a sub-cooler during heating and, same as at Mode B, as a heat source during defrosting. Also, the initiation of the TES-based reverse cycle defrosting process was the same as that in Mode B.

The positions of all the solenoid valves at the three operating modes are listed in Table 5.1.

Table 5.1 The positions of all the solenoid valves at the three operating modes

Mode		F1	F2	F3	F4	F5
A	i) Standard heating	O	C	C	C	O
	ii) Standard reverse cycle defrosting	O	C	C	C	O
B	i) Parallel TES-based heating	O	O	C	O	O
	ii) TES-based reverse cycle defrosting	C	O	C	O	C
C	i) Serial TES-based heating	O	C	O	O	C
	ii) TES-based reverse cycle defrosting	C	O	C	O	C

O: Open;　　　C: Closed.

During carrying out the comparative experiments at the above three operating modes, the frosting outdoor space in the experimental setup was maintained at 0 ± 0.1 ℃ (dry-bulb) and $90\% \pm 3\%$ relative humidity, jointly by the use of both the experimental ASHP unit and the LGUs placed there, to simulate an outdoor frosting environment for the ASHP unit so that frost can be formed on the surface of its outdoor coil. Table 5.2 shows the experimental conditions in both indoor and outdoor spaces used in experiments. For safety reason, at the end of a frosting (i.e., heating or TES-based heating) operation, compressor was switched off for one minute. After that, the four way valve was reversed for defrosting operation. Four seconds later, the compressor was turned on again and a defrosting operation was started.

Table 5.2 Experimental conditions

Parameters	Values
Heated indoor space	
Temperature (ºC)	22
RH (%)	50 ± 3
Frosting outdoor space	
Temperature (ºC)	0 ± 0.1
RH (%)	90 ± 3
Face velocity of outdoor coil (m/s)	1.8*
Heating (frosting) operation time (h)	1.5[#]

*: at the beginning of a heating (frosting) operation. It would become lower as the operation progressed.

[#]: for standard heating only

Defrosting operations were manually terminated when the tube surface temperature at the outlet of the lowest refrigerant circuit in the outdoor coil reached 18 ºC [Payne and O'Neal 1995, Ding et al. 2004, Huang et al. 2004]. Both the indoor air fan and the outdoor air fan during defrosting operations were turned off. After a defrosting operation was manually terminated, also for safety reason, the compressor was turned off for one minute. Then the four way valve was reversed to heating operation. Four seconds later, both the compressor and the outdoor air fan were turned on, but the indoor air fan remained off for a further period of 3 minutes to avoid blowing cold air

directly to the indoor heated space, when the indoor coil was still at a low temperature. When the indoor air fan was turned on, the experimental ASHP unit was in heating operation again.

5.2.2 Data reduction

During defrosting, because both indoor air fan and outdoor air fan were turned off, the input power only to compressor, P, was real time monitored, so that the actual amount of energy consumption by the experimental ASHP unit during defrosting can then be evaluated by:

$$W_d = \int_0^{t_d} P dt = \sum P \cdot \Delta t \qquad (5.1)$$

where $\Delta t = 5$ s, same as time interval used for data logging and t_d is the defrosting duration, which is the time period starting from defrosting initiation to termination.

5.3 Experimental results and discussions

5.3.1 Refrigerant side performances of the experimental ASHP unit during heating or TES-based heating process

The operating performances on the refrigerant side of the experimental ASHP unit during heating or TES-based heating process in the three operating modes are presented in this section. In order to allow the same amount of the frost as that at Mode A to form, the parallel TES-based heating process (Mode B) actually lasted for 93.7 min, while the serial TES-based heating process (Mode C) lasted for 90 min.

The measured variation profiles of the refrigerant discharge pressures and temperatures during heating or TES-based heating process in the three operating modes are shown in Figs. 5.6 and 5.7. As seen in Fig. 5.6, the measured discharge pressure in Mode A was stabilized at about 16.6 bar. However, at 10 min when the experimental ASHP unit began to operate in parallel TES-based heating (Mode B), the measured discharge pressure firstly increased sharply to 17 bar, then decreased gradually and leveled at ~16.5 bar for the next 25 minutes. Afterwards, the measured discharge pressure increased again, and reached 17.7 bar at the end of the parallel TES-based heating operation. However, in Mode C, the measured discharge pressure firstly dropped to 16 bar at ~10 min and then increased gradually to 17.2 bar.
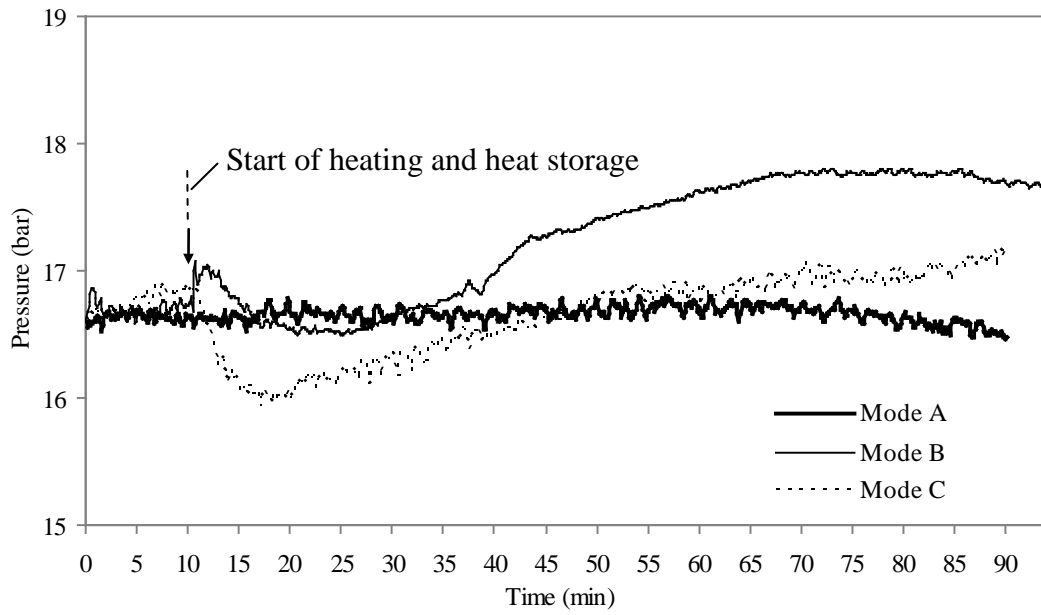
Fig. 5.6 The measured discharge pressures during heating or the TES-based heating
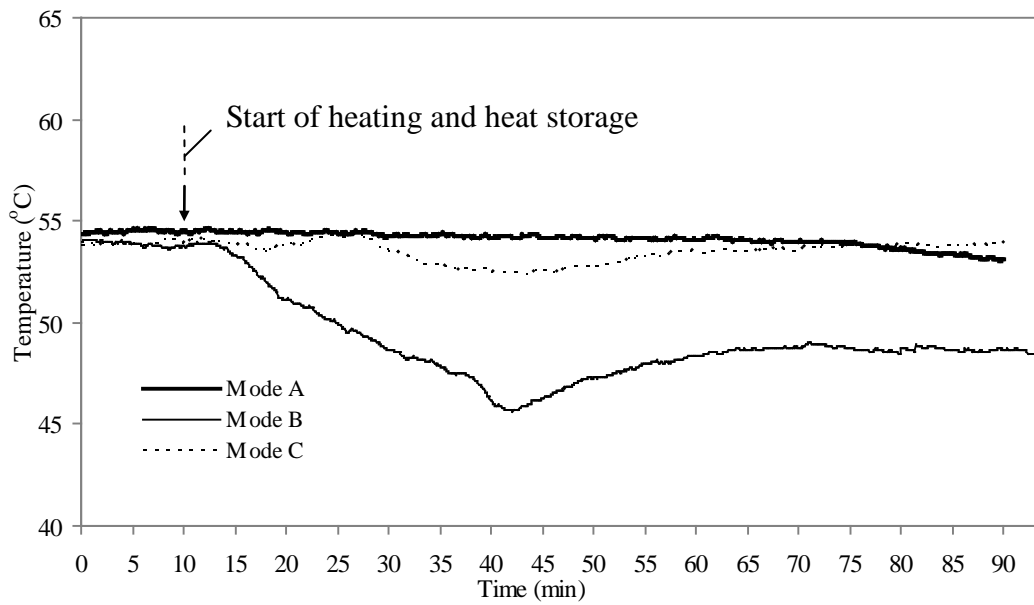
process

Fig. 5.7 The measured discharge temperatures during heating or the TES-based

heating process

As shown in Fig. 5.7, the measured refrigerant discharge temperatures were maintained at around 55.8 ^{o}C in Mode A and 53.2 ^{o}C in Mode C, respectively, while in Mode B, the measured discharge temperature began to decrease at the beginning of the parallel TES-based heating operation, and reached its minimum of 45.6 ^{o}C at ~ 42 min. Afterwards, it increased gradually and stabilized at around 48.6 ^{o}C.

The measured compressor suction pressures in the three operating modes during heating or the TES-based heating process were very close to each other, at 4.26 bar in Mode A, 4.34 bar in Mode B, and 4.26 bar in Mode C, respectively. The measured suction pressure or the evaporating temperature in Mode B was the highest, leading to the longest frosting time to obtain the same amount of frost, comparing to those in Mode A and Mode C.

The measured compressor suction temperatures during heating or TES-based heating process are presented in Fig. 5.8. As seen, the measured suction temperature in Mode B was higher than those in Mode A and Mode C. The suction temperature dropped slightly to -4.3 ^{o}C at ~ 36 min in Mode B. Afterwards, it rose gradually to -3.9 ^{o}C. In Mode C at ~18 min, the measured suction temperature began to decrease from -4.3 ^{o}C to -5 ^{o}C, and then increased gradually to -4.4 ^{o}C.
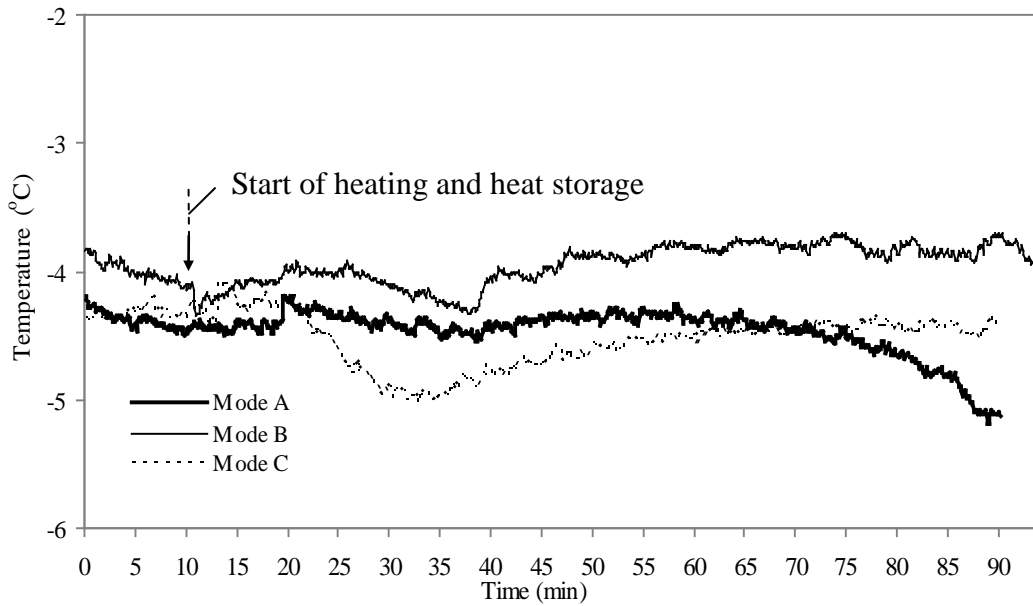
Fig. 5.8 Measured suction temperatures during heating or TES-based heating

process

Fig. 5.9 shows the results of measured refrigerant temperatures at both inlet and outlet

of the PCM-HE during the TES-based heating process in both Mode B and Mode C.

As seen, both the refrigerant temperatures at the inlet and outlet of the PCM-HE in

Mode C were lower than those in Mode B, because during the serial TES-based

heating process, the refrigerant flowing through the PCM-HE was sub-cooled. In

Mode B, the time period from 10 min to ~ 36 min could be regarded as a latent heat

storage period. Afterwards, the refrigerant temperature at PCM-HE outlet was close to

that at inlet, because the amount of heat transfer from the refrigerant to the PCM was

reduced dramatically. In Mode C, a latent heat storage period started from 10 min to

almost the end of the operation. The latent heat storage process lasted longer in Mode

C because the sub-cooled refrigerant could only discharge sensible heat to the PCM.

91
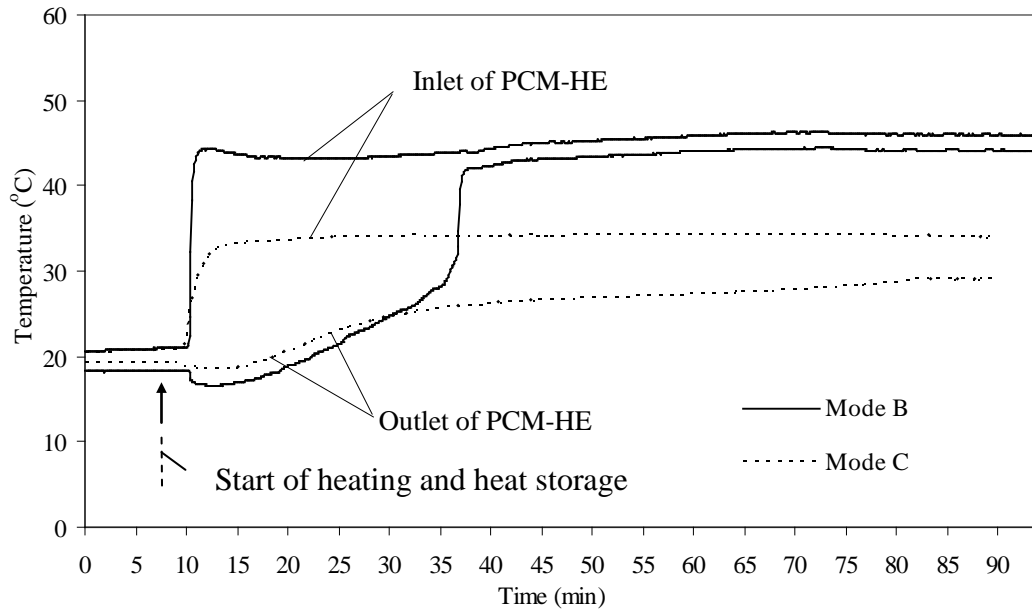
Fig. 5.9 Measured refrigerant temperatures at inlet and outlet of PCM-HE during

heating or TES-based heating process

As seen in Fig. 5.9, the PCM went through phase change from 10 min to 36 min in

Mode B. In this period, the PCM stored heat by melting, and hence the heat exchange

between refrigerant and PCM was enhanced. Then the degree of sub-cooling of

refrigerant at the outlet of the PCM-HE could be increased, leading to a higher degree

of sub-cooling of the refrigerant mixture from the PCM-HE and the indoor coil before

entering the EEV. Consequently, the suction temperature (shown in Fig. 5.8) was

reduced thus the discharge temperature (shown in Fig. 5.7) was correspondingly

reduced. When the latent heat storage process ended, heat storage ability by liquid

PCM was reduced dramatically, leading to incomplete heat transfer between the PCM

and refrigerant. The degree of sub-cooling of the refrigerant mixture dropped before

entering the EEV. Therefore, the suction temperature (shown in Fig. 5.8) was

increased, leading to an increased discharge temperature (shown in Fig. 5.7). When the experimental ASHP unit was operated in Mode C, the PCM-HE acted as a sub-cooler and the refrigerant was further sub-cooled after flowing through the PCM-HE. However, during the serial TES-based heating process, the amplitudes of variations in refrigerant temperature and pressure were smaller than those in Mode B, which may be caused by a slower heat storage process due to the fact the refrigerant in sub-cooled region could only discharge sensible heat to the PCM.

From the operating performances on the refrigerant side of the experimental ASHP unit shown in Figs. 5.6 to 5.9, it can be seen that during the parallel TES-based heating, relatively larger fluctuations in compressor discharge pressure, compressor discharge and suction temperature could occur, as compared to those during the serial TES-based heating. However, with a higher suction pressure during the parallel TES-based heating process, defrosting initiation can be delayed.

5.3.2 Refrigerant side performances of the experimental ASHP unit during defrosting process

With both the same frosting outdoor condition and the same amount of frost formed on outdoor coil surface, the operational performances of the experimental ASHP unit during defrosting using the TES-based reverse cycle defrosting method, i.e., in both

Mode B and Mode C, were different from that using standard reverse cycle defrosting method in Mode A, as shown from Figs. 5.10 to 5.14. The measured defrosting durations, were 535 s (~ 9 min) in Mode A, 340 s (5 min 40 s) in Mode B and 475 s (~ 8 min) in Mode C, respectively. Therefore, defrosting duration can be shortened by 36.4% and 11.2% when the TES-based reverse cycle defrosting method was used in Mode B and Mode C, respectively, as compared to the use of the standard reverse cycle defrosting method.

As seen in Fig. 5.10, when using the TES-based reverse cycle defrosting method (Mode B and Mode C), the surface temperatures at the exit of the lowest circuit of the outdoor coil increased at a faster pace than when the standard reverse cycle defrosting method (Mode A) was used. However, it took longer for the temperature at the exit of the lowest circuit in Mode C to reach 18 ^{o}C, than that in Mode B. This was because the heat storied in PCM-HE in Mode C was not as sufficient as that in Mode B, as reflected in Fig. 5.9. On the other hand, during defrosting in the three modes, the surface temperature significantly fluctuated, as seen in Fig. 5.10. This may have been caused by the downwards flowing of melted frost from upper circuits.
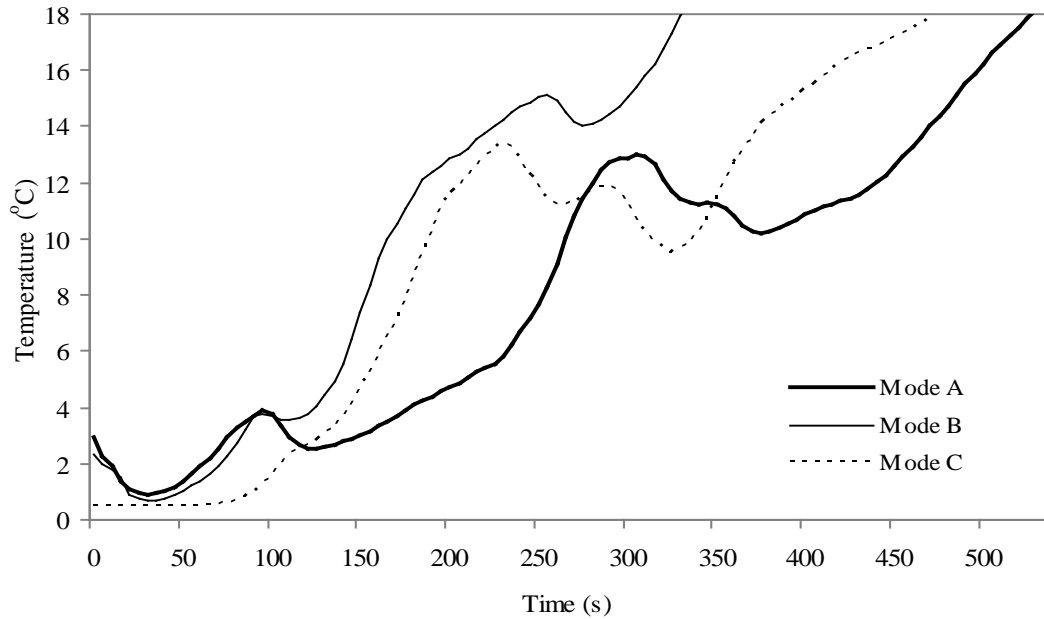
Fig. 5.10 Measured surface temperatures at the exit of the lowest circuit of the

outdoor coil during defrosting process

Figs. 5.11 and 5.12 show the measured variation profiles of compressor discharge

pressure and suction pressure during defrosting operation in the three modes. As

seen in Fig. 5.11, the measured averaged compressor discharge pressure in Mode B

was at 17.7 bar, which was higher than those in Mode A and Mode C, at 16.3 bar and

16.1 bar, respectively. In Fig. 5.13, the suction pressure in Mode B was higher than

that in Mode A. The averaged suction pressures were 4.22 bar in Mode A, 6.28 bar in

Mode B and 5.04 bar in Mode C, respectively. This was due to the fact that when

using the TES-based reverse cycle defrosting method, the PCM-HE, rather than the

indoor coil, acted as evaporator, thus a higher evaporating temperature may be

resulted in. However, when using standard reverse cycle defrosting method, the

indoor coil acted as evaporator, causing a significant reduction in evaporating
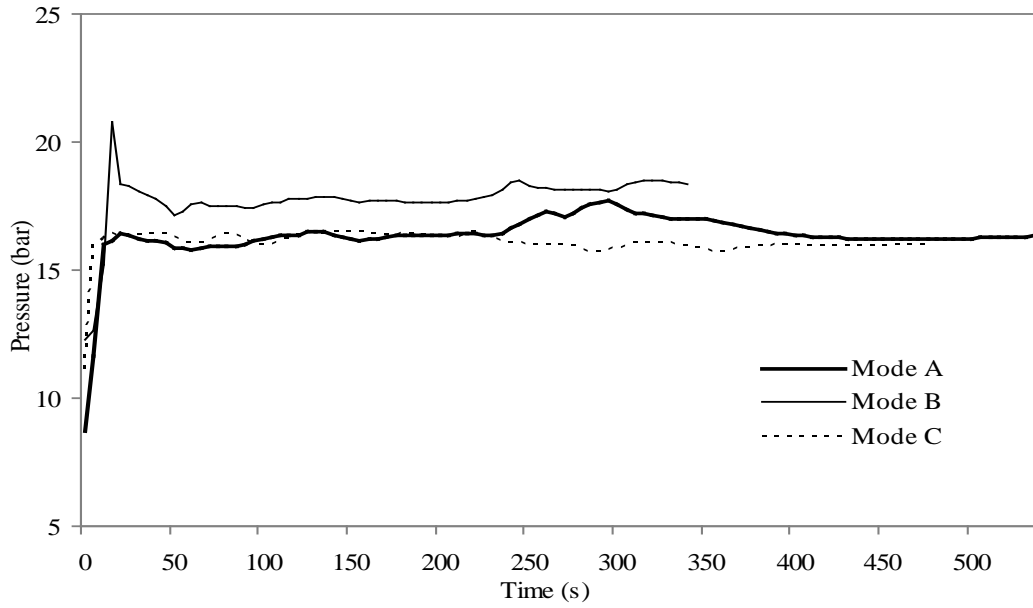
Fig.5.11 Measured discharge pressures during defrosting process
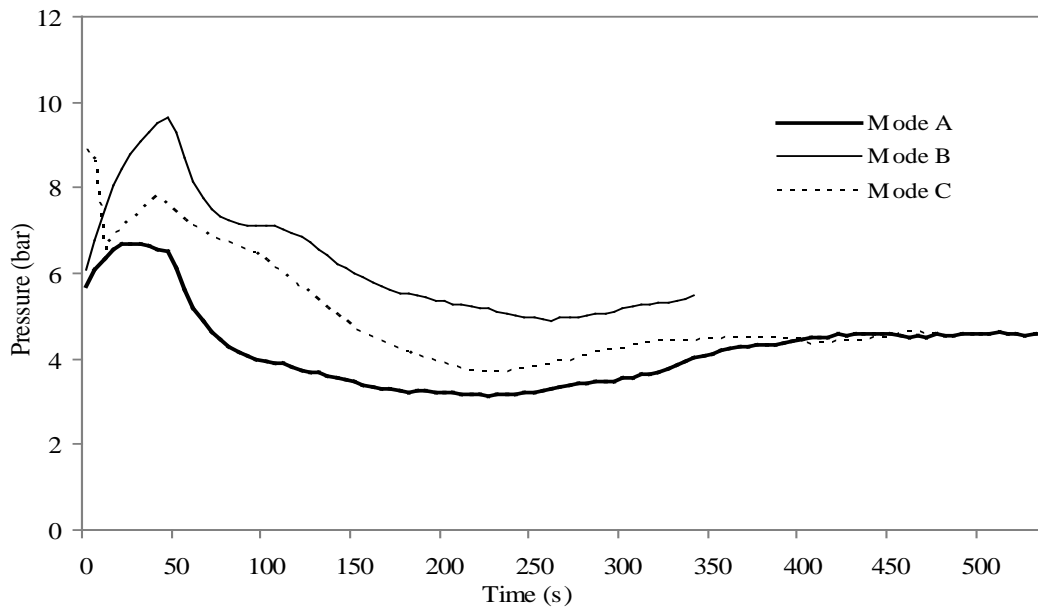
Fig.5.12 Measured suction pressures during defrosting process

temperature or suction pressure. With a higher evaporating pressure or temperature,

the risk of shutting down the ASHP unit due to low suction pressure can be

minimized, if not eliminated. Therefore, the operational stability of an ASHP unit during defrosting can be improved when using the TES-based reverse cycle defrosting method.

The refrigerant flow rates during defrosting operation in the three operating modes are shown in Fig. 5.13. Refrigerant flow rates in Mode B and Mode C were higher than that in Mode A, possibly resulting from a higher suction pressure thus a lower specific volume before entering compressor when using the TES-based reverse cycle defrosting method. Besides, the refrigerant flow rates increased at a faster pace in Mode B and Mode C than in Mode A.
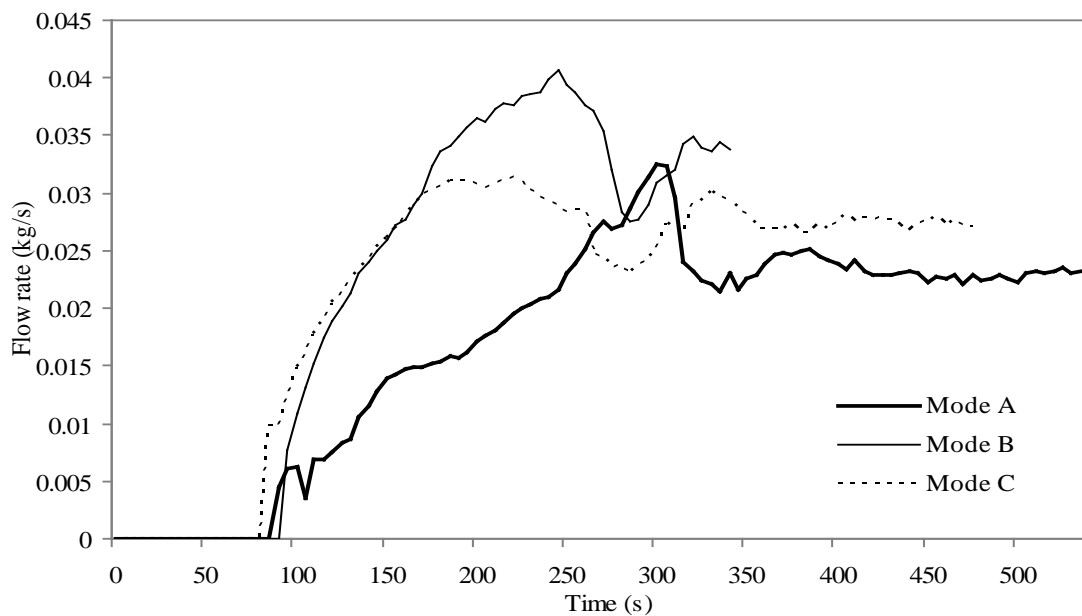
Fig. 5.13 Measured refrigerant flow rates during defrosting process

Fig. 5.14 shows refrigerant temperatures at the inlet and outlet of PCM-HE during

defrosting in both Mode B and Mode C. As seen, more heat was discharged from the

PCM in Mode B than in Mode C.
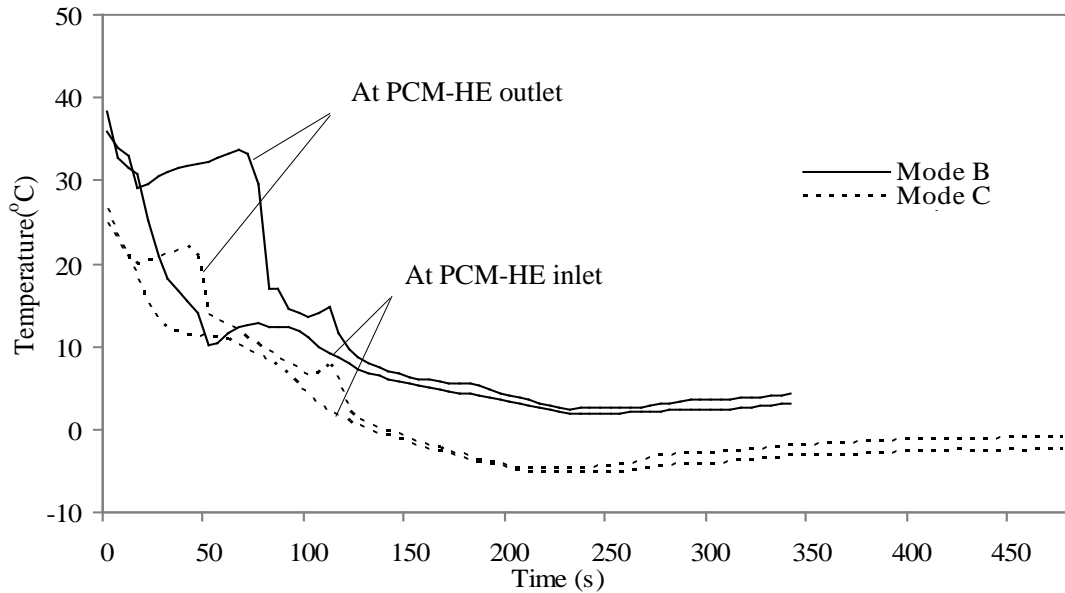
Fig. 5.14 Measured refrigerant temperatures at the inlet and outlet of PCM-HE

during defrosting process

As seen from Figs. 5.10 to 5.14, when using the novel TES-based reverse cycle

defrosting method, sufficient heat was supplied from the PCM-HE so that the

experimental ASHP unit was operated with a higher condensing temperature during

defrosting. Consequently, a higher outdoor coil surface temperature was resulted in,

which enabled a quicker defrosting process.

On the other hand, with the real time measured values of P as well as the defrosting

duration, t_d, the energy consumption for defrosting as evaluated by Eq. (5.1) was

448.5 kJ in Mode A, 266.2 kJ in Mode B and 387.5 kJ in Mode C, respectively. Therefore, the energy consumption for defrosting in Mode B was reduced by 40.6% and by 13.6% in Mode C, as compared to that in Mode A. This was due to a shorter defrosting duration when using the TES-based reverse cycle defrosting method.

5.3.3 Refrigerant side performances of the experimental ASHP unit during heating resumption process

Heating resumption followed a defrosting process. When the compressor was running again, the outdoor air fan was switched on at the same time, but the indoor air fan was remained off to avoid blowing cold air to the heated indoor space. After the compressor was running for 3 min, the indoor air fan was switched on.

Fig. 5.15 presents the measured variation profiles of compressor discharge pressure during heating resumption in the three operating modes. The discharge pressures began to increase in the earlier part of the heating resumption operation, with more increase in Mode B and Mode C than that in Mode A, suggesting that it was easier to resume space heating when using the TES-based reverse cycle defrosting method. Furthermore, there was a decrease in the discharge pressure at 3 min into heating resuming process in all the three modes, which was caused by switching on the indoor air fan.
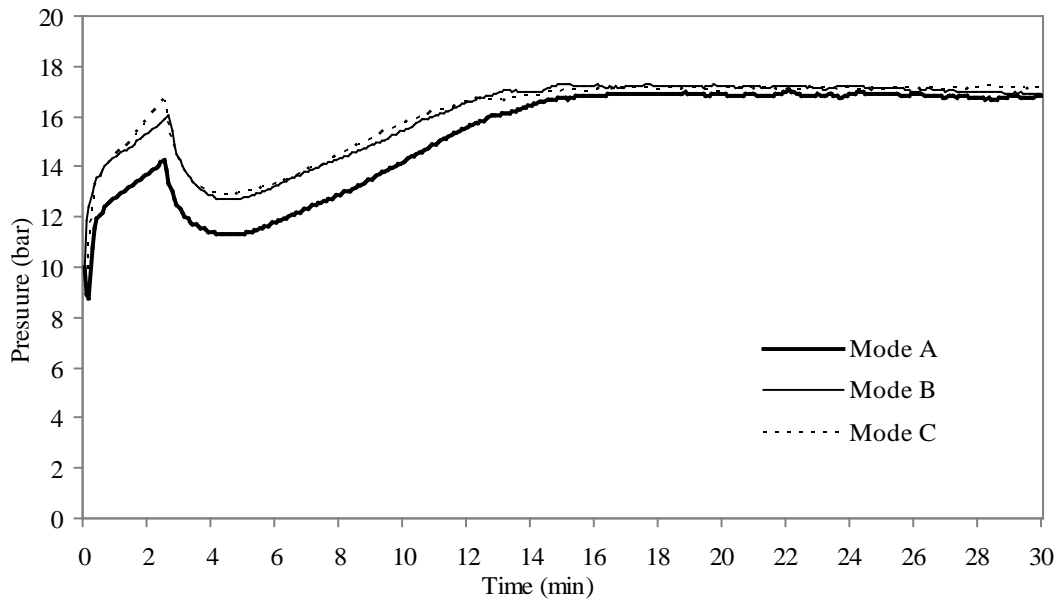
Fig. 5.15 Measured compressor discharge pressures during heating resuming process

Fig. 5.16 shows the measured compressor suction pressure during heating resumption. At about 5 min, the suction pressures in all the three operating modes reached their respective minimum values, at 2.1 bar in Mode A, 3.2 bar in Mode B and 2.6 bar in Mode C. For Mode A, the lowest suction pressure was only at 2.1 bar, so that the reliability of the ASHP unit was low since the compressor could be shut down because of low suction pressure. However, using TES-based reverse cycle defrosting can help avoid compressor shutdown because of a relatively high suction pressure.
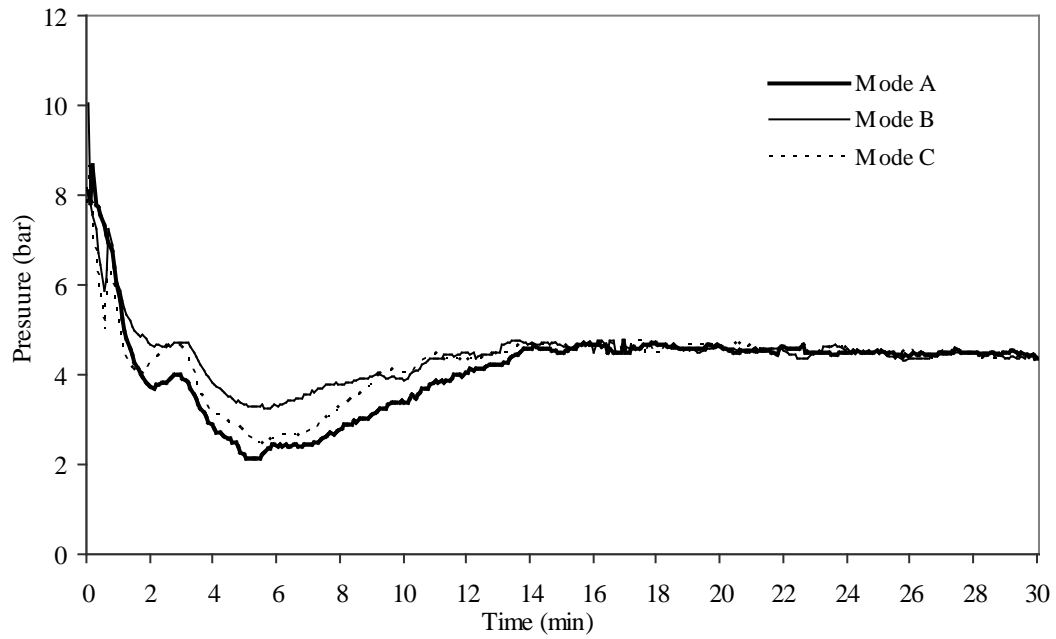
Fig. 5.16 Measured compressor suction pressures during heating resumption

5.4. Conclusions

A novel TES-based reverse cycle defrosting method for ASHPs has been developed, so as to address the fundamental problem of insufficient heat available when using the standard reverse cycle defrosting method.

Comparative experiments using both the novel TES-based reverse cycle defrosting method and the standard reverse cycle defrosting method were designed and carried out. The experimental results on the refrigerant side performances of the experimental ASHP unit suggested that the use of the novel TES-based reverse cycle

defrosting method would lead to the following advantages:

1. A shorter defrosting duration due to sufficient heat available for defrosting;

2. A smoother transition from defrosting to space heating resumption for the ASHP unit;

3. An enhanced reliablity of ASHP unit resulting from a higher suction pressure during defrosting and heating resumption;

4. A reduced energy consumption for defrosting because of a shorter defrosting duration.

The measured operating performances on the airside of the experimental ASHP unit and indoor thermal comfort characteristics using the TES-based reverse cycle defrosting method will be presented and discussed in Chapter 6.

Chapter 6

Operational Performances of the Experimental ASHP Unit Using a Novel TES-Based Reverse Cycle Defrosting Method – Airside

6.1 Introduction

In Chapter 5, the operational performances on the refrigerant side of the experiment ASHP unit using the TES-based reverse cycle defrosting method are reported. The experimental results demonstrated that using the TES-based reverse cycle defrosting method could lead to a shorter defrosting duration and a smoother transition from defrosting to heating resumption. Therefore, it becomes clear that adopting the TES-based reverse cycle defrosting method would directly and indirectly affect indoor air temperature, humidity, air velocity and mean radiant temperature (MRT), and consequently indoor thermal comfort level during defrost and heating resumption.

In this Chapter, the operational performances on the airside of the experimental ASHP unit and indoor thermal comfort characteristics using the TES-based reverse cycle defrosting method will be presented. Firstly, the well-known Fanger's thermal comfort model is briefly introduced, with appropriate assumptions and simplifications. This is followed by reporting the measured indoor thermal parameters that were necessary for evaluating indoor thermal comfort under the standard reverse cycle defrosting method and the TES-based reverse cycle defrosting

method. Finally, the calculated indoor thermal comfort indexes based on the experimental results are discussed.

6.2 Indoor thermal comfort

6.2.1 Energy exchange between a human body and its environment

According to ASHRAE Handbook Fundamentals [ASHRAE 2009], the energy balance between a human body and its environment, after combining the environmental and personal variables to produce a neutral sensation, can be expressed as follows:

$$M - W = 3.96 \times 10^{-8} f_{cl} \left[\left(t_{cl} + 273 \right)^4 - \left(\overline{t}_r + 273 \right)^4 \right] + f_{cl} h_c \left(t_{cl} - t_{adb} \right)$$
$$+ 3.05 \left[5.73 - 0.007 \left(M - W \right) - p_{av} \right] + 0.42 \left[\left(M - W \right) - 58.15 \right]$$
$$+ 0.0173 M \left(5.87 - p_{av} \right) + 0.0014 M \left(34 - t_{adb} \right) \tag{6.1}$$

where M is the rate of metabolic heat production, W the rate of mechanical work accomplished, f_{cl} clothing area factor, h_c convective heat transfer coefficient, t_{cl}, $\overline{t}_r$ and t_{adb} the clothing temperature, MRT and indoor air dry-bulb temperature, respectively, and p_{av} water vapor pressure.

The values of h_c and f_{cl} can be estimated by using Equations (6.2) to (6.5) [ASHRAE 2009]:

$$h_c = 2.38(t_{cl} - t_{adb})^{0.25} \quad \text{for} \quad 2.38(t_{cl} - t_{adb})^{0.25} > 12.1\sqrt{v_a} \quad \text{(6.2)}$$

$$h_c = 12.1\sqrt{v_a} \quad \text{for} \quad 2.38(t_{cl} - t_{adb})^{0.25} < 12.1\sqrt{v_a} \quad \text{(6.3)}$$

$$f_{cl} = 1.0 + 0.2I_{cl} \quad \text{for} \quad I_{cl} < 0.5clo \quad \text{(6.4)}$$

$$f_{cl} = 1.05 + 0.1I_{cl} \quad \text{for} \quad I_{cl} > 0.5clo \quad \text{(6.5)}$$

where v_a is the air velocity, and I_{cl} the clothing insulation value.

Clothing temperature, t_{cl}, is evaluated by [ASHRAE 2009]:

$$t_{cl} = 35.7 - 0.0275(M - W) - R_{cl}J \quad \text{(6.6)}$$

where

$$J = (M - W) - 3.05[5.73 - 0.007(M - W) - p_{av}] - 0.42[(M - W) - 58.15]$$

$$-0.0173M(5.87 - p_{av}) - 0.0014M(34 - t_{adb}) \quad \text{(6.7)}$$

where R_{cl} is the thermal resistance of clothing.

MRT or $\bar{t}_r$, a key parameter in evaluating thermal comfort for occupants, is the temperature of an imaginary isothermal black enclosure in which an occupant would exchange the same amount of heat by radiation as in the actual nonuniform environment. Using the actually measured results of globe temperature, t_g, indoor air dry-bulb temperature, t_{adb}, and air velocity, v_a, the value of $\bar{t}_r$ can be estimated. However, the accuracy of $\bar{t}_r$ determined this way would vary considerably depending on the type of environment and the accuracy of the individual measurement. The instrument most commonly used to determine t_g is a black globe thermometer because of its simplicity (see Section 6.3.3). The temperature assumed by the globe at equilibrium results from a balance between heat gained and lost by radiation and convection, and $\bar{t}_r$ can be calculated from [ASHRAE 2009]:

$$\bar{t}_r = \left[\left(t_g + 273 \right)^4 + \frac{1.10 \times 10^8 v_a^{0.6}}{\varepsilon D^{0.4}} \left(t_g - t_{adb} \right) \right]^{1/4} - 273 \tag{6.8}$$

where D is the diameter of a globe. For a standard black globe, $D = 0.15\,m.$ ε is the emissivity of a globe, and for a black globe, $\varepsilon = 0.95$.

The water vapor pressure, p_{av}, can be estimated by:

$$p_{av} = \varphi p_{asw} \tag{6.9}$$

where p_{asw} is the saturated water vapor pressure which can be estimated using

106

Equations (4.3).

Equation (6.1) can be expanded to include a range of thermal sensations by using the PMV index. Fanger [1970] related PMV to the imbalance between the actual heat flow from a human body in a given environment and the heat flow required for optimum comfort at a specified activity by the following equation:

$$PMV = [0.303\exp(-0.036M) + 0.028]L \qquad (6.10)$$

where L is the thermal load on the body, defined as the difference between the internal heat production and the heat loss to the actual environment for a person hypothetically kept at comfort values of mean skin temperature and sweat rate at the actual activity level. Hence:

$$L = M - W - 3.96 \times 10^{-8} f_{cl} \left[(t_{cl} + 273)^4 - (\bar{t}_r + 273)^4 \right] - f_{cl} h_c (t_{cl} - t_{adb})$$
$$- 3.05[5.73 - 0.007(M - W) - p_{av}] - 0.42[(M - W) - 58.15]$$
$$- 0.0173M (5.87 - p_{av}) - 0.0014M (34 - t_{adb}) \qquad (6.11)$$

After estimating the PMV using Equation (6.10), the PPD can also be estimated. Fanger [1982] related the PPD to the PMV as follows:

$$PPD = 100 - 95\exp\left[-\left(0.03353PMV^4 + 0.2179PMV^2\right)\right] \qquad (6.12)$$

A PPD of 10% corresponds to the PMV range of ± 0.5, and even with PMV=0, about 5% of the people are dissatisfied. The relationship between PMV and PPD is shown in Fig. 6.1.
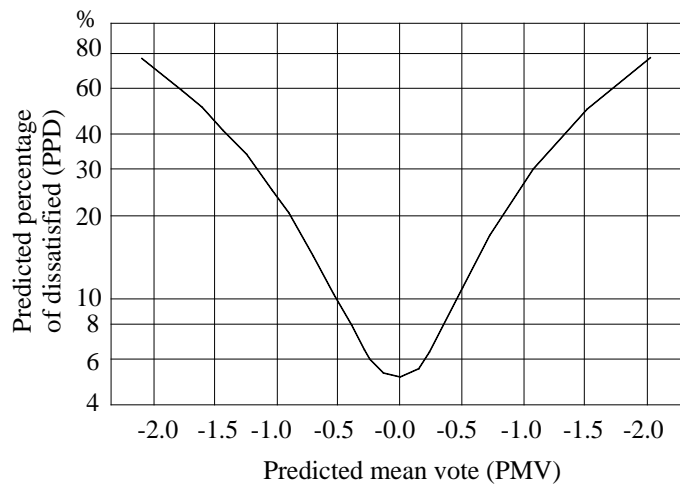
Fig. 6.1 PPD as a function of PMV [ASHRAE 2009]

Equations (6.1) to (6.12) are normally referred as Fanger's PMV-PPD model. It has been widely used and accepted for design and field assessment of thermal comfort [Yang and Su 1997, Kumar and Mahdavi 2001, Chowdhury et al. 2008, Kuchen and Fisch 2009, Hwang and Shu 2011]. Both ISO Standard 7730 [1994] and the latest version of ANSI/ASHRAE Standard 55 [ASHRAE 2010] include a short computer listing that facilitates the computing of PMV and PPD for a wide range of environmental and clothes resistance parameters.

6.2.2 Simplifications of Fanger's PMV-PPD thermal comfort model for the experimental study

Fanger's PMV-PPD thermal comfort model is normally applicable to sedentary or near sedentary physical activity levels. In this experimental study, occupants were assumed to sit quietly or relax in a heated indoor space served by the experimental ASHP unit, which could be considered as being in a sedentary physical activity level. Therefore, Fanger's PMV-PPD thermal comfort model could be adopted as a base model.

The metabolic rate for quietly seated occupants was 1.0 met. It was further assumed that occupants were immobile, therefore [ASHRAE 2010]:

$$M = 60 \ W / m^2 \tag{6.13}$$

$$W = 0 \ \ W / m^2 \tag{6.14}$$

According to ISO 7730 [1994], in winter, the clothing normally worn by occupants provided a thermal insulation of 1 clo. This clothing value was used in the current study.

Based on the above assumptions, Equations (6.4) to (6.11) could be simplified to as follows:

$$f_{cl} = 1.05 + 0.1 \times 1 = 1.15 \tag{6.15}$$

$$t_{cl} = 27.1338 - 0.6336 p_{av} - 0.013 t_{adb} \tag{6.16}$$

$$L = 34.078 - 4.554 \times 10^{-8} \left[(t_{cl} + 273)^4 - (\bar{t}_r + 273)^4 \right]$$
$$-1.15 h_c (t_{cl} - t_{adb}) + 4.088 p_{av} + 0.084 t_{adb} \tag{6.17}$$

$$PMV = 0.0629 L \tag{6.18}$$

There were four parameters: $\bar{t}_r$, t_{adb}, p_{av}, h_c in Equations (6.18) and (6.12) to determine the required indoor thermal comfort indexes, i.e., PMV and PPD, respectively. However, the convection heat transfer coefficient, h_c, was a function of air velocity, v_a; the water vapor pressure, p_{av}, was a function of both indoor air dry-bulb temperature, t_{adb}, and air RH level, φ. These may be experimentally obtained for determining PMV and PPD indexes.

6.3 Experimentation

6.3.1 Experimental conditions and operating modes

All the operational performances on the airside of the experimental ASHP unit, as

well as the indoor thermal parameters necessary for thermal comfort evaluation, were obtained under the same indoor and outdoor conditions in the three modes which are already detailed in Chapter 5: standard heating and reverse cycle defrosting operating mode (Mode A), parallel TES-based heating and reverse cycle defrosting operating mode (Mode B) and serial TES-based heating and reverse cycle defrosting operating mode (Mode C).

6.3.2 Measuring positions

The four parameters to used for evaluating airside performance of the ASHP and indoor thermal comfort, i.e., indoor air dry-bulb temperature, relative humidity (RH) of indoor air, MRT and air velocity, were experimentally measured. The indoor air dry-bulb temperature and RH were obtained by using the existing measuring instruments of the environmental chamber. For the other two parameters, i.e., air velocity and MRT, according to ANSI/ASHRAE Standard 55 [2010], within an occupied zone, measurements should be made at locations where occupants are expected to spend their time. In this experimental setup, the measuring points inside the heated indoor space are shown in Fig. 6.2.

There were totally 9 measuring points in the heated indoor space. At these 9 measuring points (see Fig. 6.2), indoor air velocity was measured at three different

levels, i.e., 0.1, 0.6 and 1.1 m above floor level, corresponding to the ankle, waist and head levels of a seated occupant (see Fig. 6.3). On the other hand, globe temperature for determining MRT was measured at 0.6 m level at these 9 measuring points.
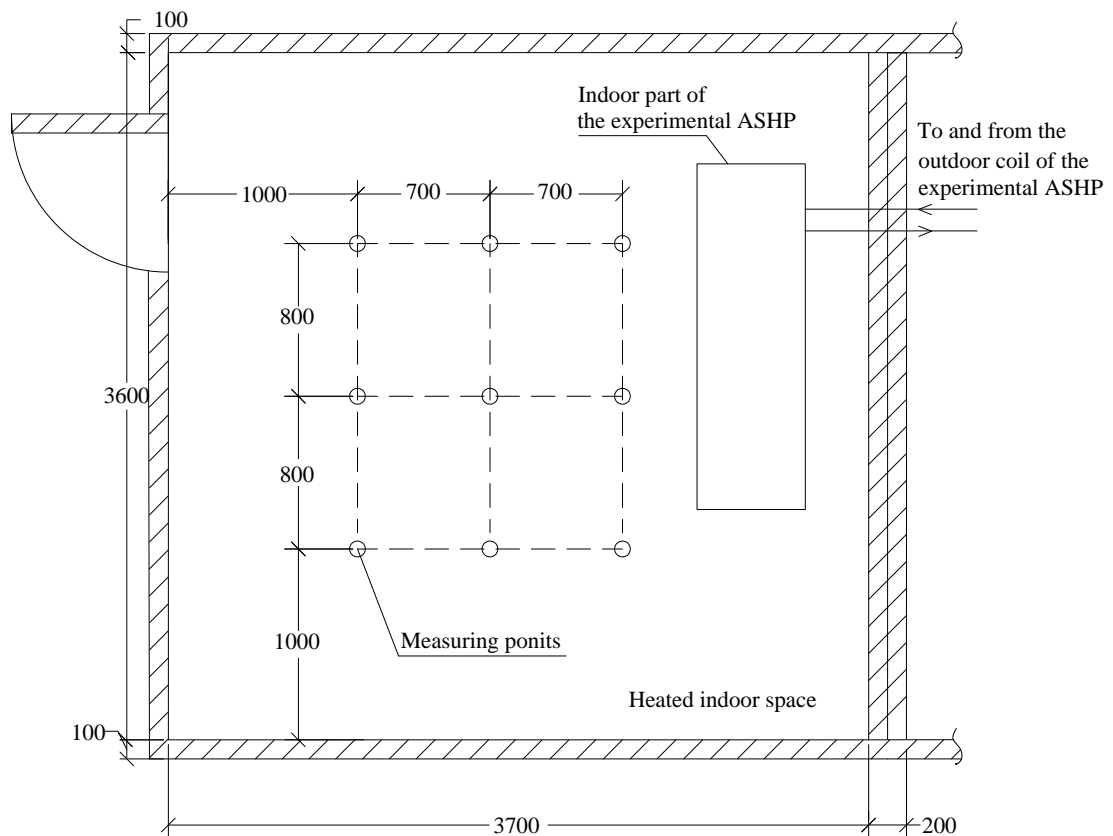
Fig. 6.2 Measuring points inside the heated indoor space of the experimental
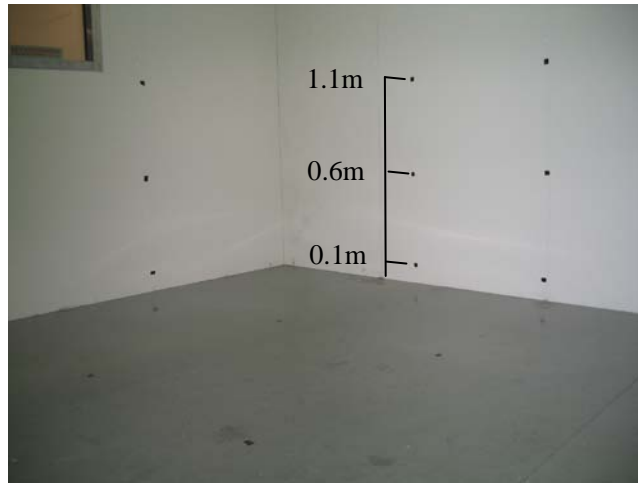
setup

Fig. 6.3 Measuring points at three different levels (0.1, 0.6 and 1.1 m)

in the heated indoor space of the experimental setup

6.3.3 Measuring instruments for air velocity and MRT

Air movement in the heated indoor space is a combination of forced flow by its ventilation system and free convection flows caused by temperature differences in the space. Air movement would therefore vary in both magnitude and direction. The air velocity is of a stochastic nature and often non-stationary. According to ANSI/ASHRAE Standard 55 [2010], the air velocity should be measured free of the influence of flow direction, therefore, an air velocity analyzer (of ± 3% accuracy) was used. The air velocity analyzer had a fast reacting omnidrectional probe tip fixed at each of the measuring points (see Fig. 6.4). On the other hand, nine black globe thermometers were used to measure globe temperature for the purpose of determining MRT [Vernon 1932, Bedford and Warmer 1934]. Under each operating

mode, the averaged room globe temperature, t_g, was obtained by averaging the readings at 0.6 m level from all the 9 measuring points. Fig. 6.5 shows the setup of measuring globe temperature using a black globe thermometer in the heated indoor space.

| (a) Velocity measuring point | (b) Velocity measuring point | (c) Velocity measuring point |
| at 0.1 m height | at 0.6 m height | at 1.1 m height |
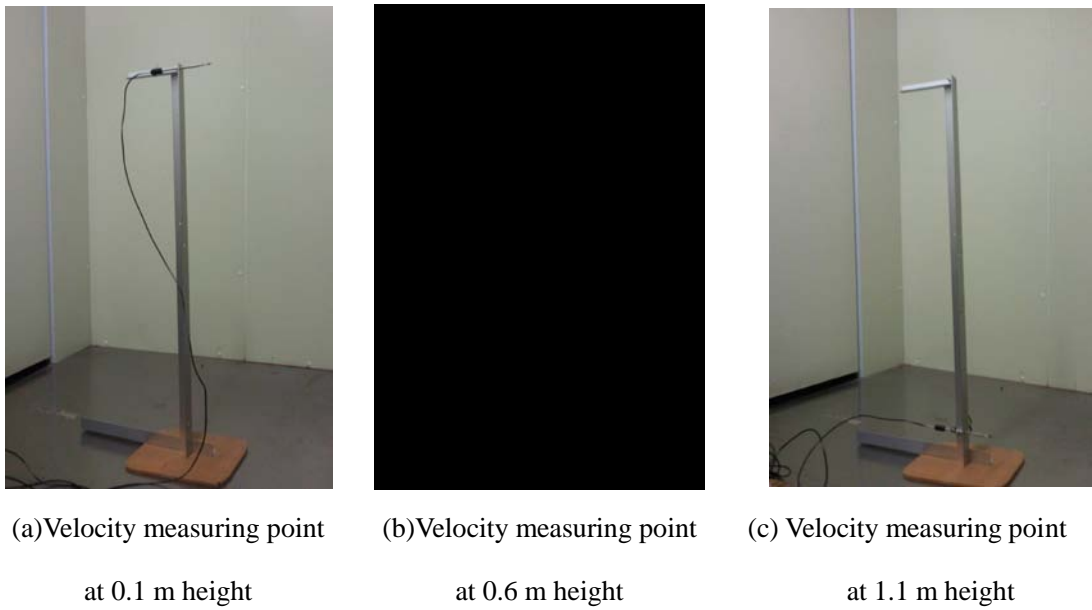
Fig. 6.4 Air velocity measurements in the heated indoor space

Fig. 6.5 A globe thermometer at 0.6 m height in the heated indoor space

6.3.4 Experimental results

6.3.4.1 Airside performances of the experimental ASHP unit during heating or
     the TES-based heating

Fig. 6.6 shows the temperature differences between supply air and indoor air in the three operating modes, which could reflect the heating capacity during heating or the TES-based heating. At the first 10 min, the temperature difference was ~10 ^{o}C. As seen, when the parallel TES-based heating began, the temperature difference between supply air and indoor air fell sharply to ~ 8 ^{o}C in Mode B, and only slightly decreased in Mode C. During heating or the TES-based heating, the average temperature differences were 9.89 ^{o}C in Mode A, 8.31 ^{o}C in Mode B and 9.47 ^{o}C in Mode C, respectively. Hence, during the parallel TES-based heating, the heating capacity was reduced to 84% of that during standard heating operation. However, during the serial TES-based heating, normal heating was not disturbed, thus the quality of space heating provided by the ASHP unit was not significantly reduced as 96% of heating capacity during standard heating operation could be provided. Finally, as heating or the TES-based heating progressed, the temperature differences in all the three operating modes gradually became smaller, because frost was gradually accumulated on outdoor coil surface, so that the performance of the ASHP unit gradually deteriorated.
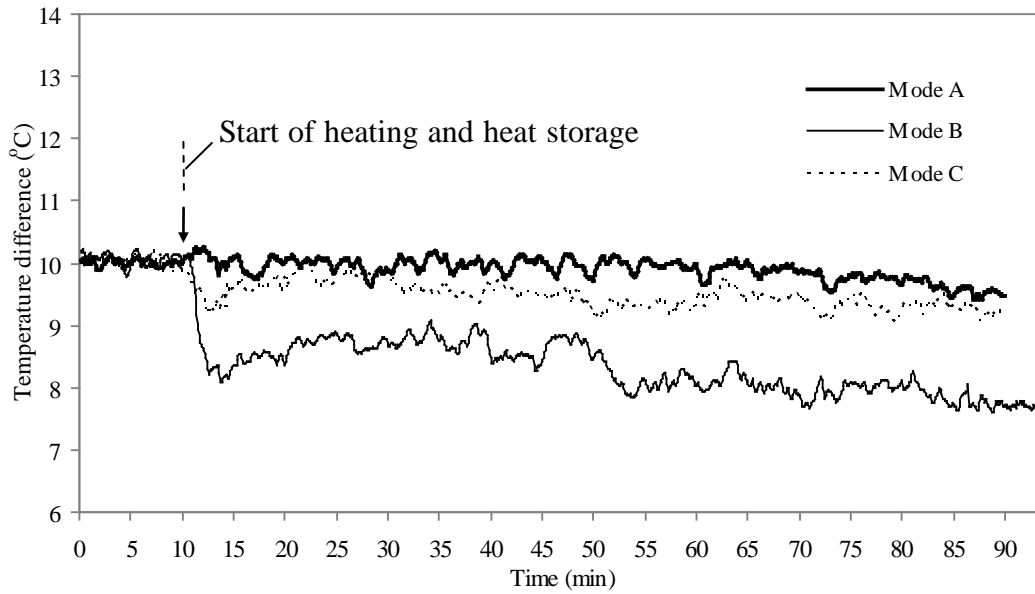
Fig. 6.6 Measured temperature differences between supply air and indoor air during

heating or TES-based heating

Based on the above observed airside performances, it can be suggested that the

parallel TES-based heating can be used at part load condition, and the serial

TES-based heating at full load condition. Alternatively, an oversized heat pump

should be employed when using the parallel TES-based heating at full load

condition.

6.3.4.2 Airside performances of the experimental ASHP unit during defrosting and heating resumption

Figs. 6.7 to 6.11 show the measured indoor air parameters during defrosting and

heating resumption in the three operating modes. In all these figures, for horizontal (time) axis, 0 min is the actual starting point of defrosting operation, and the negative values are for frosting (heating or TES-based heating) operation prior to the start of defrosting operation. The defrosting durations were 535 s (~ 9 min) in Mode A, 340 s (5 min 40 s) in Mode B and 475 s (~ 8 min) in Mode C, respectively, as reported in Chapter 5.

For the purpose of a better illustration, the comparison between measured supply air temperatures in Mode B and that in Mode A is shown in Fig. 6.7, and that between in Mode C and in Mode A in Fig. 6.8, respectively. It should be noted that during the period between defrost starting and indoor air fan starting (~13 min in Mode A , 9 min 40 s in Mode B and ~12 min in Mode C as shown in the two figures), the supply air temperature was actually the ambient air temperature measured at supply outlet of the indoor unit since the indoor air fan was switched off. As seen, in the three modes, after the indoor air fan was turned on, the supply air temperatures experienced a sharp increase in a short period of time. This was because that before the fan was turned on, compressor was already running for 3 minutes, so that the indoor coil was heated. Accordingly, the air immediately surrounding the indoor coil was also heated. Therefore, after the fan was turned on, the heated air was blown off from the indoor coil. Afterwards, the supply air temperature significantly decreased because the indoor air at a lower temperature was sucked into the indoor coil. When the indoor air temperature started to increase, as shown in Fig. 6.9, the supply air temperature in the

three modes all started to increase, and stabilized at their respective steady-state values.

Comparing with Mode A, when the TES-based reverse cycle defrosting method (Mode B and Mode C) was used, more energy could be provided by the PCM-HE, leading to a higher indoor coil temperature, and thus a higher supply air temperature. On the other hand, when using the standard reverse cycle defrosting method (Mode A), it took longer time to resume heating after defrosting because of low evaporating temperature (pressure) thus a low indoor coil temperature during defrosting. However, the increase in the supply air temperature in Mode C was not as great as that in Mode B where more heat for defrosting was available.
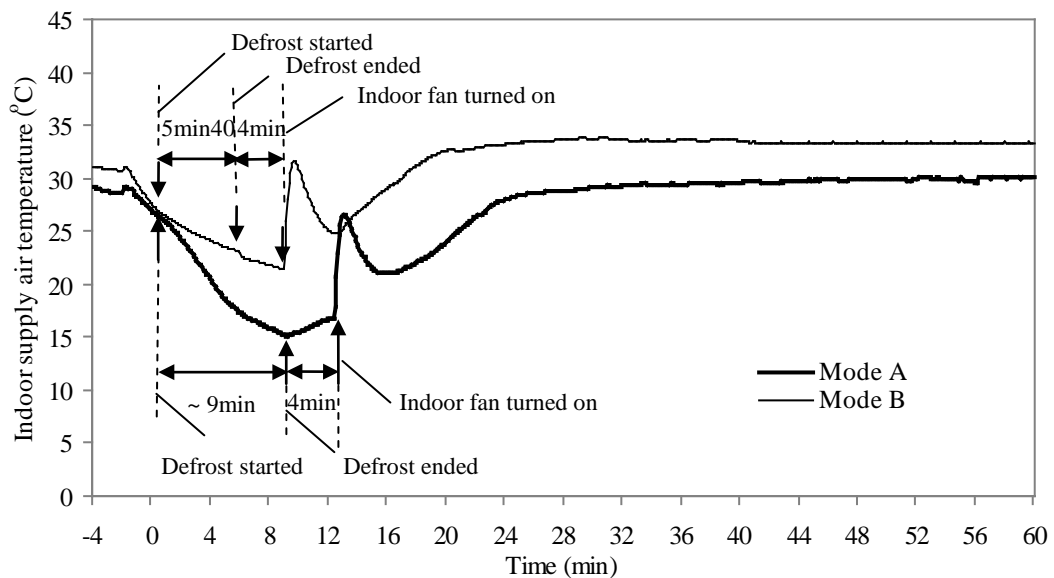
Fig. 6.7 Measured supply air temperatures in Mode A and Mode B during defrosting

and heating resumption

118
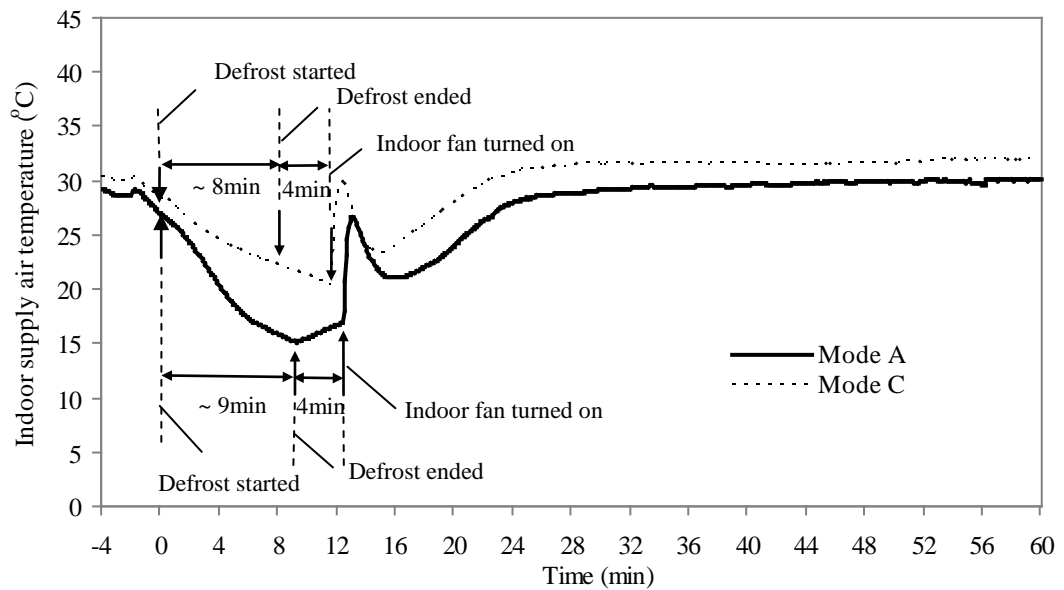
Fig. 6.8 Measured supply air temperatures in Mode A and Mode C during defrosting

and heating resumption

Fig. 6.9 illustrates the measured indoor air dry-bulb temperatures in the three modes. As seen, the measured indoor air temperatures in Mode B and Mode C were always higher than that in Mode A, resulting from a shorter defrosting period and a higher supply air temperature in Mode B and Mode C. It can be seen that indoor air temperatures started to rise ~16 minutes in Mode A, ~10 minutes in Mode B and ~12 minutes Mode C, respectively, after the defrosting started. Furthermore, the lowest indoor air dry-bulb temperatures recorded were 18.6 $^{\circ}$C in Mode A at ~16 min, 20 $^{\circ}$C in Mode B at ~10 min and 19.1 $^{\circ}$C in Mode C at ~12 min, respectively.
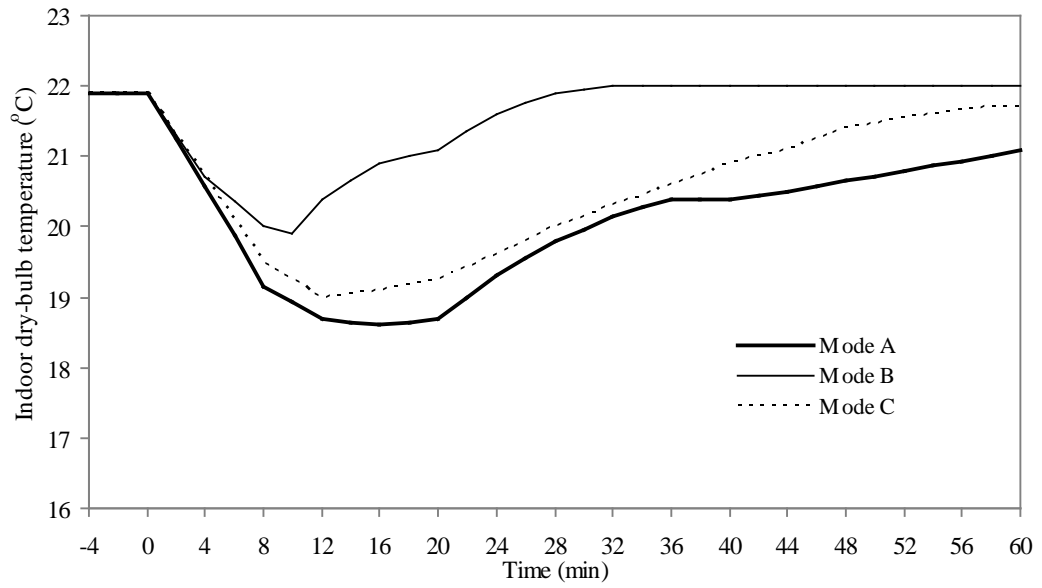
Fig. 6.9 Measured indoor air dry-bulb temperature during defrosting and heating
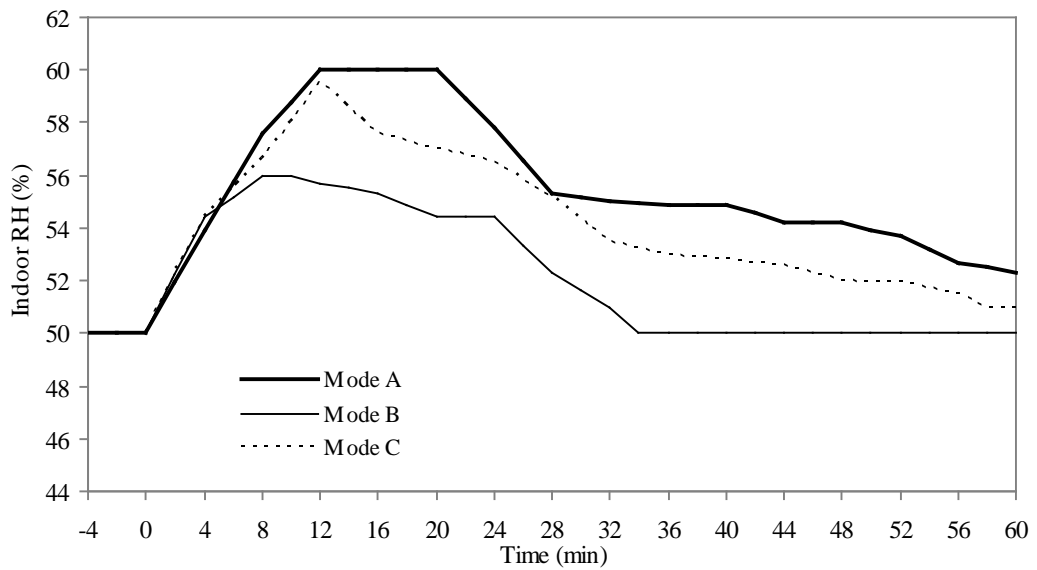
resumption

Fig. 6.10 Measured indoor RH during defrosting and heating resumption

The measured indoor air RH levels in the three modes are shown in Fig. 6.10. As a fixed moisture load in the heated indoor space was maintained during experiments in the three modes, indoor RH was higher when the indoor air dry-bulb temperature was lower, and vice versa.

On the other hand, indoor air velocity was obtained by averaging the 27 air velocity readings in the 27 (9×3 different levels) measuring points in the heated indoor space. In all the three operating modes, the averaged measured indoor air velocity was 0.37 m/s and 0.04 m/s when the indoor air fan was switched on and off, respectively.
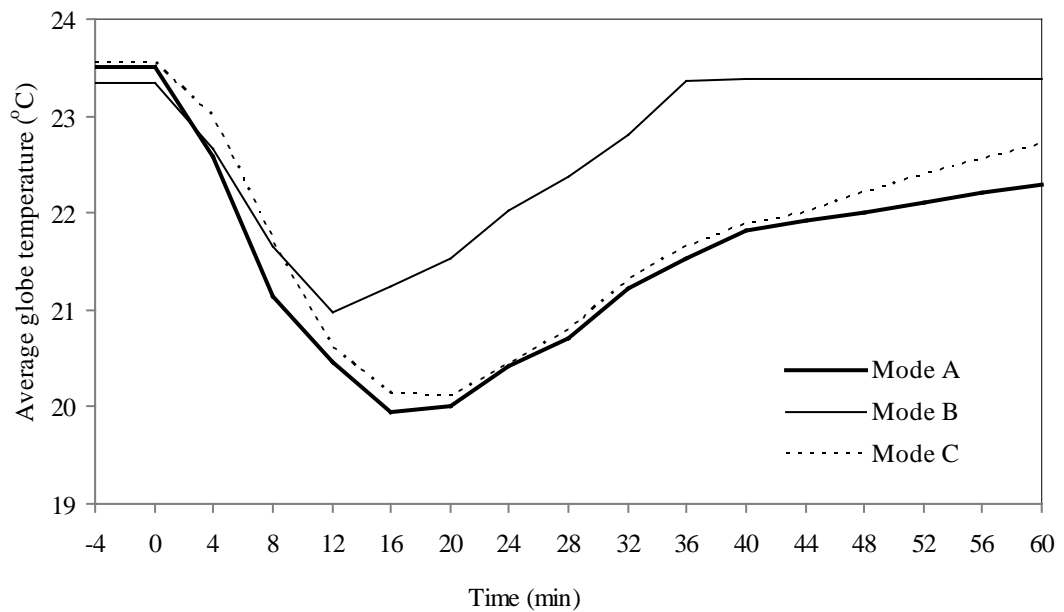
Fig. 6.11 The averaged globe temperature measured during defrosting and heating resumption

The variation patterns of the averaged globe temperature shown measured in the

three modes in Fig. 6.11 were similar to those of indoor air dry-bulb temperature (shown in Fig. 6.9). Generally, the averaged globe temperature was higher than the indoor air dry-bulb temperature by a mean value of 1.3 $^\circ$C in all the three modes.

Mean radiant temperature (MRT) in the heated indoor space was evaluated based on the known averaged indoor air velocity, indoor air dry-bulb temperature and the averaged globe temperature. Fig. 6.12 presents the variations of the evaluated MRT in the heated indoor space in the three modes. Since MRT was determined based on largely the averaged globe temperature, its variation pattern was similar to that of the averaged globe temperature. Similarly, MRT was greater than indoor air dry-bulb temperature in the three modes.
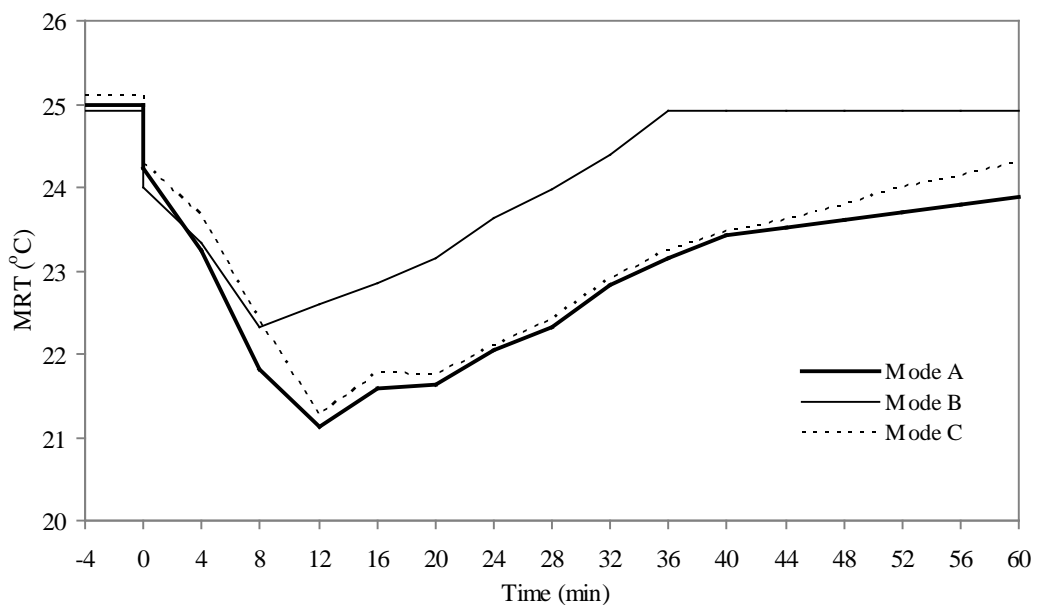
Fig. 6.12 The evaluated MRT during defrosting and heating resumption

6.3.5 Thermal comfort evaluation

With the availability of all measured and calculated parameters, the two thermal comfort indexes, PMV and PPD in the three modes, were evaluated using Equations (6.1) to (6.18). The evaluation results are shown in Fig. 6.13 for PMV and Fig. 6.14 for PPD, respectively.

As seen from Fig. 6.13, there were about 16 minutes in Mode A, 46 minutes in Mode B and 24 minutes in Mode C when PMVs were within the comfort range of -0.5<PMV<+0.5, respectively. The evaluated PMV values in three operating modes were higher than 0.5 within the first 5 minutes into defrosting operation because the indoor air fan was switched off, thus the indoor air velocity was low, but the indoor air temperature just started to decrease. On the other hand, there were about 39 minutes in Mode A, 9 minutes in Mode B and 32 minutes in Mode C when PMVs were <-0.5, respectively. This reflected that there were ~ 39 minutes in Mode A, 9 minutes in Mode B and 32 minutes in Mode C, respectively, when occupants would feel cold during and after a defrosting process. Therefore, the time duration when occupants would feel cold in Mode B was much shorter than that in Mode A, only at 23.1%, and that in Mode C was also shorter than that in Mode A, but at 82.1%. This was because when the novel TES-based reverse cycle defrosting method was used (Mode B and Mode C), the defrosting process was shorter and the supply air temperature was higher, than those in Mode A, or when the standard reverse cycle

defrosting method was used.
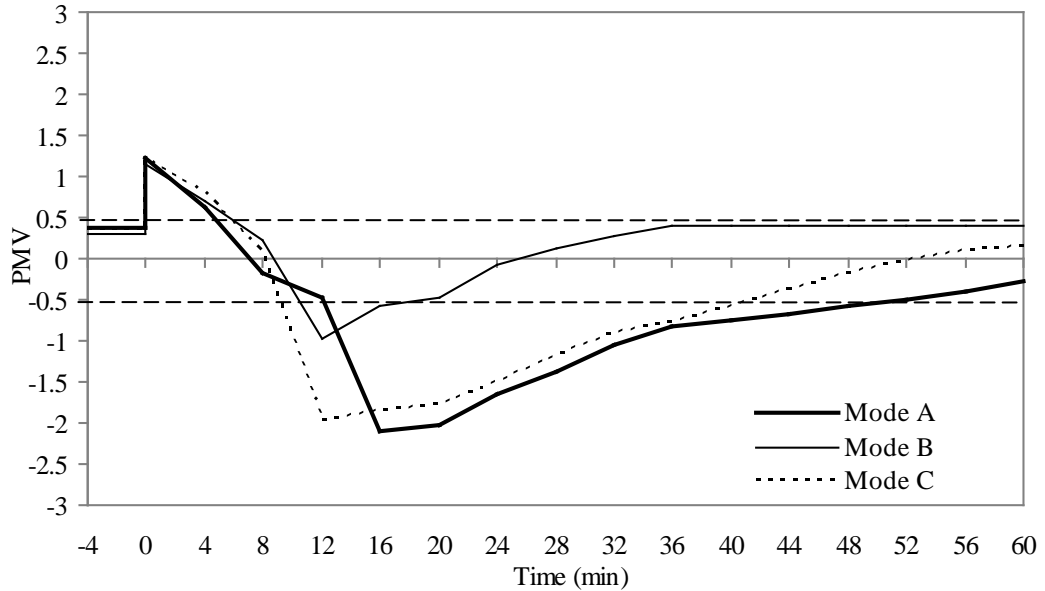
Fig. 6.13 The calculated PMV values during defrosting and heating resumption

Furthermore, in the three operating modes, for the time periods when their PMV values were also within ± 0.5, their corresponding PPD values were calculated using Equation (6.18) and are shown in Fig. 6.14. As expected, these PPD values were not greater than 10%. As seen from Fig. 6.14, there were about 16 minutes in Mode A, 46 minutes in Mode B and 24 minutes in Mode C when the calculated PPD values were not greater than 10%, respectively. The highest PPD value in Mode A was 80% but only 32.9% in Mode B and 74.7% in Mode C, respectively.

The calculated results of PMV and PPD, as shown in Figs. 6.13 and 6.14, were evaluated based on the experimentally measured indoor thermal parameters, such as

indoor air dry-bulb temperature, RH, velocity and MRT. As seen from Figs. 6.13 and 6.14, there were sharp increases in the values of both PMV value and PPD at 0 min. This was because the indoor air fan was switched off when defrosting was initiated, so that indoor air velocity changed from 0.37 m/s to 0.04 m/s at 0 min, leading to the sharp increases. However, for occupants, they may not feel such sudden changes of the indoor thermal environment due to human adaptation.
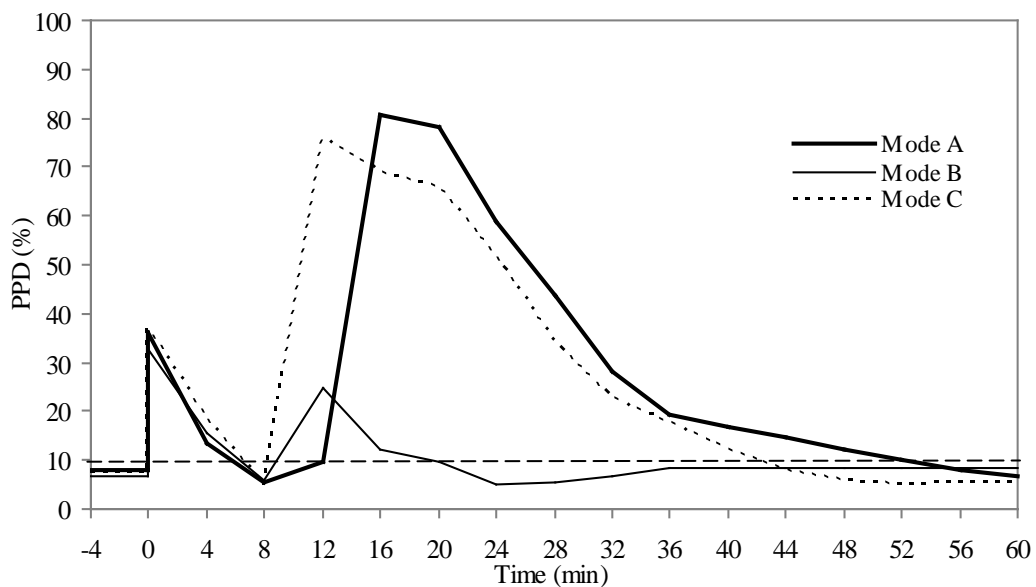
Fig. 6.14 The calculated PPD values during defrosting and heating resumption

6.4 Conclusions

To address the fundamental problem of insufficient heat available when using the standard reverse cycle defrosting method, the novel TES-based reverse cycle

defrosting method for ASHPs has been developed. After reporting the refrigerant side operating performances of the experiment ASHP unit in Chapter 5, this Chapter presents the experimental results on both the performances of the airside of the experimental ASHP unit and indoor thermal comfort characteristics when using the TES-based reverse cycle defrosting method. Indoor thermal parameters necessary for thermal comfort evaluation were measured and the indoor thermal comfort indexes evaluated based on Fanger's thermal comfort model. The experimental results of the airside performance of the ASHP unit and the evaluated indoor thermal comfort indexes (PMV and PPD) clearly suggested that the use of the novel TES-based reverse cycle defrosting method would lead to a shorter defrosting duration, a higher indoor air temperature and consequently, occupants' indoor thermal comfort can be significantly improved during reverse cycle defrosting.

On the other hand, based on the observed airside performances, it is recommended that the parallel TES-based heating can be used at part load condition, and the serial TES-based heating process at full load condition. Alternatively, an oversized heat pump should be employed when using the parallel TES-based heating at full load condition.

Chapter 7

Experimental Study of the Reverse Cycle Defrosting Performance on a Multi-circuit Outdoor Coil Unit in an ASHP

7.1 Introduction

As mentioned in Chapter 2, during defrosting, while most of the melted frost drains off from outdoor coil surface, a finned coil surface may however retain residual water which must be removed to prevent it from becoming ice when the ASHP returns to heating mode. Therefore a complete defrosting process covers both melting frost and drying coil surface. Furthermore, for outdoor coils, on its refrigerant side, multiple parallel circuits are commonly used for minimized refrigerant pressure loss and enhanced heat transfer efficiency. On its airside, however, there is usually no segmentation corresponding to the number of refrigerant circuit. Currently, terminating a defrosting operation based on surface temperature of outdoor coil is the most popular method. For an outdoor coil having multiple parallel refrigerant circuits, normally a temperature sensor is attached to the external surface of the liquid-line of its lowest circuit. The measured temperature is compared to a set point at which it is believed that an outdoor coil is free of retained water or all melted frost is drained away or vaporized. However, different set points have been reported, ranging from 12 ºC to 26.7 ºC [Stoecker et al. 1983, O'Neal 1989, Payne

and O'Neal 1995, Ding et al. 2004, Huang et al. 2004].

Although previous experimental and modeling studies on understanding the operating performance during a reverse cycle defrosting of a multi-circuit outdoor coil in ASHPs have been conducted and reported, the research work on accounting the effect of downwards flowing of the melted frost due to gravity along the surface of a multi-circuit outdoor coil on defrosting performance cannot be identified. Notably, O'Neal et al. [1989] experimentally investigated the transient defrosting performance of an ASHP unit having four-parallel refrigerant circuits. Noticeable differences in the surface temperatures at the exit of the four circuits were reported. The rates of increase in the surface temperatures at the exits of the up circuit(s) were much quicker than that of the down circuit(s). Termination of defrost was triggered when the surface temperature at the exit of the lowest circuit reached 18.3 ℃ (65 ℉). However at the same time, the surface temperature at the exit of the top circuit already reached about 37.7 ℃ (100 ℉). Similar results can also be seen in the experimental study on an outdoor coil having six rows and fourteen circuits during hot gas by-pass defrosting carried out by Stoecker et al. [1983]. Furthermore, in the study reported by Wang et al. [2008], it was shown that at six minutes into defrosting, the surfaces of down refrigerant circuit(s) in a multi-circuit outdoor coil were still covered by frost while that of up circuits were already free of frost.

Therefore, a study of the defrosting performance on the four-circuit outdoor coil in

128

the experimental ASHP unit, as part of the experimental setup reported in Chapter 4, with a particular focus on studying the impact of allowing melted frost to flow down freely along the coil surface on defrosting performance, has been carried out, using both experimental and modeling analysis approaches. This Chapter reports on the experimental part of the study and the modeling part will be reported in Chapter 8. In this Chapter, firstly the experimental procedures/conditions are described. Secondly, the experimental results are reported. This is followed by the discussion on the effects of downwards flowing of the melted frost due to gravity along a multi-circuit outdoor coil surface in an ASHP unit on defrosting performance. Finally, the evaluation of the defrosting efficiency for the experimental ASHP unit is provided.

7.2 Experimental procedures and conditions

Before defrosting, the experimental ASHP unit was operated in the heating (frosting) mode for 2 hours, at a frosting outdoor ambient of 0.5 ± 0.1 ºC (dry-bulb) and 90% ± 3% relative humidity, which was jointly maintained by the use of both experimental ASHP unit and the LGUs placed in the outdoor space. Before defrosting was started, compressor was firstly switched off. One minute after the shutdown of compressor, the four way valve was switched to defrosting mode. Four seconds later, the compressor was powered on again, and a defrosting operation was started. Defrosting operation was manually terminated when the tube surface temperature of the lowest refrigerant

circuit in the outdoor coil reached 24 ℃ [Payne and O'Neal 1995, Ding et al. 2004, Huang et al. 2004]. Both the indoor air fan and the outdoor air fan during defrosting operation were turned off.

During frosting operation, air temperature inside the heated indoor space was maintained at 20 ℃, which was jointly maintained by the use of both experimental ASHP unit and the existing air conditioning system of the environmental chamber. The experimental conditions are summarized in Table 7.1.

Table 7.1 Experimental conditions

Parameters	Values
Heated indoor space	
Temperature (℃)	20
Frosting outdoor space	
Temperature (℃)	0.5 ± 0.1
RH (%)	90 ± 3
Face velocity of outdoor coil (m/s)	1.8 *
Heating (frosting) operation time (h)	2

*: at the beginning of a heating (frosting) operation. It would become lower as the operation progressed.

7.3 Experimental results

Eight photographs illustrating the frost melting process on the airside of the four-circuit outdoor coil are shown in Fig. 7.1. These photographs show the airside conditions of the outdoor coil up to 7.5 minutes into the defrosting operation when there was no solid frost left on the coil surface. It further took 2.5 minutes for the tube surface temperature of the lowest refrigerant circuit in the outdoor coil to reach 24 ℃ when defrosting was ended. The entire defrosting duration was 600 s (10 minutes). As seen from the photographs, frost melting on the coil surface of the up refrigerant circuit(s) was quicker than that on the coil surface of down refrigerant circuit(s). For example, in Fig. 7.1 d), the airside condition of the outdoor coil at 3 minutes into the reverse cycle defrosting operation is depictured. It can be seen that while the airside of the highest circuit was already free of frost, there was still quite an amount of frost on the airside of the down circuit(s) waiting to be melted. Fig. 7.1 f) shows the airside condition 5 minutes into defrosting when only the airside of the lowest circuit was still covered with frost. As observed from these photos, the defrosting operation on the airside of the four refrigerant circuits did not end at the same time, although their starting time points were all the same.

131

a) 0 minute (start of the defrosting)
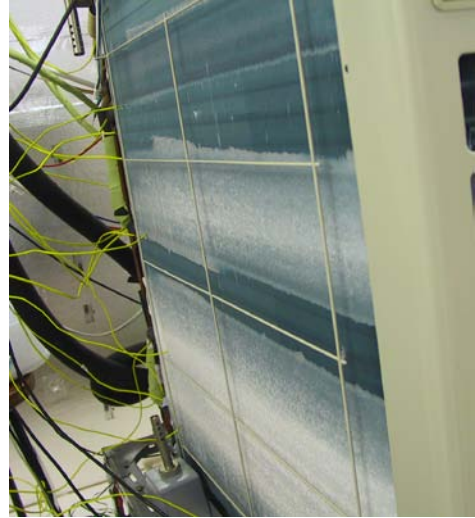
b) 1 minute into defrosting operation

c) 2 minutes into defrosting operation

d) 3 minutes into defrosting operation

e) 4 minutes into defrosting operation
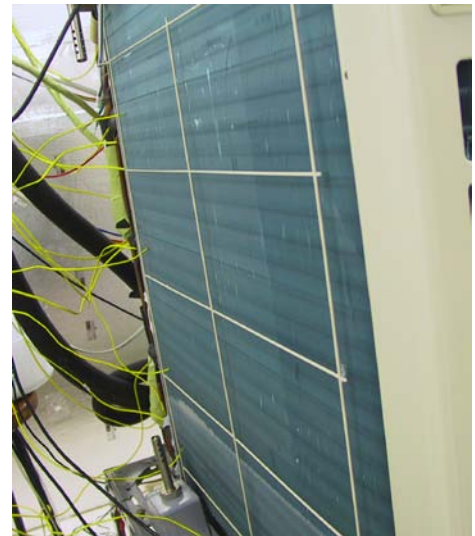
f) 5 minutes into defrosting operation

g) 6 minutes into defrosting operation   h) 7.5 minutes into defrosting operation

Fig. 7.1 Airside conditions of the outdoor coil during frosting (8 photographs)

The measured operating performances of the experimental ASHP unit during defrosting are presented in Figs. 7.2 to 7.5. In all these figures, for their time (horizontal) axis, 0 second is the actual starting time for defrosting operation.

Fig. 7.2 presents the measured tube surface temperatures at the exits (T_e in Fig. 4.2) of the four refrigerant circuits. It was noted that the variation trends of these temperatures were similar to those reported by O'Neal et al. [1989]. Given their locations, these temperatures could indirectly reflect the characteristics of the frost melting taking place on the airside of each circuit. It can be seen from the diagram that the measured temperatures at the top three circuits began to increase sharply at ~ 60 s, 100 s, and 250 s into defrosting, respectively. These may be considered as the time points when frost melting process (latent heat transfer) diminished. These clear time lags of sharp temperature rise directly reflected the different airside defrosting

performances as observed from photographs in Fig. 7.1. For the measured tube surface temperature at the exit of the lowest circuit, no sharp increase was observed until ~ 500 s into defrosting, suggesting its thermal load imposed was significantly higher. The exit temperature of the lowest circuit reached 24 °C finally when the defrosting operation was terminated, but at that instance, the tube surface temperatures at the exits of the top and the second top circuit already reached ~ 42 °C. Hence, termination of the defrosting operation for the entire coil was directly influenced by the defrosting performance on the airside of the lowest circuit.
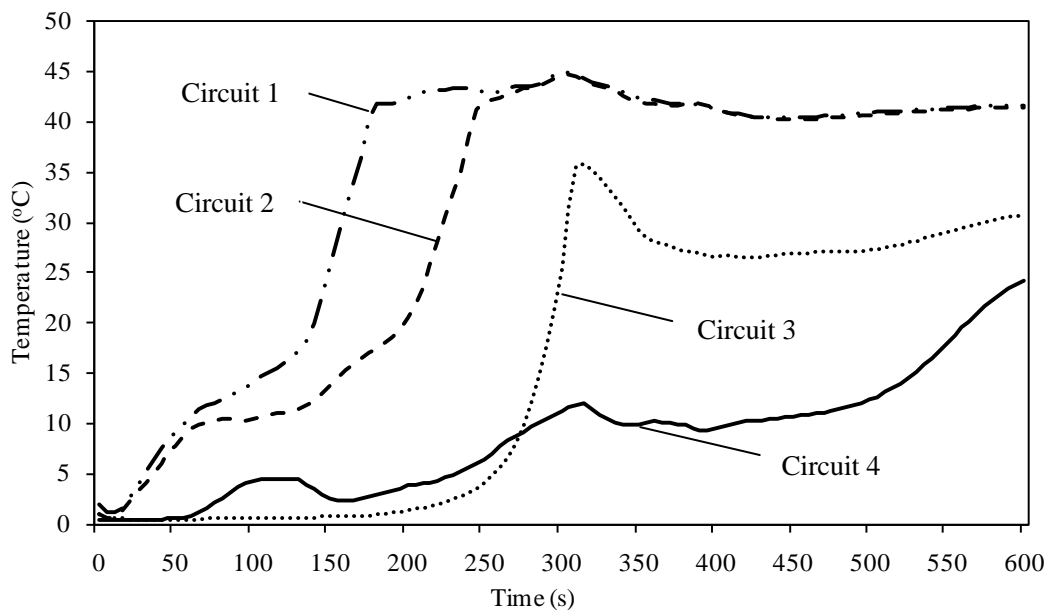
Fig. 7.2 Measured tube surface temperatures at the exits of the four refrigerant circuits during defrosting operation

Fig. 7.3 shows the measured variation profiles of compressor discharge pressure and suction pressure during defrosting operation. Both were relatively stable at ~ 16 bar

(discharge) and 4 bar (suction), respectively. In addition, the measured total refrigerant flow rate during the entire defrost operation is presented in Fig. 7.4. As seen, the refrigerant flow rate increased to its maximum value of 0.030 kg/s at ~ 305 s into defrosting, and then it stabilized at about 0.024 kg/s.
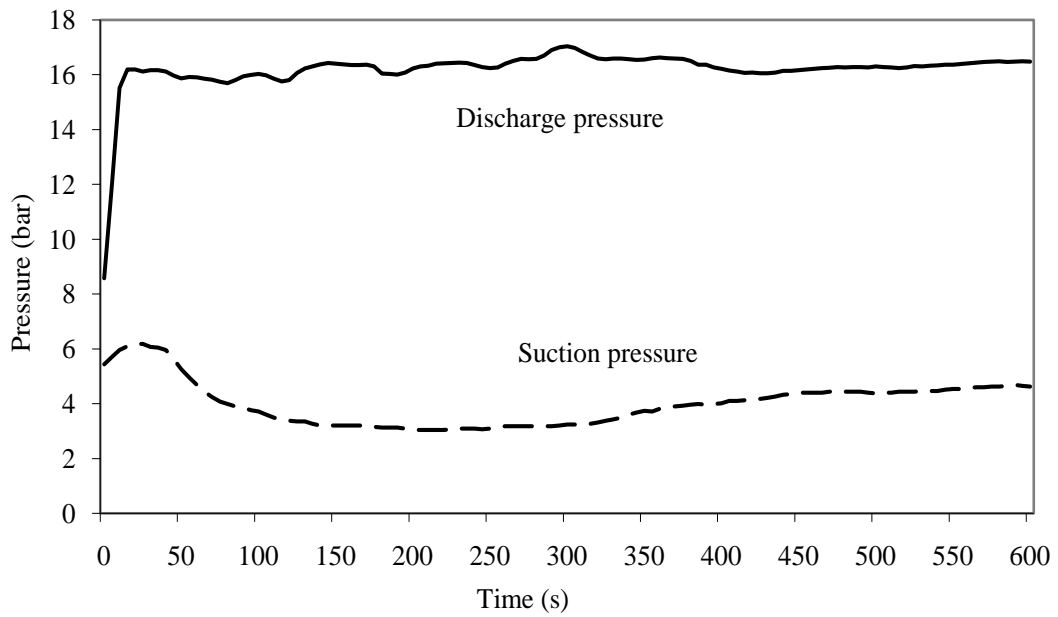
Fig. 7.3 Measured compressor discharge pressure and suction pressure during

defrosting operation
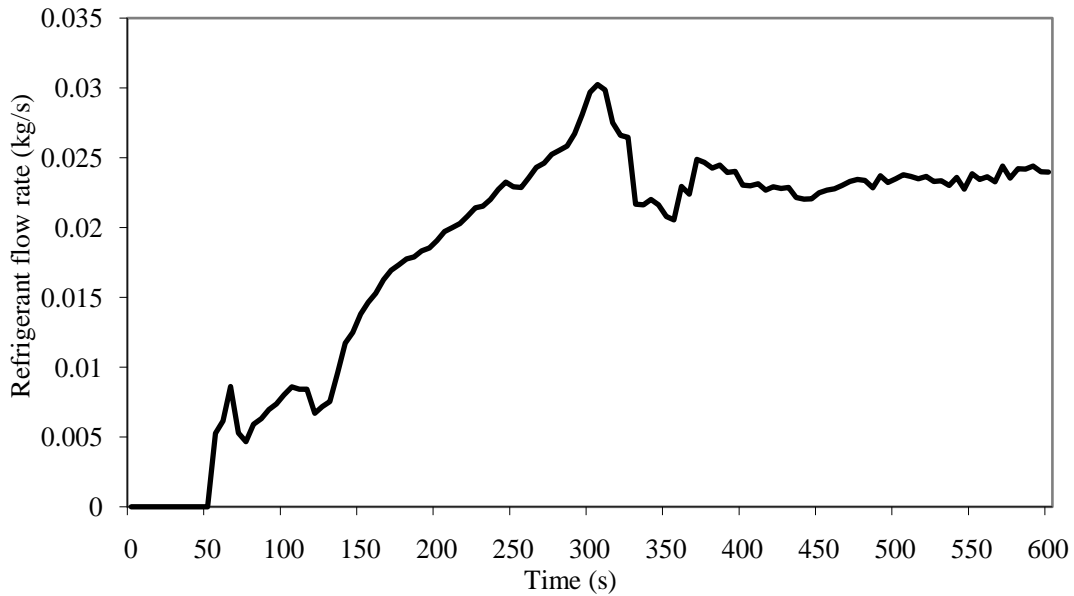
Fig. 7.4 Measured refrigerant flow rate during defrosting operation

Furthermore, melted frost flowing downwards by gravity from high level along the coil surfaces of lower circuit(s) was finally collected in the water collecting pan. Fig. 7.5 shows the measured temperature variation profile of the melted frost collected in the pan during defrosting. As seen, water temperature increased steadily from ~ 120 s into defrosting operation and reached its maximum of 26 ºC at 340 s. Thereafter, water temperature gradually dropped. At the end of defrosting operation, water temperature at the collecting pan was at about 17 ºC. Therefore, there existed a peak of the measure temperature of the melted frost, occurring at ~ 340 s. There can be two possible reasons for this. Firstly, as seen in Fig. 7.4, the measured refrigerant flow rate began to decrease at ~ 305 s, hence the heat provided to the melted frost was also reduced, causing a decrease in the temperature of the melted frost collected in the pan. Secondly, after all the frost on the coil surface was melted, no more

136

melted frost would flow into the collecting pan. Therefore, the temperature of the melted frost, which was warmer than ambient air, would drop as it lost heat to ambient air and water vaporization.
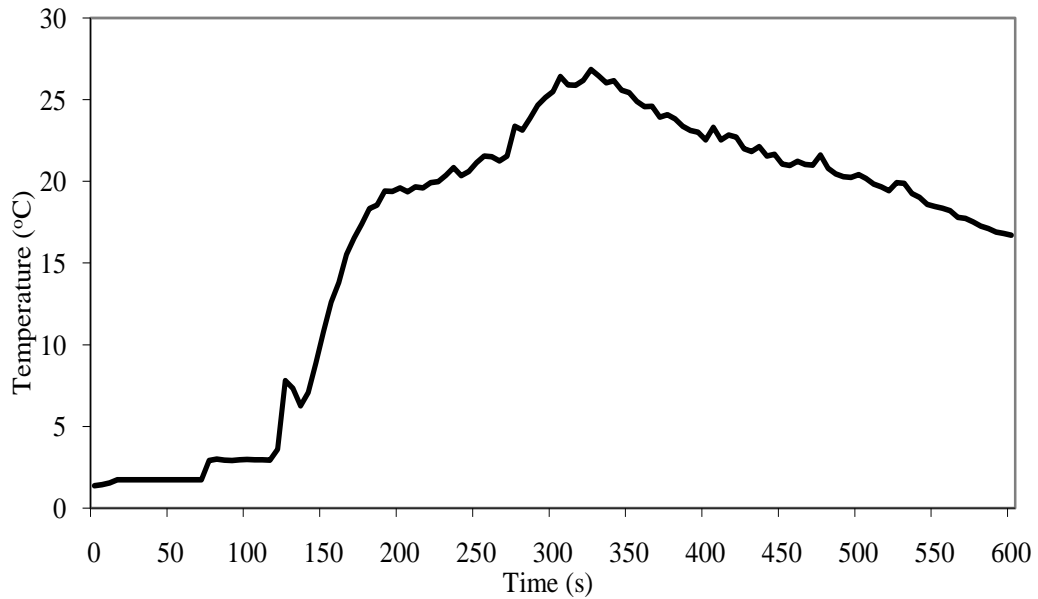
Fig. 7.5 Measured temperature variation profile of melted frost in the water collecting pan during defrosting operation

7.4 Effects of downwards flowing of melted frost along coil surface on defrosting performance

As understood, a number of factors, such as the total mass and structure of frost formed on outdoor coil surface, the ambient air temperature/humidity, etc., may affect defrosting performance of an ASHP unit. However, although the defrosting

137

performance on the airside of an outdoor unit having multiple refrigerant circuits may be influenced by these factors, the downwards flowing melted frost, or water, due to gravity, along coil surface would certainly have a role to play during defrosting, leading to two problems as observed in the experimental work reported in this Chapter.

Firstly, the melted frost was at a temperature significantly lower than that of the outdoor coil surface. Allowing it to travel longer on coil surface than necessary resulted in some heat taken away by the melted frost, causing energy waste by unnecessarily heating up the melted frost. As a result, the temperature of melted frost in the water collecting pan increased with time, as illustrated in Fig. 7.5.

Secondly, on the airside of lower level circuits in a multi-circuit outdoor coil, there were not only the frost formed there, but also the melted frost flowing downwards from the upper level circuits, leading to a greater thermal load there. This was believed to be an important reason why it took a longer time for the surface temperature at the exit of the bottom circuit to reach the termination temperature, as suggested by Fig. 7.2. A delayed ending time certainly increased the total amount of heat provided to the outdoor coil, reducing the defrosting efficiency accordingly.

To practically solve the above two problems observed, i.e., taking heat away from the outdoor coil by the downwards flowing of the melted frost and a prolonged

defrosting duration, a water collecting pan on the airside directly under each of the circuits may be added. With this, the melted frost can only freely flow down by gravity within the airside surface area of a particular refrigerant circuit itself and will not interfere with the operation on the airside of the other circuits, so that the two observed problems might practically solved.

7.5 Evaluation of defrosting efficiency

Defrosting efficiency was an important parameter for evaluating defrosting operation [Kerschbaumer 1971, Stoecker et al. 1983, Krakow et al. 1993b, Jhee et al. 2002, Hoffenbecker et al. 2005]. It was defined as a ratio of the actual amount of heat required both to melt the accumulated frost and to vaporize the retained water to the total amount of heat provided to the outdoor coil during the entire defrosting operation.

Defrosting efficiency for the experimental ASHP unit was evaluated by:

$$\eta_d = \frac{Q_m + Q_v}{\sum Q_j} \qquad (7.1)$$

where Q_m and Q_v are the heat needed to melt the frost and to vaporize the retained

water, respectively, as evaluated by Eqs. (7.2) and (7.3):

$$Q_m = M_f L_{sf} \tag{7.2}$$

$$Q_v = M_v L_v \tag{7.3}$$

where M_f and M_v are the total mass of frost formed on the outdoor coil and the mass of vaporized melted frost, respectively. L_{sf} and L_v are latent heat of melting and latent heat of evaporation of water, respectively.

In this study, the total mass of frost formed on the outdoor coil calculated by using Equations (4.1) to (4.4), M_f, and the melted frost collected in the collecting pan at the end of defrosting operation were 1.34 kg and 1.22 kg, respectively. The difference between the two, 0.12 kg, was taken as the mass of vaporized melted frost, M_v.

To estimate the total amount of heat provided to the outdoor coil during the entire defrosting operation, $\sum Q_j$, the refrigerant flow rate to each circuit was assumed to be the same. Then the heat supplied to each circuit, Q_j, can be evaluated by:

$$Q_j = \int_0^{t_d} q_j dt \quad (j\text{=}1\text{-}4) \tag{7.4}$$

$$q_j = m_{r,j}(h_i - h_e) \quad (j\text{=}1\text{-}4) \tag{7.5}$$

where j=1 refers to the top circuit, j=2 the 2nd top circuit, j=3 the 3rd top circuit and j=4 the bottom circuit, respectively. t_d is the duration of defrosting operation, and was 600 s in the current study.

Using Equations (7.1) to (7.5), the defrosting efficiency was evaluated at 34.5%, which was smaller than the defrosting efficiency range of 40.4% and 58% obtained in a previous simulation study for a single circuit outdoor coil [Krakow et al. 1993b]. This was considered reasonable as in a multi-circuit outdoor coil, allowing melted frost to freely flow downwards would lead to a prolonged defrost operation, thus a lower defrosting efficiency was expected. Furthermore, there can be other factors influencing the defrosting efficiency, including, for example, ambient air dry-bulb temperature and RH, duration for heating (frosting) operation, etc, all of which would affect the amount and the density of frost formed on the coil surface. In addition, the distribution of the frost formation on the outdoor coil during frosting and the distribution of refrigerant flow during defrosting would also affect on the defrosting efficiency.

In order to quantitatively analyze the effects of downwards flowing of melted frost along a multi-circuit outdoor coil surface of an ASHP unit on its defrosting performance, a modeling analysis has been carried out, to be reported the in Chapter 8.

7.6 Conclusions

This Chapter reports on the experimental part of a study of reverse cycle defrosting performance on a four-circuit outdoor coil in a 6.5 kW heating capacity experimental ASHP unit. It was observed that defrosting was quicker on the airside of upper circuits than that on the lower circuits. The effects of downwards flowing of the melted frost along a multi-circuit outdoor coil surface were discussed, and finally, the defrosting efficiency was evaluated at 34.5%. On the other hand, the modeling part of the study is to be reported in next Chapter.

Chapter 8

Modeling Analysis of the Reverse Cycle Defrosting Performance on a Multi-circuit Outdoor Coil Unit in an ASHP

8.1 Introduction

A study on the impact of allowing melted frost to flow down freely along the multi-circuit coil surface on defrosting performance has been carried out, using both experimental and modeling analysis approaches. The experimental part of the study on the defrosting performance on a four-circuit outdoor coil surface in the experimental ASHP unit is reported in Chapter 7. This Chapter presents the modeling part.

As mentioned in Chapter 2, although defrosting models were previously developed and used in studying defrosting performance, none of them in fact considered the effects of downwards flowing of the melted frost due to gravity along an outdoor coil surface on the defrosting performance, by either assuming a stable water layer or the absence of water retention on coil surface [Krakow et al. 1992a, 1992b, 1993a, 1993b, Liu et al. 2003, Sherif and Hertz 1998, Al-Mutawa and Sherif 1998a, 1998b, Alebrahim and Sherif 2002, Hoffenbecker et al. 2005, Dopazo et al. 2010]. However, the experimental study on a nominal 3-ton residential ASHP unit reported by Payne and O'Neal [1995] suggested that after ~ 1 hour frosting at 1.7 ºC dry-bulb

temperature and 80% relative humidity, and ~ 7 min defrosting, over 1.6 liter of melted frost was collected. This amount of water flowing downwards due to gravity on the entire outdoor coil would affect defrosting as additional thermal resistance was introduced [Cheng and Seki 1991]. On the other hand, the experimental results and their related discussion presented in Chapter 7 also clearly suggested that downwards flowing of the melted frost along the surface of a multi-circuit outdoor coil of an ASHP unit would have negative effects on defrosting performance, in terms of both taking heat away from the outdoor coil and prolonging a defrost operation.

In this Chapter, firstly, a semi-empirical defrosting model for the four-circuit outdoor coil of the experimental ASHP unit, the first of its kind, which was developed based on both the fundamentals of mass and energy conservation and using the experimental data reported in Chapter 7, is presented. Secondly, the model was validated by comparing the predicted defrosting duration and the temperature variation of the collected melted frost with the corresponding experimental results reported in Chapter 7. Finally, using the validated model, the negative effects of downwards flowing of the melted frost along the surface of a multi-circuit outdoor coil on defrosting performance were quantitatively analyzed and are reported.

8.2 Development of the semi-empirical mathematical model

In this study, a defrosting process on the airside of an outdoor coil was subdivided into three stages: frost melting without water flow, frost melting with water flow and water layer vaporizing. A defrosting process began with frost melting without water flow. In this stage, all the melted frost could be held on finned coil surface due to surface tension until the mass of the melted frost held reached its maximum [Krakow et al. 1992b, Hu 2010]. Then the second stage started. Along with the frost melting, the melted frost flowed downwards by gravity. When coil surface was free of frost, the second stage ended and the water layer vaporizing stage began. The retained water was vaporized into ambient air until the coil surface became dry, when the third stage as well as the entire defrosting process ended.

When developing the semi-empirical model, the entire airside of the four-circuit outdoor coil surface was divided into four control volumes, respectively, as shown in Fig. 8.1. For each control volume, the lumped parameter modeling approach was applied. In addition, the water collecting pan placed under the bottom circuit to collect the melted frost flowing down from the outdoor coil surface was also modeled as part of the semi-empirical model. When modeling the collecting pan, three stages were also assumed during defrost. In the first stage, the melted frost or water flowing down from the airside of the bottom (or the fourth) circuit would stay on the pan surface due to surface tension until the arrival of the maximum that could

be held by the pan, when the second stage started. In the second stage, the amount of melted frost flowing out from the collecting pan was equal to that flowing into the pan, i.e., the flow of collected melted frost in the pan was in a dynamic equilibrium. Finally in the third stage, after the frost melting process, no melted frost fell into the collecting pan. The temperature of the melted frost was measured by a thermal couple placed near the drainage outlet, as shown in Fig. 8.1.
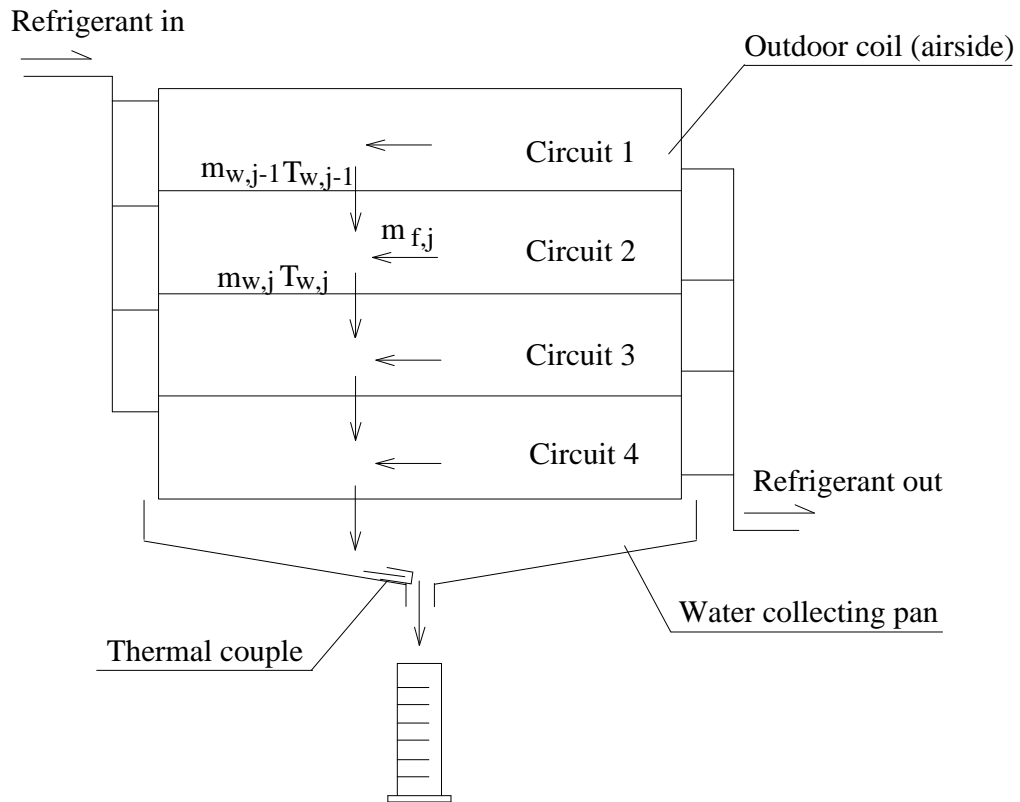
Fig. 8.1 Conceptual model for the airside of the four-circuit outdoor unit during

reverse cycle defrosting

8.2.1 Assumptions and calculation conditions

The model was developed based on fundamentals of mass and energy conservation, heat and mass transfer within each of control volumes at each stage of the defrosting process, and using also experimental data reported in Chapter 7.

When establishing the model, the following were assumed:

i)   During the second stage, the retained water in each control volume was in a dynamic equilibrium, i.e., the difference between the mass of water entering and that leaving a control volume was equal to the rate of frost melting within the control volume.

ii) The heat conductivities of the tubes and fins were much higher than those of frost and melted frost, and hence their heat resistances were neglected.

iii) The mass flow rate of refrigerant was evenly distributed into the four refrigerant circuits during defrosting, and the frost was assumed to be uniformly accumulated over the coil surface before starting defrosting.

iv) Heat exchanges between refrigerant and frost/ambient air in the superheated region and the sub-cooling region in the outdoor coil were very small, and therefore neglected during defrosting. The entire outdoor coil was regarded as having a two-phase region only.

v) During defrosting, the melted frost infiltrated into frost's porous structure. The contact area between the melted frost and frost would increase as water flowing downwards, suggesting that the flow resistance increased downwards along the outdoor coil. Therefore, the velocity of water layer in each control volume should decrease from top to bottom circuit.

vi) The movement of the water layer was considered to be a flowing boundary. Because the velocity of the water flow was very small as observed during experiments, water layer flowed in laminar regime.

vii) In the process of melted frost falling into the pan, the heat dissipated from the melted frost to the ambient air was negligible because the falling distance was small.

Furthermore, the following experimental data reported in Chapter 7 were also used in assisting the model development:

a) The total mass of the frost experimentally obtained was at 1.34 kg, thus following Assumption iii), the mass of frost formed on the surface of each circuit, $M_{f,j}$ (j=1-4), was 0.335 kg (1.34/4 kg).

b) The mass of vaporized melted frost experimentally obtained was at 0.12 kg, so that the maximum surface water on each circuit, $M_{w,max}$, was 0.03 kg (0.12/4 kg).

c) At 90 s into defrosting, the melted frost on the water collecting pan reached its maximum that could be held.

d) The experimentally obtained refrigerant flow rate, inlet and exit temperature of the outdoor coil, and the compressor discharge pressure during the defrosting process, as shown in Figs. 7.2 to 7.4 in Chapter 7, were used as the inputs to the model developed.

8.2.2 Model development

8.2.2.1 Outdoor coil

Using assumptions and experimental data as detailed in Section 8.2.1, the semi-empirical model was developed as follows.

The applications of the mass and energy conservation, for control volume j, in each stage shown in Fig. 8.2, are given by Equations (8.1) to (8.14).
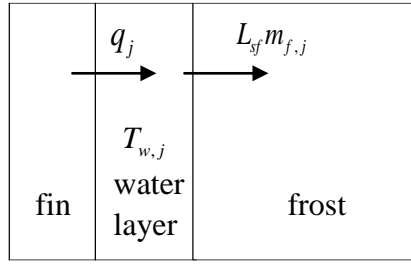
a) first stage
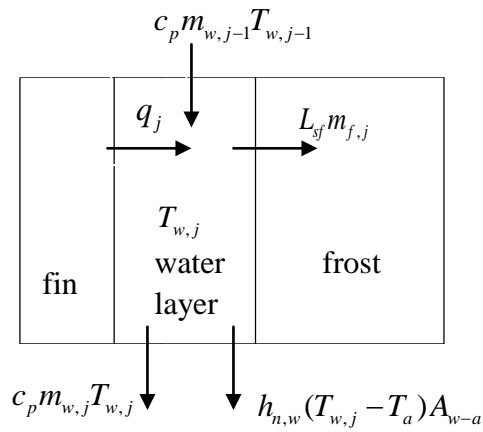
b) second stage
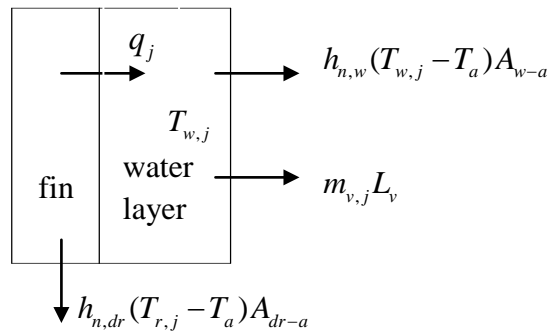
c) third stage

Fig. 8.2 Schematics of the airside heat transfer among fin, water layer and frost in

each of the four control volumes during the three stages

<u>First stage: frost melting without water flow</u>

At this stage, as shown in Fig. 8.2 a), energy and mass conservation in control volume j yielded:

$$q_j \Delta t = L_{sf} m_{f,j} \Delta t + c_p \Delta(M_{w,j} T_{w,j}) \tag{8.1}$$

As $\Delta t \rightarrow 0$, Eq. (8.1) can be written as follows:

$$q_j = L_{sf} m_{f,j} + c_p \frac{d(M_{w,j} T_{w,j})}{dt} \tag{8.2}$$

where $M_{w,j}$ is accumulated mass of retained melted frost in the control volume, j:

$$M_{w,j} = \int_0^t m_{f,j} dt \tag{8.3}$$

Meanwhile, the heat transfer in control volume j could be expressed as:

$$q_j = \frac{T_{r,j} - T_{ICW,j}}{R_r} \tag{8.4}$$

where T_{ICW} is the temperature at the interface between the coil surface and the water layer.

On the other hand, q_j was evaluated by:

$$q_j = m_{r,j}(h_{r,i} - h_{r,e}) \qquad (8.5)$$

where $m_{r,j}$ is refrigerant mass flow rate in control volume j. Enthalpies of refrigerant at both inlet and exit of the outdoor coil, $h_{r,i}$ and $h_{r,e}$, were evaluated from the measured inlet and outlet temperatures and the measured compressor discharge pressure.

Second stage: frost melting with water flow

As shown in Fig. 8.2 b), energy conservation in control volume j, taking into account the convective heat transfer between the water layer and the ambient air, required:

$$q_j + c_p m_{w,j-1} T_{w,j-1} = L_{sf} m_{f,j} + c_p M_{w,max} \frac{dT_{w,j}}{dt}$$
$$+ c_p m_{w,j} T_{w,j} + h_{n,w}(T_{w,j} - T_a) A_{f-a} \qquad (8.6)$$

where $M_{w,max}$ is the maximum mass of surface water on each refrigerant circuit, and $h_{n,w}(T_{w,j} - T_a) A_{f-a}$ is the heat transferred to the ambient air from effective airside surface area covered by only the melted frost in control volume j.

Mass conservation in control volume j was:

$$m_{w,j} = m_{f,j} + m_{w,j-1} \qquad (8.7)$$

On the other hand, the heat transferred from the water layer to frost layer for melting the frost and to the ambient air was:

$$h_w(T_{w,j} - T_{tp})A_o = L_{sf}m_{f,j} + h_{n,w}(T_{w,j} - T_a)A_{f-a} \qquad (8.8)$$

Third stage: water layer vaporizing

In the third stage, the surface of outdoor coil was free of frost, and vaporization of retained water took place. As illustrated in Fig. 8.2 c), energy and mass conservation in control volume j yielded:

$$q_j = c_p \frac{d(M_{w,j}T_{w,j})}{dt} + h_{n,w}(T_{w,j} - T_a)A_{w-a}$$
$$\qquad\qquad (8.9)$$
$$+ h_{n,dr}(T_{r,j} - T_a)A_{dr-a} + m_{v,j}L_v$$

where $h_{n,w}(T_{w,j} - T_a)A_{w-a}$ is the heat transferred to the ambient air from the water layer in control volume j, and the $h_{n,dr}(T_{r,j} - T_a)A_{dr-a}$ the heat transferred to the ambient air from the dry coil surface in control volume j.

$$M_{w,j} = M_{w,max} - \int_0^t m_{v,j}dt \qquad (8.10)$$

where $m_{v,j}$ is the vaporization rate of surface water and was proportional to the difference in vapor pressure between the exposed water surface and the ambient air as described by Mills [1995] , expressed as:

$$m_{v,j} = h_D A_{w-a} (\rho_{vs,j} - \rho_{va})$$ (8.11)

where A_{w-a} is the effective wetted airside surface area of the refrigerant circuit in the third stage. As the vaporizing process continued, the area was diminishing. The relationship between the effective wetted airside surface area and the equivalent airside surface area of the refrigerant circuit was [Krakow et al. 1992b, Hu 2010]:

$$A_{w-a} = A_o \left(\frac{M_{w,j}}{M_{w,max}} \right)^{1.5}$$ (8.12)

Effective airside surface area covered by only the melted frost of a refrigerant circuit in the second stage, A_{f-a}, was similarly evaluated:

$$A_{f-a} = A_o \left(\frac{\int_0^t m_{f,j} dt}{M_{f,j}} \right)^{1.5}$$ (8.13)

Then, the effective dry airside surface area of the refrigerant circuit in the third stage, A_{dr-a}, was:

$$A_{dr-a} = A_o - A_{w-a} \tag{8.14}$$

The heat transfer resistance on the refrigerant side, R_r, was determined by:

$$R_r = \frac{1}{h_{tp} A_i} \tag{8.15}$$

where A_i is the internal surface area of the refrigerant tube in a four-circuit outdoor coil. h_{tp} is the heat transfer coefficient on the refrigerant side in the two-phase region, determined by [Shah 1979]:

$$h_{tp} = h_L (0.55 + \frac{2.09}{p_r^{0.38}}) \tag{8.16}$$

where h_L is the refrigerant side heat transfer coefficient assuming that all refrigerant is liquid, evaluated using the *Dittus-Boelter* Equation [Kays and London 1984]:

$$h_L = 0.023 \, \mathrm{Re}_r^{0.8} \, \mathrm{Pr}_r^{0.4} \, \lambda / D \tag{8.17}$$

and p_r is the reduced pressure, determined by [Shah 1979]:

$$p_r = \frac{P_{sat}}{P_c} \tag{8.18}$$

where P_{sat} is the saturated discharge pressure of refrigerant and P_c is critical pressure

for R22, equals to 4.99MPa.

The coefficient of convective heat transfer caused by water flow adopted that for

local laminar forced convective heat transfer [Liu et al. 2003]:

$$h_{w,x} = 0.332 \frac{\lambda}{x} \text{Re}_{w,x}^{\frac{1}{2}} \text{Pr}_w^{\frac{1}{3}}$$

(8.19)

The average coefficient of convective heat transfer caused by water flow inside a

control volume was evaluated by:

$$h_w = \int_{jH}^{(j+1)H} h_{w,x} dx \bigg/ H$$

(8.20)

To obtain the coefficient of convective heat transfer caused by water flow, based on

Assumption v) and the experimental observation, the velocity of water layer in each

control volume would decrease from top to bottom circuit, and could be estimated

by:

$$v_{w,j} = \frac{H}{t_{d,1}} 0.85^{j-1}$$

(8.21)

where $t_{d,1}$ is defrosting duration in Circuit 1. The exact numerical values used in

Equation (8.21) were chosen based on experimental data obtained, for example, a value of 150 s was used for $t_{d,1}$.

During the entire defrosting process, the outdoor air fan was switched off and the heat transfer from the outdoor coil to the ambient air was dominated by natural convection. The Nusselt Number of natural convection and the corresponding coefficient of natural convective heat transfer coefficient were used [Jaluria 1980]:

$$Nu = \frac{h_n H}{\lambda_a} = 0.13(Gr\,Pr_a)^{\frac{1}{3}}, \text{ for } 10^9 < GrPr_a < 10^{13} \qquad (8.22)$$

where

$$Gr = \frac{g\beta(T_w - T_a)}{v^2} H^3 \qquad (8.23)$$

The coefficient of convective mass transfer, h_D, was related to the coefficient of natural convective heat transfer, h_n, by the Lewis Analogy [Threlkeld 1970, Padki et al. 1989]:

$$h_D = \frac{h_n}{c_p \rho_a (Le)^{\frac{2}{3}}} \qquad (8.24)$$

where Le is the Lewis number for air and water vapor mixtures and a fixed value of

0.845 was adopted in this study [ASHRAE 2009].

8.2.2.2 Water collecting pan

$$h_n A_{pw}(T_{pw} - T_a) \uparrow \qquad \downarrow c_p m_{w,4} T_{w,4}$$

$$\boxed{T_{pw}}$$

a) first stage

$$h_n A_{pw}(T_{pw} - T_a) \uparrow \qquad \downarrow c_p m_{w,4} T_{w,4}$$

$$\boxed{T_{pw}}$$

$$\downarrow c_p m_{w,4} T_{pw}$$

b) second stage

$$h_n A_{pw}(T_{pw} - T_a) \uparrow \qquad \uparrow m_{v,pw} L_v$$

$$\boxed{T_{pw}}$$
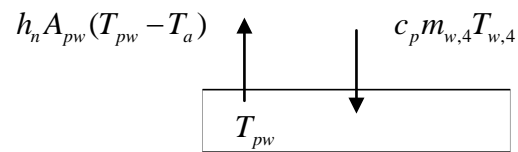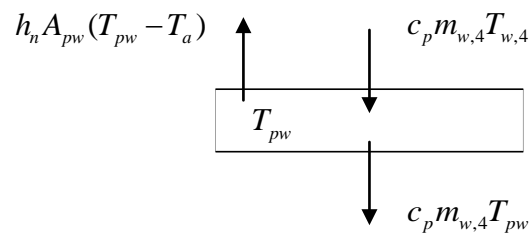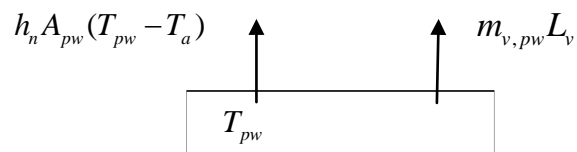
c) third stage

Fig. 8.3 Schematics of the heat transfer in the water collecting pan during the three

stages

Fig. 8.3 shows the schematics of the heat transfer in the collecting pan. Eq. (8.25) is

for the energy conservation of the collected melted frost in the first stage:

$$c_p m_{w,4} T_{w,4} = c_p \frac{d(M_{pw} T_{pw})}{dt} + h_n A_{pw}(T_{pw} - T_a) \tag{8.25}$$

where M_{pw} is the accumulated mass of the retained melted frost in the water

collecting pan, which can be evaluated using Eq. (8.3).

In the second stage, energy conservation yielded:

$$c_p m_{w,4} T_{w,4} = c_p M_{pw,max} \frac{dT_{pw}}{dt} + h_n A_{pw}(T_{pw} - T_a) + c_p m_{w,4} T_{pw} \tag{8.26}$$

where $M_{pw,max}$ is the maximum mass of the retained water in the water collecting pan.

In the third stage, energy conservation of the collected melted frost required:

$$c_p \frac{d(M_{pw} T_{pw})}{dt} = m_{v,pw} L_v + h_n A_{pw}(T_{pw} - T_a) \tag{8.27}$$

where M_{pw} can be evaluated using Eq. (8.10).

Eqs. (8.25) to (8.27) are the governing equations for predicting melted frost temperature in the collecting pan.

8.2.3 Calculation method

Euler's method [Gerald and Wheatley 2003] was applied to solving all the differential equations (8.2), (8.6), (8.9) and (8.25) to (8.27), with a time step of 5 s. The mass flow rate and temperature of melted frost leaving a control volume were regarded as those of the melted frost entering the adjacent lower control volume. Similarly, the thermal properties of the melted frost leaving the bottom control volume (i.e., j=4) were regarded as those of melted frost entering the water collecting pan.

8.3 Results and discussions

8.3.1 Model validation

The model presented in Section 8.2 was validated by comparing the predicted defrosting duration and the temperature variation of collected melted frost with corresponding experimental data reported in Chapter 7. The experimental defrosting

duration, as reported in Chapter 7, was 600 s. Using the model developed, at 600 s

into defrosting operation, 96.2% of the water retained on the surface of the entire

outdoor coil was vaporized.
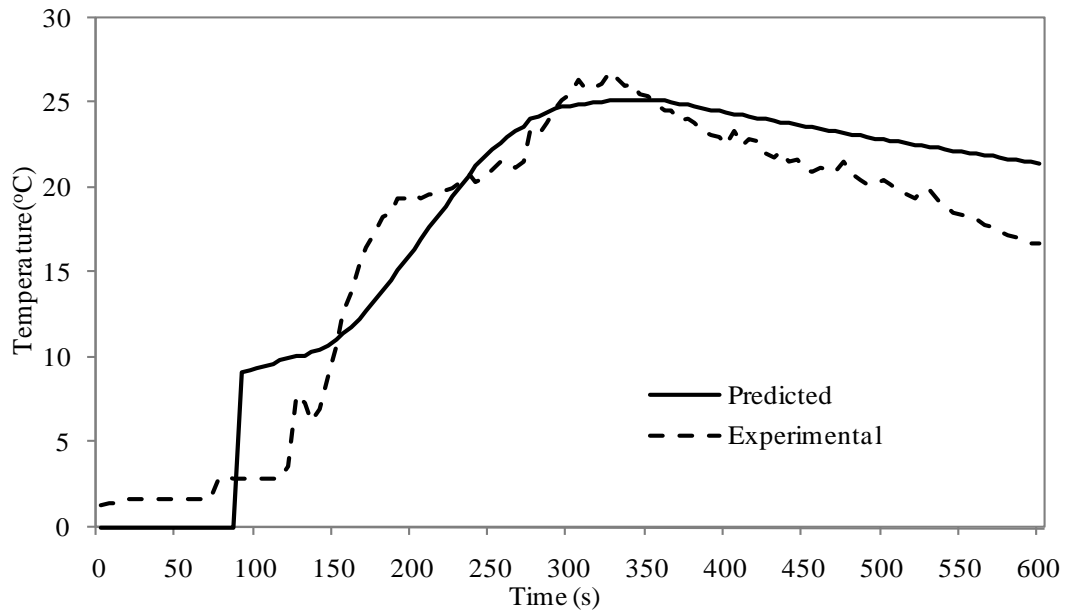
Fig. 8.4 Experimental and predicted temperatures of the melted frost in the water

collecting pan

Furthermore, Fig. 8.4 shows the experimental and predicted melted frost

temperatures in the water collecting pan. As seen, the predicted temperature of the

melted frost in the collecting pan began to increase at 90 s into defrosting. At 360 s

into defrosting, melting on the bottom circuit ended, and no melted frost flowed

down to the water collecting pan thereafter. Then the melted frost temperature in the

collecting pan began to decrease due to both the heat transfer from the melted frost

to ambient air and water vaporization. As seen in Fig. 8.4, the predicted temperature

of the melted frost using the model developed agreed reasonably well with the experimental data.

8.3.2 Modeling analysis of the negative effects of downwards flowing melted frost

The validated semi-empirical model was used to analytically study the negative effects of downwards flowing of the melted frost along the experimental four-circuit outdoor coil surface on defrosting performance.

Figs. 8.5 and 8.6 show the predicted mass flow rate and temperature of melted frost flowing over the surface of each of the four circuits. As shown in Fig. 8.5, the mass flow rates of melted frost increased from the Circuit 1 to Circuit 4. This was because the downwards flowing melted frost along the surface of a circuit should be the summary of the melted frost flowing in from the circuit above and the melted frost generated inside this circuit.

As shown in Fig. 8.6, the temperature of melted frost on the surface of each of the four circuits increased with the defrosting time. When the melted frost began to flow downwards at 55 s, the melted frost temperature on each circuit was all at ~ 17 $^{\circ}$C. Afterwards, the temperature of melted frost on each of the four circuits decreased for
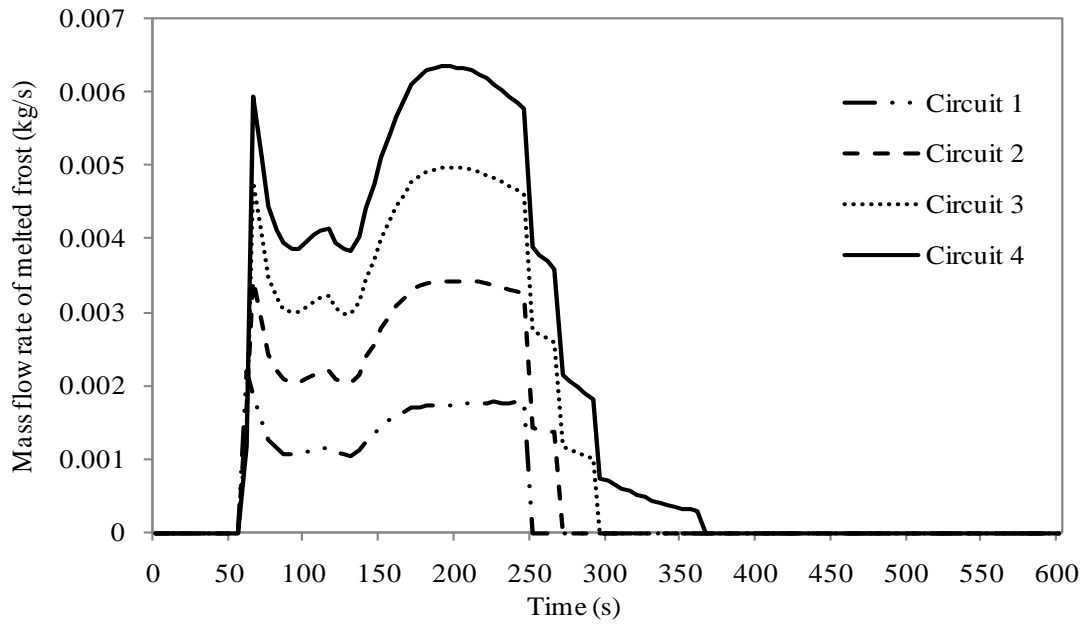
Fig. 8.5 Predicted mass of melted frost flowing over the surface of each of the four

circuits using the validated model
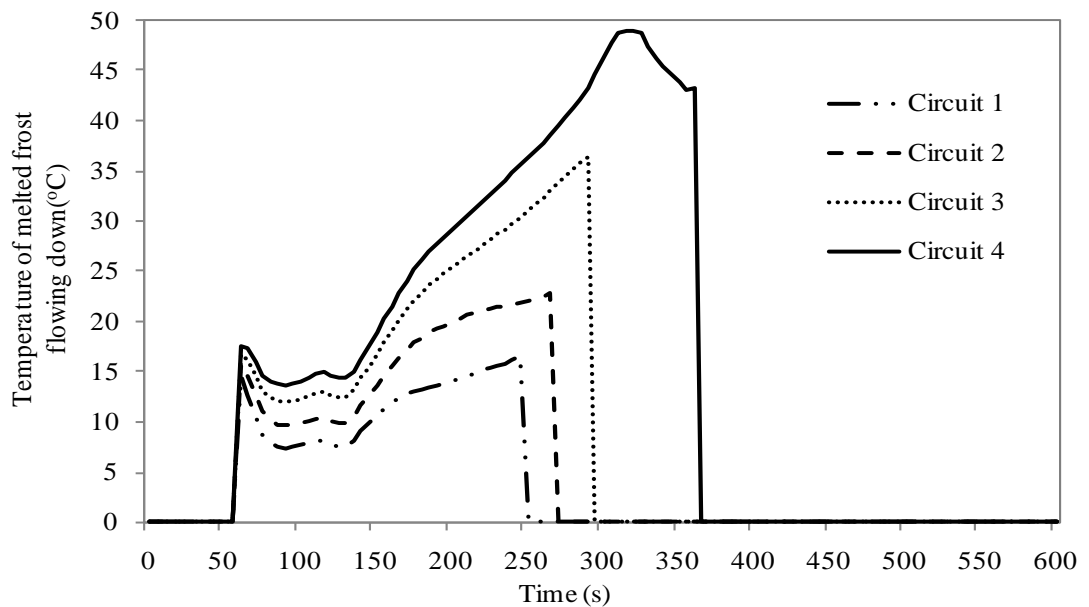
Fig. 8.6 Predicted temperature of melted frost flowing over the surface of each of the

four circuits using the validated model

163

a while before starting to increase. This may be explained by the fact that heat from the downwards flowing melted frost was initially absorbed by the frost, causing the decrease in water temperature. As the defrosting process went by, more frost was melted, so that less heat was absorbed by frost, and the temperature of melted frost would increase. At the respective end of frost melting process in each circuit, the temperatures of melted frost on Circuit 1 to Circuit 4 reached 16.6 $^{\circ}$C, 23.0 $^{\circ}$C, 36.5 $^{\circ}$C and 49.0 $^{\circ}$C, respectively.

The predicted frost-melting rate on the surface of each of the four circuits is presented in Fig. 8.7. As seen, the frost-melting rates on all four circuits were the same up to 55 s into defrosting operation, following the Assumption iii). Thereafter, when the melted frost started to move downwards, all frost-melting rates increased because frost absorbed heat from not only the outdoor coil itself but also moving melted frost. On the other hand, frost-melting rates at circuits of different levels were not the same, the higher the level, the higher the melting rate. This was because as the melted frost flowed downwards, more melted frost would flow through the circuits at lower level, taking more heat away, and leading to a longer defrosting duration there. Towards the end of frost melting, frost-melting rate on each of the four circuits was respectively reduced, because of the reduced refrigerant mass flow rate (shown in Fig. 7.4 in Chapter 7) and the increased heat loss from the exposed water layer to ambient air.
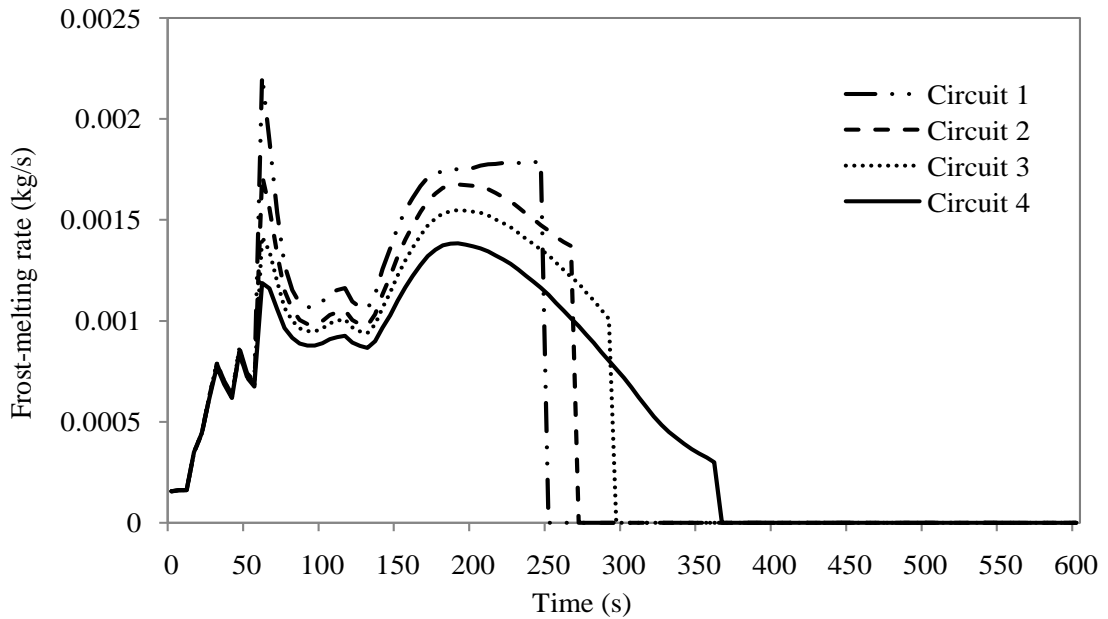
Fig. 8.7 Predicted frost-melting rate on the surface of each of the four circuits using

the validated model

Furthermore, using the validated model, the predicted heat used to melt the frost, to vaporize the retained water, to heat up the melted frost, and heat loss to the ambient air accounted for 20.3%, 14%, 10%, and 55.7% of the total amount of heat provided to the outdoor coil, respectively. As discussed in Chapter 7, the downwards flowing of the melted frost along the outdoor coil surface not only took away part of the heat supposed to be used for defrosting, but also prolonged the defrosting on lower level circuits, and thus the entire defrosting operation. Model predictions indicated that the frost melting ended at 245 s, 265 s, 290 s, and 360 s, from the top circuit to the bottom circuit (Circuit 1 to Circuit 4), respectively. This was consistent with the experimental observation that frost melting process on higher level circuits ended earlier than that on lower level circuits.

Consequently, energy was wasted because while frost-melting was still going on at lower circuits, higher level circuit(s) was already free of frost or even retained water, and heat loss to ambient air surrounding the higher level circuits took place. Therefore, a decrease in defrosting efficiency would be resulted in. If melted frost can be drained locally without flowing downwards along the surface of lower level circuits, the defrosting duration at all circuits may be leveled. Using the validated model, the predicted defrosting efficiency would be 40.8% when melted frost was locally drained. Comparing to the defrosting efficiency (34.5%) reported in Chapter 7, an increase of 18.3% in defrosting efficiency can be achieved.

8.4 Conclusions

In order to quantitatively analyze the effects of downwards flowing of the melted frost along the multi-parallel circuit outdoor coil surface of the experimental ASHP unit on its defrosting performance, a semi-empirical mathematical model, the first of its kind, has been developed and is reported in this Chapter. The model was validated by comparing the predicted defrosting duration and the temperature variation of the collected melted frost with those corresponding experimental results reported in Chapter 7.

Using the validated model, the effects of downwards flowing of the melted frost of along the four-circuit outdoor coil surface on defrosting performance were quantitatively analyzed. The analysis showed that frost melting ended at 245 s, 265 s, 290 s, and 360 s, respectively, from the top circuit to the bottom circuit. This was consistent with the experimental observation that frost melting at upper level circuits ended earlier than that on lower level circuits.

The model prediction results also suggested that although the energy used to heat the melted frost only accounted for about 10% of the total amount of heat provided to the outdoor coil during defrosting, downwards flowing of melted frost along outdoor coil surface actually prolonged the defrosting process at lower level circuits, thus prolonging the entire defrosting operation and reducing the defrosting efficiency. If the melted frost may be drained away locally, an increased of 18.3% in defrosting efficiency, as compared to allowing it to flow downwards, was predicted.

The uneven defrosting performances, as observed experimentally, have been re-confirmed through this modeling analysis, as shown in Figs. 8.5 to 8.7. As long as the melted frost was allowed to flow downwards due to gravity along the circuit surface, uneven defrosting would take place in any outdoor coils even when the frost was uniformly formed on the entire outdoor coil surface and the initial operating conditions on the refrigerant side were the same, as reflected by the assumption used in model development. The model developed and reported in this Chapter provided a

useful tool for studying and understanding the effects of downwards flowing melted

frost on the defrosting performance of a multi-circuit outdoor coil in an ASHP unit.

Chapter 9

An Experimental Investigation on Reverse Cycle Defrosting Performance for an ASHP Unit Using an Electronic Expansion Valve

9.1 Introduction

For a heat pump/refrigeration system, an expansion device is a key component for refrigerant mass flow control to maintain the refrigerant in a superheated state before entering compressor. With a faster response to load variation, a wider range of flow rate regulation and a higher control precision, an electronic expansion valve (EEV) has a robust adaptability to all refrigerants in use under different operating conditions, and therefore can be used to replace other types of expansion devices or throttle regulators, such as a TEV or a capillary tube. In fact, the ranges of EEV applications have expanded gradually and successfully from small-scale to large-scale systems, especially in inverter driven variable speed compressor systems and/or multi-evaporator systems [He et al. 1997, Aprea and Mastrullo 2002, Choi and Kim 2002, Li et al. 2004, Chen et al. 2005, Chen et al. 2008, Jiang et al. 2011].

As mentioned in Chapter 2, the reported studies on the impacts of using various throttle regulators on defrosting performance of ASHPs are available but limited. O'Neal et al. [1991] found that increasing the orifice diameter of a short-tube would

lead to a shorter defrosting duration. Ding et al. [2004] suggested using a solenoid valve to by-pass the TEV in an air-to-water heat pump during defrosting to improve defrosting performance, with a smooth resumption of heating operation after the termination of defrosting. However, no reported studies on the influence of adopting various control strategies for an EEV on the reverse cycle defrosting performance for space heating ASHPs may be identified.

This Chapter reports on an experimental investigation on reverse cycle defrosting operation for the experimental ASHP unit using an EEV as a refrigerant flow throttle regulator. The experimental procedures are firstly presented. This is followed by reporting the results of comparative experiments under two control strategies for the EEV to study their effects on defrosting performance: the EEV being fully open and the EEV being regulated by a degree of refrigerant superheat (DS) controller during defrosting. The experimental results revealed that when the EEV was regulated by the DS controller during defrosting, a higher defrosting efficiency and less heat wastage would be resulted in.

9.2 Experimental method and procedure

The details of the experimental ASHP unit are shown in Chapter 4. The EEV used in the experimental ASHP unit controlled the refrigerant flow through an evaporator by

means of monitoring both refrigerant pressure and temperature at compressor suction. The pressure was used to determine the evaporating temperature, and then difference between the suction temperature and the evaporating temperature was the operating DS. The opening of the EEV was regulated by a proportional-integral-derivative (PID) DS controller to maintain a fixed DS during the ASHP's operation.

Before defrosting, the experimental ASHP unit was operated in the heating (frosting) mode at a frosting outdoor ambient environment of 0 ± 0.1 ℃ (dry-bulb) and 90% $\pm$ 3% relative humidity. During frosting operation, the air temperature inside the heated indoor space was maintained at 22 ℃. The experimental conditions are summarized in Table 9.1.

Defrost was manually initiated after 2 hours of heating (frosting) operation. The compressor in the experimental ASHP unit was firstly switched off, and at the same time the EEV was fully open to accelerate balance the system pressure. One minute after the shut down of compressor, the four way valve was switched to defrosting mode. Four seconds later, the compressor was powered on again and a defrosting operation was started. Both the indoor air fan and the outdoor air fan during defrosting operation were turned off.

Table 9.1 Experimental conditions

Parameters	Values
Heated indoor space	
Temperature (ºC)	22
Frosting outdoor space	
Temperature (ºC)	0 ± 0.1
RH (%)	90 ± 3
Face velocity of outdoor coil (m/s)	1.8 *
Heating (frosting) operation time (h)	2

*: at the beginning of a heating (frosting) operation. It would become lower as the operation progressed.

During defrosting operation, the effects of two control strategies for the EEV on defrosting performance were experimentally investigated: the EEV being fully open (Strategy A), and the EEV being regulated by the DS controller with a DS setting of 5 ºC (Strategy B). The minimum EEV opening was set at 30% of the full opening to avoid a very small refrigerant flow. Defrosting operation was manually terminated when the tube surface temperature at the exit of the lowest refrigerant circuit in the outdoor coil reached 18 ºC [Payne and O'Neal 1995, Ding et al. 2004, Huang et al. 2004].

The following three operating parameters were used to evaluate the defrost

performance under the two EEV control strategies: defrosting duration, defrosting coefficient of performance (COP_d) and defrosting efficiency. Defrosting duration was the time period from defrost initiation to defrost termination. COP_d, was defined as the ratio of the total output heat, $\sum Q_j$, to the electrical energy consumption, W_d, during a defrosting period, t_d.

COP_d was evaluated by:

$$COP_d = \frac{\sum Q_j}{W_d} \qquad (9.1)$$

where W_d and $\sum Q_j$ can be evaluated by Eqs. (5.1) and (7.4), respectively.

Finally, defrosting efficiency was evaluated by Eq. (7.1).

9.3 Experimental results and discussions

Experiments using the experimental ASHP unit on the defrosting performance under the two control strategies for EEV were carried out, and the experimental data were collected only after completing two successively frost/defrost cycles to ensure measuring stability and accuracy. The measured operating performance parameters

during the experiments are presented in this section. The overall system performances during a defrosting period under each of the two control strategies are summarized in Table 9.2.

Table 9.2 Measured defrosting performance of the experimental ASHP unit under the two EEV control strategies

Performance parameter	Strategy A	Strategy B	Unit
Defrosting duration period, t_d	590	575	s
Total output heat during defrosting, Q_d	2628.0	1769.4	kJ
Energy consumption during defrosting, W_d	604.6	592	kJ
Calculated mass of accumulated frost, M_f	1.34	1.34	kg
Collected melted frost	1.22	1.22	kg
Water vaporized, M_v	0.12	0.12	kg
COP_d	4.35	2.98	–
Defrosting efficiency, η_d	28.2	42.9	%

Strategy A: EEV fully open;   Strategy B: EEV regulated by DS controller

The measured defrosting performance parameters are shown in Fig. 9.1 to 9.5. In all these figures, for their time (horizontal) axis, 0 second was the actual starting time for a defrosting operation.

As seen in Fig. 9.1, the opening of the EEV under control Strategy B decreased

gradually from 100% to 30% of its maximum, while it stayed at 100% under Strategy A. In Fig. 9.2, the measured refrigerant flow rates under both control strategies were almost the same in approximately the first 280 s into defrosting operation when the EEV opening was at about 60% of its maximum under Strategy B, and the refrigerant flow rate started to drop and reached its minimum of 0.48 l/min when the opening of the EEV reached its minimum preset value of 30% of its maximum.
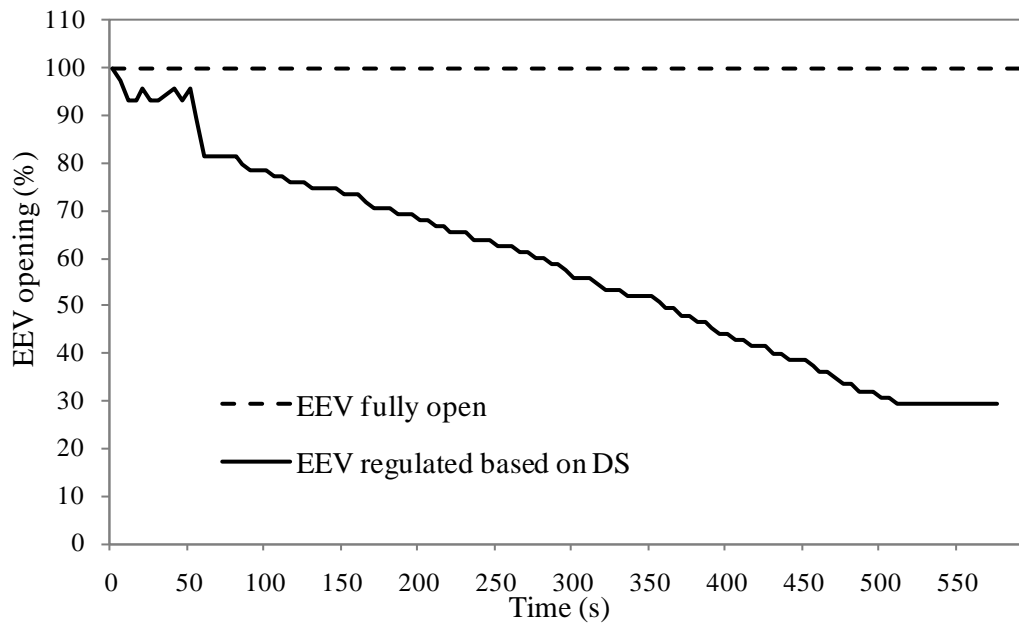
Fig. 9.1 The opening of the EEV during defrosting under the two EEV control
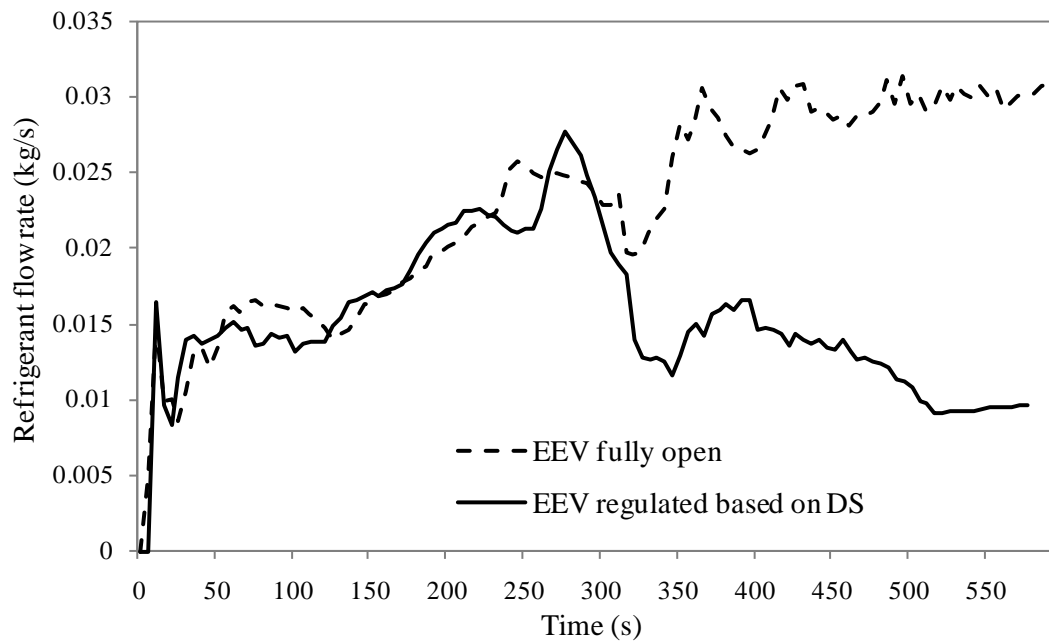
strategies

Fig. 9.2 Measured refrigerant flow rates during defrosting under the two EEV

control strategies

Fig. 9.3 shows the measured variation profiles of compressor discharge pressure and

suction pressure during defrosting when the EEV was under the two control

strategies. During the first half of the defrosting operation, the measured compressor

discharge pressures were almost identical, fluctuating around 17.5 bar. However,

during the 2nd half of the defrosting operation, discharge pressures started to increase,

with that under Strategy B increasing more. On the other hand, the variations of the

measured compressor suction pressures were almost identical.
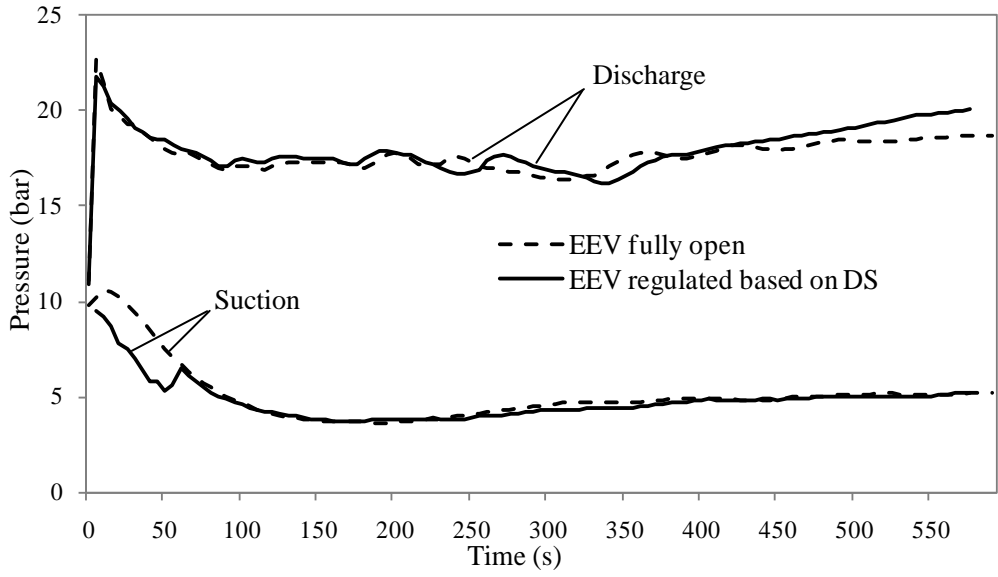
Fig. 9.3 Measured compressor discharge and suction pressures under the two EEV

control strategies
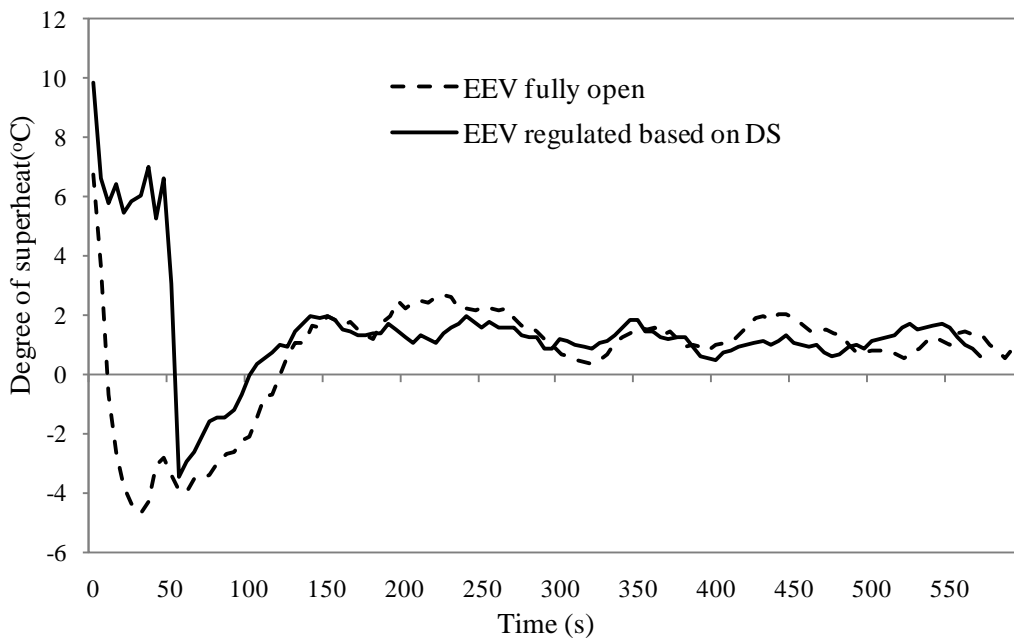
Fig. 9.4 Measured degree of superheat during defrosting under the two EEV

control strategies

The measured variations in DS in the comparative experiments are shown in Fig. 9.4.

The variations of the DS in both modes were similar, with the average values of DS in Strategy A and Strategy B being 0.68 $^{\circ}$C and 1.56 $^{\circ}$C, respectively. This suggested that the experimental ASHP unit was operated on a safer side when its EEV was under Strategy B.
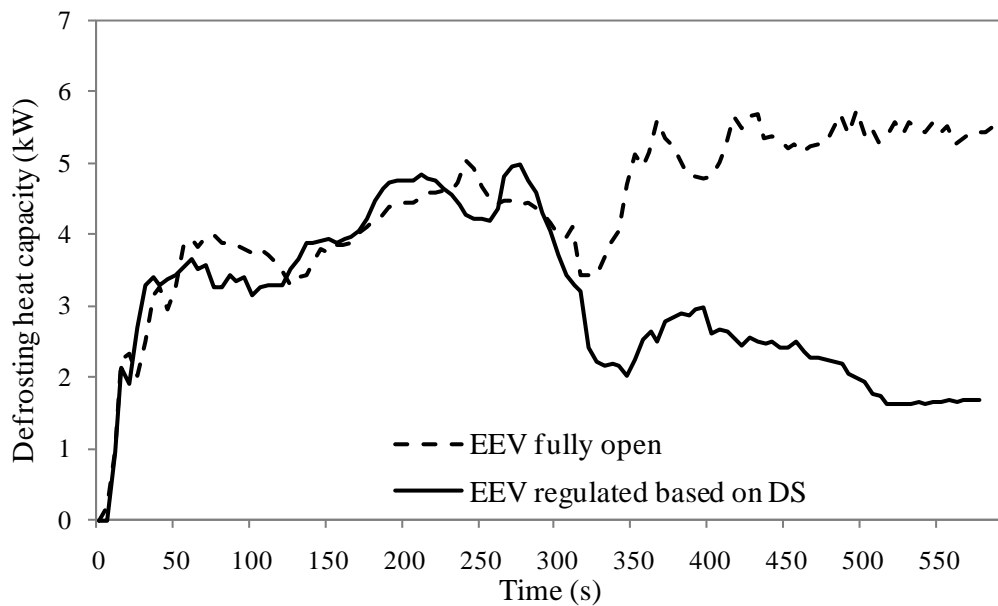
Fig. 9.5 Evaluated defrosting heating capacity during defrosting under the two

EEV control strategies

The evaluated values of defrosting heating capacity during defrosting are illustrated in Fig. 9.5. Similar variation patterns to that shown in Fig. 9.2 can be seen. Defrosting heating capacity decreased with the decrease of refrigerant flow rate. As seen, the heating capacity of the experimental ASHP unit when its EEV was under the control Strategy B was reduced rapidly starting from 280 s into defrosting operation when the opening of EEV was at ~ 60% of its maximum. At the end of the

defrosting operation, defrosting heating capacity under EEV control Strategy A was 3.3 times of that under EEV control Strategy B.

By using Equation (7.4), the total heat outputs from the experimental ASHP unit during defrosting when the EEV was under the two control strategies were evaluated, at 2628 kJ (under Strategy A) and 1769.4 kJ (under Strategy B), respectively. Therefore the total output heat can be reduced by 33.7% when the EEV was regulated by a DS controller, as compared to fully opening EEV during defrosting, with similar defrost duration and performance.

On the other hand, as shown in Table 9.2, the defrosting time periods, t_d, under Strategies A and B, were 590 s and 575 s, respectively, with the latter being slightly faster. Furthermore, the total electrical energy consumptions during defrosting of the experimental ASHP unit under the two control strategies differed only by less than 2%. Therefore, the defrosting coefficient of performance (COP_d) evaluated by Equation (9.1) were 4.35 and 2.98, under Strategies A and B, respectively. It appeared though that fully opening an EEV during defrosting can result in a higher system efficiency. This traditionally defined COP_d may therefore not be able to adequately reflect the reality. In fact, the total output heat during defrosting was used for not only melting frost, vaporizing melted frost on outdoor coil surface, but also warming up the coil metal, and lastly heating the ambient air through convection. In other words, part of the total output heat produced was wasted during defrosting.

Thus, using COP_d may not make too much sense in evaluating the operating efficiency of a heat pump during defrosting.

As shown in Fig. 7.1, for an outdoor coil having multi parallel circuits, defrosting ended later on its lower circuits than on its higher circuits. Hence, much heat can be wasted through heating up ambient air by the hot coil surface of higher circuits. Therefore, using the defrosting efficiency, as defined by Equation (7.1), to evaluate the performance of a defrosting operation may make more sense. In this experimental study reported in this Chapter, the defrosting efficiencies evaluated using Equation (7.1) were 28.2% under control Strategy A and 42.9% under control Strategy B, respectively. Those suggested that the control Strategy A, or fully opening an EEV, would lead to more heat wastage through heating up the ambient air by convection, which was particularly true for an outdoor coil consisting of multi parallel circuits. On the other hand, when the EEV was controlled by a DS controller during defrosting, less heat was wasted, since refrigerant mass flow rate was correspondingly reduced at the later part of defrosting, as shown in Fig. 9.2. Given that the total input electrical energy consumptions during defrosting under the two strategies were similar, less heat was taken from heated indoor space when the EEV was controlled by a DS controller (Strategy B). The disturbance to the thermal environment in the heated indoor space was therefore less than that when the EEV remained fully open during defrosting (Strategy A).

9.4 Conclusions

This Chapter reports an experimental investigation on the performance of a reverse cycle defrosting operation for the experimental ASHP unit when its EEV was under the two different control strategies: fully open and controlled by a DS controller. Experimental results suggested that when the EEV was regulated by a DS controller during defrosting, a higher defrosting efficiency was obtained. The refrigerant flow rate was reduced during the later part of a defrosting operation and thus less heat was provided, consequently a higher defrosting efficiency and less heat wastage would be resulted in.

Chapter 10

Conclusions and Future Work

10.1 Conclusions

A programmed research work on developing a novel TES-based reverse cycle defrosting method and evaluating the operating performance for the experimental ASHP unit has been successfully carried out and is reported in this thesis. The conclusions of the thesis are:

1) A novel TES-based reverse cycle defrosting method for ASHPs has been developed to address the fundamental problem of insufficient heat available when using the standard reverse cycle defrosting method. Comparative experiments using both the novel TES-based reverse cycle defrosting method and the standard reverse cycle defrosting method were designed and carried out. The experimental results on the refrigerant side performances of the experimental ASHP unit reported in Chapter 5 suggested that the use of the novel TES-based reverse cycle defrosting method would lead to the following advantages: a smoother transition from defrosting to space heating resumption for the ASHP unit; an enhanced reliablity of ASHP unit resulting from a higher suction pressure during defrosting and heating resumption, and a reduced energy consumption for defrosting because of a shorter defrosting duration.

2) Chapter 6 presents the experimental results of the airside performances of the experimental ASHP unit and indoor thermal comfort characteristics when using the TES-based reverse cycle defrosting method. Indoor thermal parameters necessary for thermal comfort evaluation were measured and the indoor thermal comfort indexes evaluated based on Fanger's thermal comfort model. The experimental results of the airside performance of the ASHP unit and the evaluated indoor thermal comfort indexes (PMV and PPD) clearly demonstrated that the use of the novel TES-based reverse cycle defrosting method would lead to a shorter defrosting duration because of sufficient heat available for defrost, a higher indoor air temperature and consequently, occupants' indoor thermal comfort can be significantly improved during a reverse cycle defrosting operation.

3) The experimental part of a study of the reverse cycle defrosting performance on the four-circuit outdoor coil in the experimental ASHP unit is reported in Chapter 7. It was observed that defrosting was quicker on the airside of upper circuits than that on the lower circuits. The effects of downwards flowing of the melted frost along a four-circuit outdoor coil surface were discussed, and the defrosting efficiency was evaluated at 34.5%.

4) The modeling part of the study is presented in Chapter 8. In order to quantitatively analyze the effects of downwards flowing of the melted frost along the surface of the four-circuit outdoor coil in the experimental ASHP unit on its defrosting performance, a semi-empirical mathematical model, the first of its kind, has been developed and is reported. The model prediction results

suggested that although the energy used to heat the melted frost only accounted for about 10% of the total amount of heat provided to the outdoor coil during defrosting, downwards flowing of melted frost along outdoor coil surface actually prolonged the defrosting process at lower level circuits, thus prolonging the entire defrosting operation and reducing the defrosting efficiency. If the melted frost may be drained away locally, an increased of 18.3% in defrosting efficiency, as compared to allowing it to flow downwards, was predicted. The model developed and reported in this Chapter provided a useful tool for studying and understanding the effects of downwards flowing melted frost on the defrosting performance of a multi-circuit outdoor coil in an ASHP unit.

5) Chapter 9 reports an experimental investigation on the performance of a reverse cycle defrosting operation for the experimental ASHP unit when its EEV was under the two different control strategies: fully open and controlled by a DS controller. Experimental results suggested that when the EEV was regulated by a DS controller during defrosting, a higher defrosting efficiency was obtained. The refrigerant flow rate was reduced during the later part of a defrosting operation and thus less heat was provided. Consequently a higher defrosting efficiency and less heat wastage would be resulted in.

The project reported in this thesis has made important contributions to the advancement of heat pump technology through developing the novel TES-based reverse cycle defrosting method for ASHPs and studying the defrosting performance on a multi-circuit outdoor unit in an ASHP. The novel TES-based reverse cycle defrosting method can be used to eliminate the fundamental problem of insufficient

184

heat available for defrosting encountered when using the standard reverse cycle defrosting method for ASHPs. The long-term significance of the project is that the project outcomes helped increase energy efficiency of, and enhance the reliability of an ASHP unit, and improve indoor thermal comfort for occupants. This would in turn encourage a wider use of ASHPs, contributing to energy conservation and sustainable development worldwide.

10.2 Proposed future work

A number of future studies following on the successful completion of the project reported in this thesis are proposed:

1) Two heat storage operating modes of using the novel TES-based reverse cycle defrosting method for ASHPs, i.e., parallel TES-based heating and serial TES-based heating, were investigated and the study results are presented in Chapter 5 and Chapter 6. It is proposed to develop a mathematic model for the experimental ASHP unit when operated in both parallel TES-based heating and serial TES-based heating modes. The model will include a sub-model specifically for the PCM-HE. Based on the model, the amount of the PCM and the size of PCM-HE may be determined for optimized defrosting performance.

2) A comparison of the annual total energy consumption for the experimental ASHP unit when using the TES-based heating method and standard heating

method is not included in current study. However, the annual total energy consumption is an important parameter when evaluating the performance of an ASHP unit. Therefore, a detailed analysis on the annual total energy consumption by an ASHP unit at different heating methods should be carried out.

3) The model developed in Chapter 8 provided a useful tool for studying and understanding the effects of downwards flowing melted frost on the defrosting performance in a multi-circuit outdoor coil of an ASHP unit. Lumped parameter modeling approach was applied, assuming only a two-phase region for the entire outdoor coil without considering the existence of a superheated region and the sub-cooling region. Further development work should be directed to considering all three regions for an improved modeling accuracy.

Appendix A

Table A1 Properties of PCMs with melting points between 20 $^{\circ}$C and 30 $^{\circ}$C

Compound	Melting temperature ($^{\circ}$C)	Heat of fusion (kJ/kg)	Thermal conductivity (W/mK)	Density (kg/m^3)
$Mg(NO_3)_2 \cdot 6H_2O$	25.8	125.9	n.a	1738 (liquid, 20 $^{\circ}$C) 1728 (liquid, 40 $^{\circ}$C) 1795 (solid, 5 $^{\circ}$C)
$CaCl_2 \cdot 6H_2O$	29	190.8	0.540 (liquid, 38.7 $^{\circ}$C)	1562 (liquid, 32 $^{\circ}$C)
	29.2	171	0.561 (liquid, 61.2 $^{\circ}$C)	1496 (liquid)
	29.6	174.4	1.088 (solid, 23 $^{\circ}$C)	1802 (solid, 23 $^{\circ}$C)
	29.7	192		1710 (solid, 25 $^{\circ}$C)
	30			1634
	29-39			1620
66.6% $CaCl_2 \cdot 6H_2O$+ 33.3% $MgCl_2 \cdot 6H_2O$	25	127	n.a.	1590
48% $CaCl_2$ +4.3%NaCl +0.4%KCl +47.3% H_2O	26.8	188.0	n.a.	1640
47% $Ca(NO_3)_2 \cdot 4H_2O$ + 33% $Mg(NO_3)_2 \cdot 6H_2O$	30	136	n.a.	n.a.
Paraffin C16-C18	20-22	152	n.a.	n.a.

Table A1 Properties of PCMs with melting points between 20 ^{o}C and 30 ^{o}C (*Continued*)

Polyglycol E600	22	127.2	0.189	1126
			(liquid, 38.6 ^{o}C)	(liquid, 25 ^{o}C)
			0.187	1232
			(liquid, 67.0 ^{o}C)	(solid, 4 ^{o}C)
Paraffin C13-C24	22-24	189	0.21	0.760
			(solid)	(liquid,70 ^{o}C)
				0.900
				(solid, 20 ^{o}C)
1-Dodecanol	26	200	n.a.	n.a
Paraffin C18	28	244	0.148	0.774
			(liquid,40 ^{o}C)	(liquid, 70 ^{o}C)
	27.5	243.5	0.15	0.814
			(solid)	(solid,20 ^{o}C)
			0.358	
			(solid, 25 ^{o}C)	
Capric-lauric acid (45-55%)	21	143	n.a.	n.a.
Dimethyl sebacate	21	120-135	n.a.	n.a.
34% Mistiricacid +	24	147.7	0.164	888
66% Capricacid			(liquid, 39.1 ^{o}C)	(liquid, 25 ^{o}C)
			0.154	1018
			(liquid, 61.2 ^{o}C)	(solid, 1 ^{o}C)
Vinlystearate	27-29	122	n.a.	n.a.

% in weight, n.a.: not available

Appendix B

Photos of the experimental setup
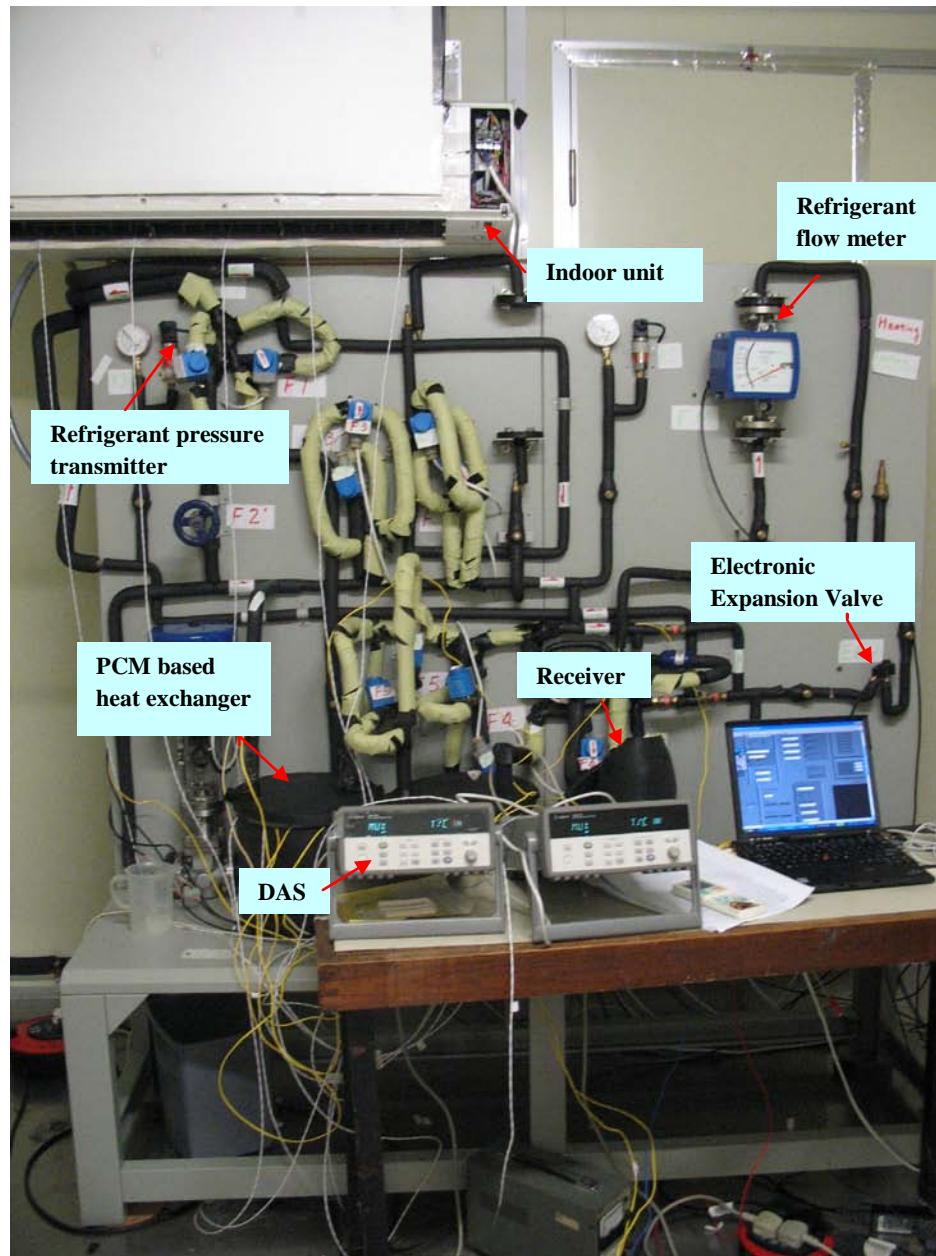
Photo 1 Overview of the indoor part of the experimental setup
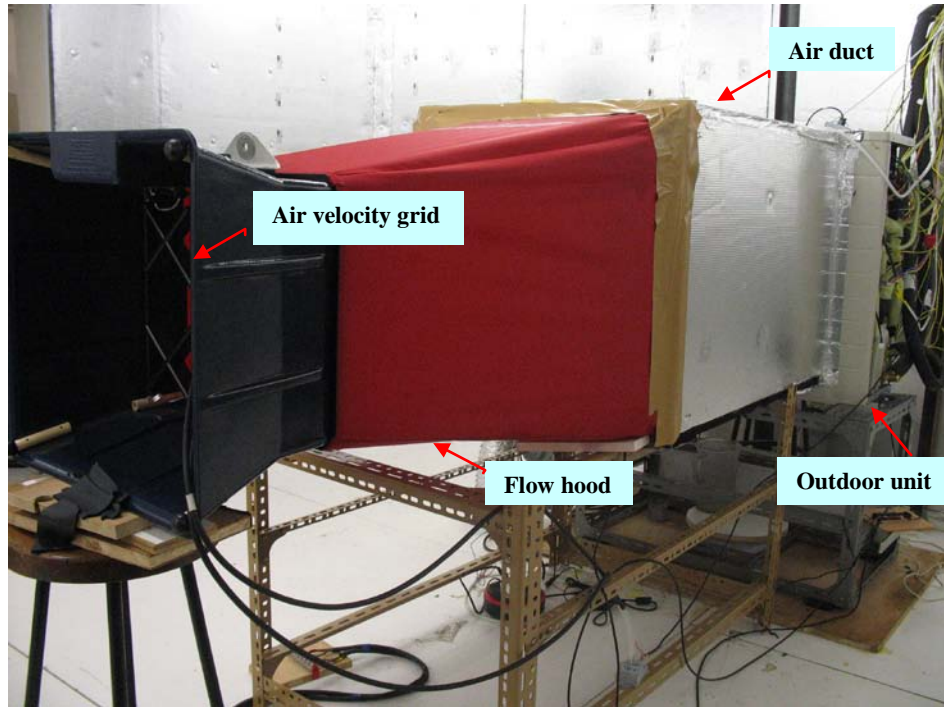
Photo 2 Overview of the outdoor part of the experimental setup
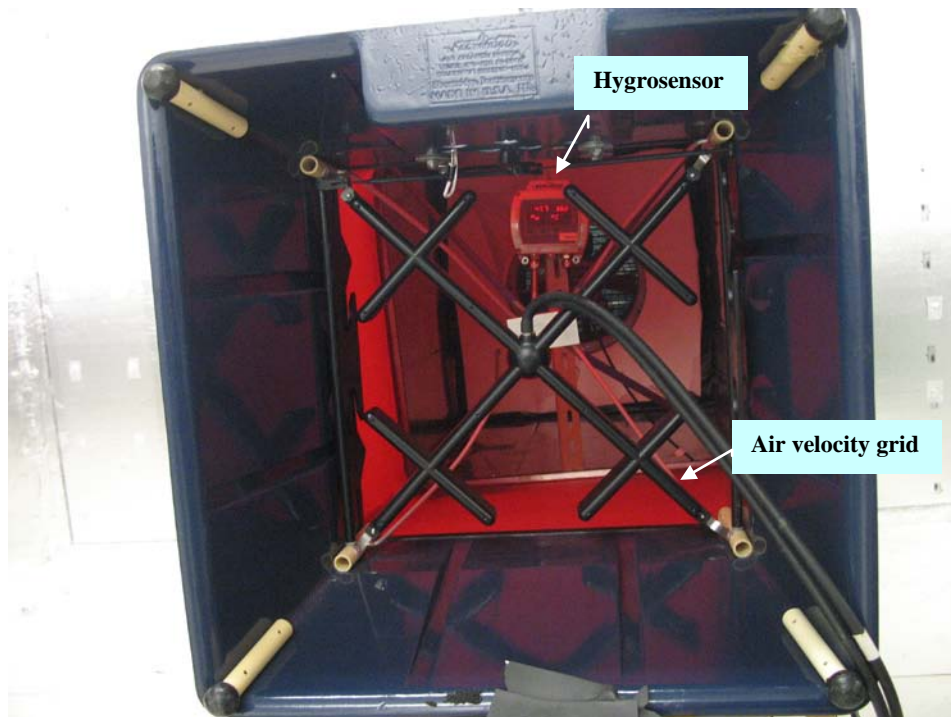
Photo 3 Air velocity grid and hygrosensor on the outdoor part of the experimental setup
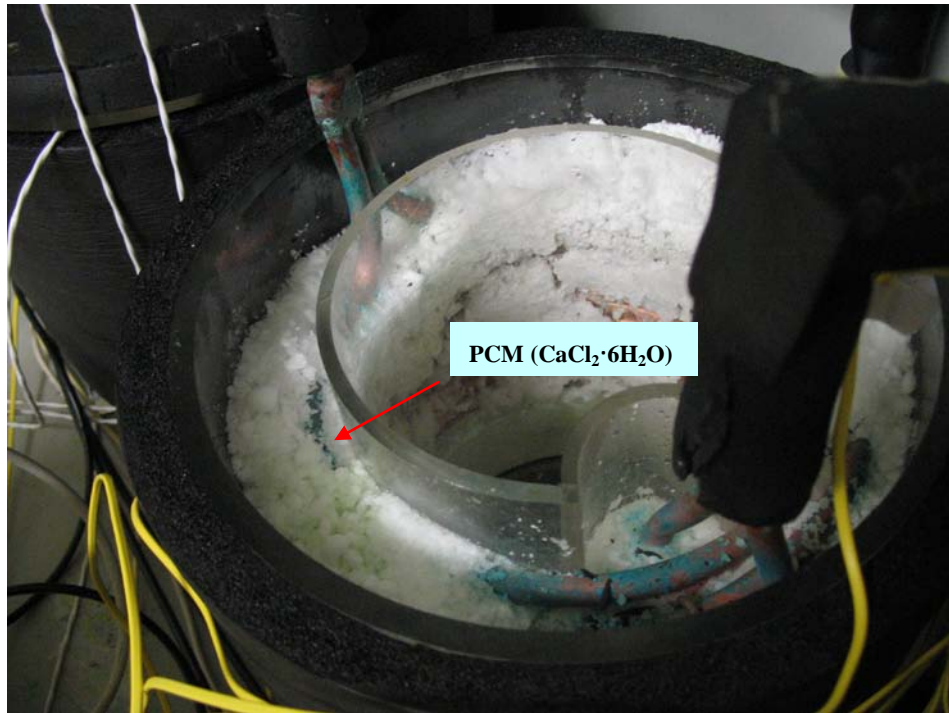
Photo 4 PCM-based heat exchanger in the experimental ASPH unit

Photo 5 Air sampling device in the experimental ASPH unit (1)
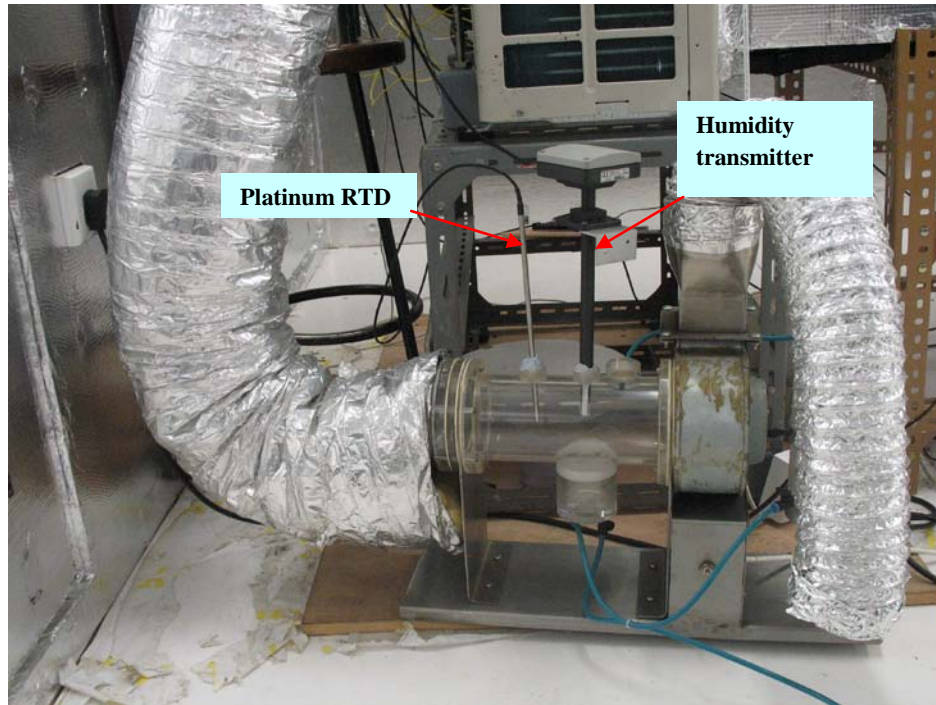
Photo 6 Air sampling device in the experimental ASPH unit (2)
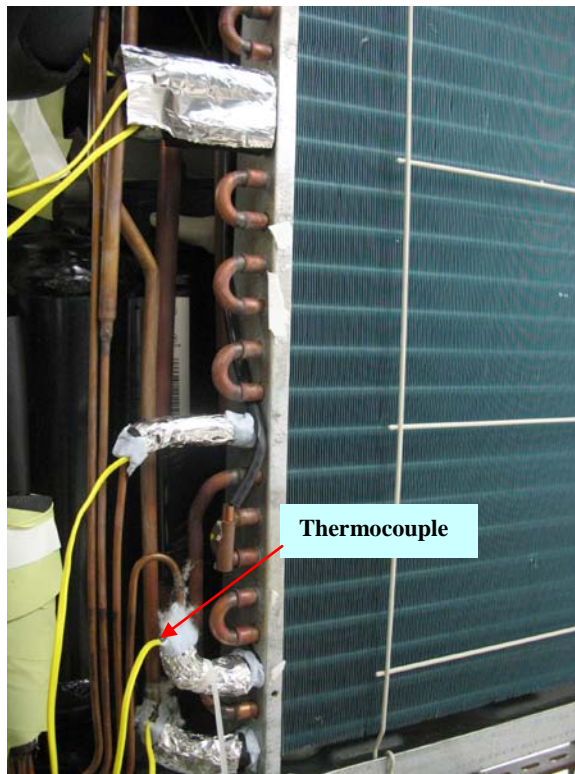
Photo 7 Outdoor coil and its instrumentations in the experimental ASPH unit

Appendix C

Table C1 List of the measured parameters

Measured parameter	Location	Instrument/ sensor	Number	Accuracy
RT	Compressor discharge	TC (K-type)	1	± 0.3 ℃
RT	Compressor suction	TC (K-type)	1	± 0.3 ℃
RT	Indoor coil outlet	TC (K-type)	1	± 0.3 ℃
RT	Receiver inlet	TC (K-type)	1	± 0.3 ℃
RT	EEV outlet	TC (K-type)	1	± 0.3 ℃
RT	Top circuit inlet	TC (K-type)	1	± 0.3 ℃
RT	Second top circuit inlet	TC (K-type)	1	± 0.3 ℃
RT	Second bottom circuit inlet	TC (K-type)	1	± 0.3 ℃
RT	Bottom circuit inlet	TC (K-type)	1	± 0.3 ℃
RT	Top circuit exit	TC (K-type)	1	± 0.3 ℃
RT	Second top circuit exit	TC (K-type)	1	± 0.3 ℃
RT	Second bottom circuit exit	TC (K-type)	1	± 0.3 ℃
RT	Bottom circuit exit	TC (K-type)	1	± 0.3 ℃
RT	Outdoor coil exit	TC (K-type)	1	± 0.3 ℃
RT	PCM-HE outlet	TC (K-type)	1	± 0.3 ℃
PCM temperature	Inserted in the middle of PCM-HE	TC (K-type)	1	± 0.3 ℃
Melted frost temperature	water collecting pan outlet	TC (K-type)	1	± 0.3 ℃
Air temperature	Supply air temperature from indoor unit	Pt100	5	Class A ± 0.1 ℃
Air temperature	Upstream of the outdoor unit	Pt100	1	Class A ± 0.1 ℃
RH	Upstream of the outdoor unit	Humidity transmitter	1	± 3.0%
Air temperature	Downstream of the outdoor unit	Hygrosensor	1	± 0.2 ℃
RH	Downstream of the outdoor unit			± 1.0%
RP	Compressor discharge	Pressure transmitter	1	± 0.3%
RP	Compressor suction	Pressure transmitter	1	± 0.3%
RP	Receiver inlet	Pressure transmitter	1	± 0.3%
RP	EEV outlet	Pressure transmitter	1	± 0.3%
RF	Between EEV and receiver	Flow meter	1	± 1.6%
Air flow rate	Air flow rate passing	Flow hood	1	± 3%

	through the outdoor coil			
Air velocity	supply outlet of the indoor coil	Velocity transducer	5	± 1.0%
Amount of the melting water	Under the water collecting pan	Measuring cylinder	1	± 0.1 liter
Power consumption	Compressor	PWM digital power meter	1	± 2%

RT: Refrigerant temperature

RP: Refrigerant pressure

RF: Refrigerant flowrate

TC: Thermocouple

References

1 Abdel-Wahed et al. 1983
Abdel-Wahed, R.M., Hifni, M.A., and Sherif, S.A.
Hot water defrosting of a horizontal flat plate cooling surface. *International Journal of Refrigeration*, Vol. 6, No. 3, pp. 152-154 (1983)

2 Alebrahim and Sherif 2002
Alebrahim, Al.M. and Sherif, S.A.
Electrical defrosting analysis of a finned tube evaporator coil using the enthalpy method. *Proceedings of the Institution of Mechanical Engineers, Part C: Journal of Mechanical Engineering Science*, Vol. 216, No. 6, pp. 655-673 (2002)

3 Al-Mutawa and Sherif 1998a
Al-Mutawa, N.K. and Sherif, S.A.
An analytical model for hot-gas defrosting of a cylindrical coil cooler, Part I: Model development. *ASHRAE Transactions,* Vol. 104, Part 1, pp. 1722-1730 (1998)

4 Al-Mutawa and Sherif 1998b
Al-Mutawa, N.K. and Sherif, S.A.
An analytical model for hot-gas defrosting of a cylindrical coil cooler, Part II: Model results and conclusions. *ASHRAE Transactions,* Vol. 104, Part 1, pp. 1731-1737 (1998)

5 Al-Mutawa and Sherif 1998c
Al-Mutawa, N.K. and Sherif, S.A.
Determination of coil defrosting loads, Part 1: Experimental facility description. *ASHRAE Transactions*, Vol. 104, Part 1, pp. 268-288 (1998)

6 Al-Mutawa and Sherif 1998d
Al-Mutawa, N.K. and Sherif, S.A.
Determination of coil defrosting loads, Part 4: Refrigeration defrost cycle dynamics. *ASHRAE Transactions*, Vol. 104, Part 1, pp.313-343 (1998)

7 Al-Mutawa and Sherif 1998e
Al-Mutawa, N.K. and Sherif, S.A.
Determination of coil defrosting loads, Part 5: Analysis of loads. *ASHRAE Transactions*, Vol. 104, Part 1, pp. 344-355 (1998)

8 Ameen et al. 1993
Ameen, F.R., Coney, J.E.R. and Sheppard, C.G.W.
Experimental study of warm-air defrosting of heat-pump evaporators. *International Journal of Refrigeration*, Vol. 16, No. 1, pp. 13-18 (1993)

9   Anand et al. 1989
    Anand, N.K., Schiesing J.S., O'Neal, D.L. and Peterson, K.T.
    Effects of outdoor coil fan pre-start on pressure transients during the reverse cycle defrost of heat pump. *ASHRAE Transactions*, Vol. 95, Part 2, pp. 699-704 (1989)

10 Aprea and Mastrullo 2002
    Aprea, C. and Mastrullo, R.
    Experimental evaluation of electronic and thermostatic expansion valves performances using R22 and R407C. *Applied Thermal Engineering*, Vol. 22, No. 2, pp. 205-218 (2002)

11 ASHRAE 2007
    ASHRAE
    Handbook of HVAC Applications (2007)

12 ASHRAE 2009
    ASHRAE
    Handbook of Fundamentals (2009)

13 ASHRAE 2010
    ASHRAE
    ANSI/ASHRAE Standard 55-2010, Thermal Environment Conditions for Human Occupancy (2010)

14 Arkar et al. 2007
    Arkar, C., Vidrih, B. and Medved, S.
    Efficiency of free cooling using latent heat storage integrated into the ventilation system of a low energy building. *International Journal of Refrigeration*, Vol. 30, No. 1, pp. 134-143 (2007)

15 Bajnoczy et al. 1999
    Bajnoczy, G., Pálffy, E.G., Prépostffy, E. and Zöld, A.
    Heat storage by two grade phase change material. *Periodica Polytechnica-Chemical Engineering*, Vol. 43, No. 2 , pp. 137-147 (1999)

16 Barrow 1985
    Barrow, H.
    A note on frosting of heat pump evaporator surfaces. *Heat Recovery System*, Vol. 5, No. 3, pp. 195-201 (1985)

17 Bauer and Wirtz 2000
    Bauer, C.A. and Wirtz, R.A.
    Thermal characteristics of a compact, passive thermal energy storage device. *Proceedings of the 2000 ASME IMECE*, Orlando, Florida, USA (2000)

18 Baxter and Moyers 1984
    Baxter, V.D. and Moyers, J.C.
    Air source heat pump: field measurement of cycling, frosting, and defrosting losses, 1981-1983. *Oak Ridge National Laboratory Report ORNL/CON-150.*

(1984)

19 Bedford and Warmer 1934
Bedford, T. and Warmer, C.G.
The globe thermometer in studies of heating and ventilating. *Journal of Hygiene*, Vol. 34, No. 4, pp. 458-473 (1934)

20 Brown et al. 1998
Brown, R.C., Rasberry, J.D. and Overmann, S.P.
Microencapsulated phase-change materials as heat transfer media in gas-fluidized beds. *Powder Technology*, Vol. 98, No. 3, pp. 217-222 (1998)

21 Byun et al. 2006
Byun, J.S., Jeon, C.D., Jung, J.H. and Lee, J.
The application of photo-coupler for frost detecting in an air-source heat pump. *International Journal of Refrigeration*, Vol. 29, No. 2, pp. 191-198 (2006)

22 Byun et al. 2008
Byun, J.S., Lee, J. and Jeon, C.D.
Frost retardation of an air-source heat pump by the hot gas bypass method. *International Journal of Refrigeration*, Vol. 31, No. 2, pp. 328-334 (2008)

23 Chen et al. 2005
Chen, W., Zhou, X.X. and Deng, S.M.
Development of control method and dynamic model for multi-evaporator air conditioners (MEAC). *Energy Conversion Management*, Vol. 46, No. 3, pp. 451-465 (2005)

24 Chen et al. 2008
Chen, Y.M., Deng, S.M., Xu, X.G. and Chan, M.Y.
A study on the operational stability of a refrigeration system having a variable speed compressor. *International Journal of Refrigeration*, Vol. 31, No. 8, pp. 1368-1374 (2008)

25 Chen et al. 2009
Chen, Y.G., Guo, X.M. and Yang, Z.
Dynamic defrosting characteristics of air source heat pump and effects of outdoor air parameters on defrost cycle performance. *Applied Thermal Engineering*, Vol. 29, No. 13, pp. 2701-2707 (2009)

26 Cheng and Seki 1991
Cheng, K.C. and Seki, N.
Freezing and melting heat transfer in engineering: selected topics on ice-water systems and welding and casting processes, Taylor & Francis. 1991

27 Cheng and Shiu 2002
Cheng, C.H. and Shiu, C.C.
Frost formation and frost crystal growth on a cold plate. *International Journal of Heat and Mass Transfer*, Vol. 45, No. 21, pp. 4289-4303 (2002)

28 Choi and Kim 2002
    Choi, J.M. and Kim, Y.C.
    The effects of improper refrigerant charge on the performance of a heat pump with an electronic expansion valve and capillary tube. *Energy*, Vol. 27, No. 4, pp. 391-401 (2002)

29 Choi et al. 2011
    Choi, H.J., Kim, B.S., Kang, D. and Kim, K.C.
    Defrosting method adopting dual hot gas bypass for an air-to-air heat pump. *Applied Energy*, Vol. 88, No. 12, pp. 4544-4555 (2011)

30 Chowdhury et al. 2008
    Chowdhury, A.A., Rasul, M.G. and Khan, M.M.K.
    Thermal-comfort analysis and simulation for various low-energy cooling-technologies applied to an office building in subtropical climate. *Applied Energy*, Vol. 85, No. 6, pp. 449-462 (2008)

31 Cole 1989
    Cole, R.A.
    Refrigeration loads in a freezer due to hot gas defrost and their associated costs. *ASHRAE Transactions*, Vol. 95, Part 1, pp. 1149-1154 (1989)

32 Coley 1983
    Coley, M.B.
    The Cost of Frost. *ASHRAE Journal*, Vol. 25, pp. 29-31 (1983)

33 Datta and Tassou 1997
    Datta, D. and Tassou, S.
    Frost prediction on evaporator coils of supermarket display cabinets using artificial neural networks. *Proceedings of CLIMA 2000 Conference*, Brussels, Belgium, pp. 98 (1997)

34 Datta and Tassou 2002
    Datta, D. and Tassou, S.
    Implementation of a defrost on demand control strategy on a retail display cabinet. *Proceedings of IIF-IIR=COMMISSION D1/B1*, Urbana, IL, USA (2002)

35 Ding et al. 2004
    Ding, Y.J, Ma, G.Y. and Chai, Q.H.
    Experiment investigation of reverse cycle defrosting methods on air source heat pump with TXV as the throttle regulator. *International Journal of Refrigeration*, Vol. 27, pp. 617-678 (2004)

36 Domingorena and Ball 1980
    Domingorena, A.A. and Ball, S.J.
    Performance evaluation of a selected three-ton air-to-air heat pump in the heating mode. *ORNT/CON-34. Oak Ridge National Laboratory* (1980)

37   Dopazo et al. 2010
     Dopazoa A.J., Fernandez-Seara, J., Uhía, F. J. and Diz, R.
     Modeling and experimental validation of the hot-gas defrost process of an air-cooled evaporator. *International Journal of Refrigeration*, Vol. 33, No. 4, pp. 829-839 (2010)

38   Eckman 1987
     Eckman, R.L.
     Heat pump defrost controls: a review of past, present, and future technology. *ASHRAE Transactions*, Vol. 93, Part 1 , pp. 1152-1156 (1987)

39   Emery and Siegel 1990
     Emery, A.F. and Siege, B.L.
     Experimental measurements of the effects of frost formation on heat exchanger performance. *Proceedings of AIAA/ASME Thermo physics and Heat Transfer Conference*, ASME HTD 139, pp. 1-7 (1990)

40   Esen and Ayhan 1996
     Esen, M. and Ayhan, T.
     Development of a model compatible with solar assisted cylindrical energy storage tank and variation of stored energy with time for different phase change materials. *Energy conversion Management*, Vol. 37, No. 12 , pp. 1775-1785 (1996)

41   Ettouney et al. 2004
     Ettouney, H.M., Alatigi, I., Al-Sahali, M. and Al-Ali, S.A.
     Heat transfer enhancement by metal screens and metal spheres in phase change energy storage systems. *Renewable Energy*, Vol. 29, No. 6, pp. 841-860 (2004)

42   Fanger 1970
     Fanger, P.O.
     Thermal Comfort. *Danish Technical Press*, Copenhagen. 1970

43   Fanger 1982
     Fanger, P.O.
     Thermal Comfort. *Robert E. Krieger Publishing Company*, Malabar, FL. 1982

44   Farid and Kanzawa 1989
     Farid, M.M. and Kanzawa, A.
     Thermal performance of heat storage module using PCMs with different melting temperatures: mathematical modeling. *Transactions of ASME, Journal of Solar Energy Engineering*, Vol. 111, No.2, pp. 152-157 (1989)

45   Fossa and Tanda 2002
     Fossa, M. and Tanda, G.
     Study of free convection frost formation on a vertical plate. *Experimental Thermal and Fluid Science*, Vol. 26, No. 6-7, pp. 661-668 (2002)

46   Fukai et al. 2000
     Fukai, J., Kanou, M., Kodama, Y. and Miyatake, O.

Thermal conductivity enhancement of energy storage media using carbon fibers. *Energy Conversion and Management*, Vol. 41, No. 14, pp. 1543-1556 (2000)

47   Fukai et al. 2002
Fukai, J., Hamada, Y., Morozumi, Y. and Miyatake, O.
Effect of carbon-fiber brushes on conductive heat transfer in phase change materials. *International Journal of Heat and Mass Transfer*, Vol. 45, No. 24, pp. 4781-4792 (2002)

48   Gerald and Wheatley 2003
Gerald, C.F. and Wheatley, P.O.
Applied numerical analysis,7th ed. *Addison-Wesley Publishing Co*. 2003

49   Goodman and Shea 1960
Goodman, T.R. and Shea, J.J.
The melting of finite slabs. *Journal of Applied Mechanics*, Vol. 27, pp. 16-24 (1960)

50   Griffiths and Eames 2007
Griffiths, P.W. and Eames, P.C.
Performance of chilled ceiling panels using phase change material slurries as the heat transport medium. *Applied Thermal Engineering*, Vol. 27, No. 10, pp. 1756-1760 (2007)

51   Gu et al. 2004
Gu, Z., Liu, H. and Li, Y.
Thermal energy recovery of air conditioning system–heat recovery system calculation and phase change materials development. *Applied Thermal Engineering*, Vol. 24, No. 17-18, pp. 2511-2526 (2004)

52   Guo et al. 2008
Guo, X.M., Chen, Y.G., Wang, W.H. and Chen, C.Z.
Experimental study on frost growth and dynamic performance of air source heat pump system. *Applied Thermal Engineering*, Vol. 28, No. 17-18, pp. 2267-2278 (2008)

53   Hamada and Fukai 2005
Hamada, Y. and Fukai, J.
Latent heat thermal energy storage tanks for space heating of buildings: comparison between calculations and experiments. *Energy Conversion and Management*, Vol. 31, No. 13, pp. 2025-2041 (2005)

54   Hao et al. 2002
Hao, Y. L., Iragorry, J., Castro, D., Tao, Y. X. and Jia, S.
Microscopic characterization of frost surface during liquid-ice phase change period. *Proceedings of the 2002 ASME International Mechanical Engineering Congress & Exposition, New Orleans, LA*, No. IMECE2002-32797 (2002)

55 Hawlader et al. 2003
    Hawlader, M. N. A., Uddin, M. S. and Khin, M.M.
    Microencapsulated PCM thermal-energy storage system. *Applied Energy*, Vol. 74, No. 1-2, pp. 195-202 (2003)

56 Hayashi et al. 1977
    Hayashi, Y., Aoki, A., Adachi, S. and Hori, K.
    Study of frost properties correlating with frost formation types. *Journal of Heat Transfer*, Vol. 99, No. 2, pp. 239-244 (1977)

57 He et al. 1997
    He, X.D., Liu, S. and Asada, H.H.
    Modeling of vapor compression cycles for multi variable feedback control of HVAC systems. *ASMEJ. Dynamic Systems, Measurement, and Control*, Vol. 119 , No. 2, pp. 183-191 (1997)

58 He et al. 2003
    He, Z., Peng, X., Xing, Z. and Shu, P.
    Operating characteristics of an air-source heat pump under frosting defrosting conditions. *Proceedings of the Institution of Mechanical Engineers, Part A: Journal of Power and Energy*, Vol. 217, No. 6, pp. 623-629 (2003)

59 Herrick 1982
    Herrick, C.S.
    Multi-freeze cycle life testing of Glauber's salt in a rolling cylinder heat store. *Solar Energy*, Vol. 28, No. 2, pp. 99-104 (1982)

60 Hewitt and Huang 2008
    Hewitt, N. and Huang, M.J.
    Defrost cycle performance for a circular shape evaporator air source heat pump. *International Journal of Refrigeration*, Vol. 31, No. 3, pp. 444-452 (2008)

61 Hoffenbecker et al. 2005
    Hoffenbecker, N., Klein, S.A. and Reindl, D.T.
    Hot gas defrost model development and validation. *International Journal of Refrigeration*, Vol. 28, No. 4, pp. 605–615 (2005)

62 Hoogendoorn and Bart 1992
    Hoogendoorn, C.J. and Bart, G.C.J.
    Performance and modeling of latent heat stores. *Solar Energy*, Vol. 48, No. 1, pp. 53-58 (1992)

63 Hosoda and Uzuhashi 1967
    Hosoda, T. and Uzuhashi, H.
    Effects of frost on the heat transfer coefficient. *Hitachi Review*, Vol. 16, No. 6, pp. 254-259 (1967)

64   Hu 2010
      Hu, W.J.
      Study on the dynamic characteristic of a novel PCM based defrosting for air source heat pump. PhD Thesis (in Chinese), Harbin Institute of Technology, (2010)

65   Huang et al. 2004
      Huang, D., Yuan, X.L. and Zhang, X.Q.
      Effects of fan-starting methods on the reverse-cycle defrost performance of an air-to-water heat pump. *International Journal of Refrigeration*, Vol. 27, No. 8, pp. 869-875 (2004)

66   Huang et al. 2007
      Huang, D., He, Z.L. and Yuan, X.L.
      Dynamic characteristics of an air-to-water heat pump under frosting/defrosting conditions. *Applied Thermal Engineering*, Vol. 27, No. 11-12, pp. 1996-2002 (2007)

67   Huang et al. 2008
      Huang, J.M, Hsieh, W.C., Ke, X.J. and Wang, C.C.
      The effects of frost thickness on the heat transfer of finned tube heat exchanger subject to the combined influence of fan types. *Applied Thermal Engineering*, Vol. 28, No. 7, pp. 728-737 (2008)

68   Hwang and Shu 2011
      Hwang, R. and Shu, S.
      Building envelope regulations on thermal comfort in glass facade buildings and energy-saving potential for PMV-based comfort control. *Building and Environment*, Vol. 46, No. 4, pp. 824-834 (2011)

69   Iragorry and Tao 2005
      Iragorry, J. and Tao, Y.X.
      Frost temperature relations for defrosting sensing system. *Journal of Heat Transfer*, Vol. 127, No. 3, pp. 344-349 (2005)

70   Ismail and Henriquez 2002
      Ismail, K.A.R. and Henriquez, J.R.
      Numerical and experimental study of spherical capsules packed bed latent heat storage system. *Applied Thermal Engineering*, Vol. 22, No. 15, pp. 1705-1716 (2002)

71   Ismail and Jesus 2001
      Ismail, K.A.R. and Jesus, A.B.
      Parametric study of solidification of PCM around a cylinder for ice-bank applications. *International Journal of Refrigeration*, Vol. 24, No. 8, pp. 809-822 (2001)

72   Ismail et al. 2001
      Ismail, K.A.R., Alves, C.L.F. and Modesto, M.S.
      Numerical and experimental study on the solidification of PCM around a vertical axially finned isothermal cylinder. *Applied Thermal Engineering*, Vol. 21, No. 1, pp. 53-77 (2001)

73   Jaluria 1980
      Jaluria, Y.
      Natural convection, HMT, the science and applications of heat and mass transfer. Vol. 5. *Pergamon Press*, New York. 1980

74   Jhee et al. 2002
      Jhee, S., Lee, K.S. and Kim, W.S.
      Effect of surface treatments on the frosting defrosting behavior of a fin-tube heat exchanger. *International Journal of Refrigeration*, Vol. 25, No. 8, pp. 1047-1053 (2002)

75   Jiang et al. 2011
      Jiang, M., Wu, J., Wang, R. and Xu, Y.
      Research on the control laws of the electronic expansion valve for an air source heat pump water heater. *Building and Environment*, Vol. 46, No. 10, pp. 1954-1961 (2011)

76   Jones and Parker 1975
      Jones, B.W. and Parker, J.D.
      Frost formation with varying environmental parameters. *Journal of Heat Transfer*, Vol. 97, No. 2, pp. 255-259 (1975)

77   Kalaiselvam et al. 2008
      Kalaiselvama, S., Veerappan, M., Arul Aaron, A. and Iniyan, S.
      Experimental and analytical investigation of solidification and melting characteristics of PCMs inside cylindrical encapsulation. *International Journal of Thermal Sciences*, Vol. 47, No. 7, pp. 858-874 (2008)

78   Kays and London 1984
      Kays W. M. and London A. L.
      Compact heat exchangers. *McGraw-Hill Book Company*, New York, U.S.A., 1984

79   Kelly and Bean 1977
      Kelly, G. and Bean, J.
      Dynamic performance of a residential air-to-air heat pump. *National Bureau of Standards Building Science Series*, BSS 93, Washington, D.C., March 1977

80   Kerschbaumer 1971
      Kerschbaumer, H.G.
      Analysis of the influence of frost formation on evaporators and of the defrost cycles on performance and power consumption of refrigeration systems. *Proceedings of XIII International Congress of Refrigeration*, Washington, D.C. (1971)

81 Krakow et al. 1992a
Krakow, K.I., Yan, L. and Lin, S.
A model of hot gas defrosting of evaporators, Part 1: Heat and mass transfer theory. *ASHRAE Transactions*, Vo. l98, Part 1, pp. 451-461 (1992)

82 Krakow et al. 1992b
Krakow, K.I., Yan, L. and Lin, S.
A model of hot gas defrosting of evaporators, Part 2: Experimental analysis. *ASHRAE Transactions*, Vo. l98, Part 1, pp. 462-474 (1992)

83 Krakow et al. 1993a
Krakow, K.I., Yan, L. and Lin, S.
An idealized model of reversed-cycle hot gas defrosting of evaporators, Part 1: Theory. *ASHRAE Transactions*, Vol. 99, Part 2, pp. 317-328 (1993)

84 Krakow et al. 1993b
Krakow, K.I., Lin, S and Yan, L.
An idealized model of reversed-cycle hot gas defrosting of evaporators, Part 2: Experimental analysis and validation. *ASHRAE Transactions*, Vol. 99, Part 2, pp. 329-338 (1993)

85 Koizumi 2004
Koizumi, H.
Time and spatial heat transfer performance around an isothermally heated sphere placed in a uniform downwardly directed flow (in relation to the enhancement of latent heat storage rate in a spherical capsule. *Applied Thermal Engineering,* Vol. 24, No. 17-18, pp. 2583-2600 (2004)

86 Kondepudi et al. 1995
Kondepudi, S., Murali, K., Lorsch, H. and Bhalerao, A.
Voiding heat pump evaporator frost through the use of desiccants. *ASME-JSES-JSME international solar energy conference*, New York, Part 1, pp. 25-29 (1995)

87 Kondepudi and O'Neal 1989
Kondepudi, S.N. and O'Neal, D.L.
Effect of frost growth on the performance of louvered finned tube heat exchangers. *International Journal of Refrigeration*, Vol.12, No. 3, pp. 151-158 (1989)

88 Kondepudi and O'Neal 1990
Kondepudi, S.N. and O'Neal, D.L.
Effects of different fin configuration on the performance of finned-tube heat exchanger under frosting conditions. *ASHRAE Transactions*, Vol. 96, Part 2, pp. 439-444 (1990)

89 Kondepudi and O'Neal 1991
Kondepudi, S.N. and O'Neal, D.L.
Frosting performance of finned-tube heat exchanger with wavy and corrugated

fins. *Experimental Thermal and Fluid Science*, Vol. 4, No. 5, pp. 613-618 (1991)

90   Kuchen and Fisch 2009
      Kuchen, E. and Fisch, M.N.
      Spot monitoring: Thermal comfort evaluation in 25 office buildings in winter. *Building and Environment*, Vol. 44, No. 4, pp. 839-847 (2009)

91   Kumar and Mahdavi 2001
      Kumar, S. and Mahdavi, A.
      Integrating thermal comfort field data analysis in a casebased building simulation environment. *Building and Environment*, Vol. 36, No. 6, pp. 711-720 (2001)

92   Kuwahara et al. 1986
      Kuwahara, E., Kuwahara, T. and Yamazaki, M.
      Shortening the defrost time on a heat-pump air conditioner. *ASHRAE Transactions*, Vol. 92, Part 1, pp. 20-29 (1986)

93   Kwak and Bai 2010
      Kwak, K. and Bai, C.
      A study on the performance enhancement of heat pump using electric heater under the frosting condition Heat pump under frosting condition. *Applied Thermal Engineering*, Vol. 30, No. 6-7, pp. 539-543 (2010)

94   Kwon et al. 2006
      Kwon, J.T., Lim, H.J., Kwon, Y.C., Koyama, S., Kim, D.H. and Kondou, C.
      An experimental study on frosting of laminar air flow on a cold surface with local cooling. *International Journal of Refrigeration*, Vol. 29, No. 5, pp. 754-760 (2006)

95   Lawrence and Evans 2008
      Lawrence, J.M.W. and Evans, J.A.
      Refrigerant flow instability as a means to predict the need for defrosting the evaporator in a retail display freezer cabinet. *International Journal of Refrigeration*, Vol. 31, No. 1, pp. 107-112 (2008)

96   Lee and Ro 2001
      Lee, Y.B. and Ro, S.T.
      An experimental study of frost formation on a horizontal cylinder under cross flow. *International Journal of Refrigeration*, Vol. 24, No. 6, pp. 468-474 (2001)

97   Lee and Ro 2002
      Lee, Y.B. and Ro, S.T.
      Frost formation on a vertical plate in simultaneously developing flow. *Experimental Thermal and Fluid Science*, Vol. 26, No. 8, pp. 939-945 (2002)

98   Li et al. 2004
Li, X.Q., Chen, J.P., Chen, Z.J., Liu, W.H., Hu, W. and Liu, X.B.
A new method for controlling refrigerant flow in auto mobile air conditioning. *Applied Thermal Engineering*, Vol. 24, No. 7, pp. 1073-1085 (2004)

99   Li et al. 2011
Li, Y., Chen, G., Tang, L. and Liu, L.
Analysis on performance of a novel frost-free air-source heat pump system. *Building and Environment*, Vol. 46, No. 10, pp. 2051-2059 (2011)

100   Liang et al. 2010
Liang, C.H., Zhang, X.S., Li, X.W. and Chen, Z.Q.
Control strategy and experimental study on a novel defrosting method for air-source heat pump. *Applied Thermal Engineering*, Vol. 30, No. 8-9, pp. 892-899 (2010)

101   Liu et al. 2003
Liu, Z.Q., Tang, G.F. and Zhao, F.Y.
Dynamic simulation of air source heat pump during hot-gas defrost. *Applied Thermal Engineering*, Vol. 23, No. 6, pp. 675-685 (2003)

102   Liu et al. 2006
Liu, L., Wang, H.Y., Zhang, X.H., Meng, S. and Ma, C.F.
An experimental study on minimizing frost deposition on a cold surface under natural convection conditions by use of a novel anti-frosting paint, Part I: Anti-frosting performance and comparison with the uncoated metallic surface. *International Journal of Refrigeration*, Vol. 29, No. 2, pp. 229-236 (2006)

103   Long and Zhu 2008
Long, J.Y. and Zhu, D.S.
Numerical and experimental study on heat pump water heater with PCM for thermal storage. *Energy and Buildings*, Vol. 40, No. 4, pp. 666-672 (2008)

104   Lüer and Beer 2000
Lüer, A. and Beer, H.
Frost deposition in a parallel plate channel under laminar flow conditions. *International Journal of Thermal Science*, Vol. 39, No. 1, pp. 85-95 (2000)

105   Machielsen and Kerschbaumer1989
Machielsen, C.H.M. and Kerschbaumer, H.G.
Influence of frost formation and defrosting on the performance of air coolers: standards and dimensionless coefficients for the system designer. *International Journal of Refrigeration*, Vol. 12, No. 5, pp. 283-290 (1989)

106   Mago and Sherif 2003
Mago, P.J. and Sherif, S.A.
Heat and mass transfer on a cylinder surface in cross flow under supersaturated frosting conditions. *International Journal of Refrigeration*, Vol. 26, No. 8, pp. 889-899 (2003)

107 Mao et al. 1999
    Mao, Y., Besant, R.W. and Chen, H.
    Frost characteristics and heat transfer on a flat plate under freezer operating conditions, Part I: Experimentation and correlations. *ASHRAE Transactions*, Vol. 105, Part 2, pp. 231-251 (1999)

108 Martinez-Frias and Aceves 1999
    Martinez-Frias, J. and Aceves, S.M.
    Effects of evaporator frosting on the performance of an air to air heat pump. *Journal of Energy Resources Technology, Trans*actions *of the ASME*, Vol. 121, No. 1, pp. 60-65 (1999)

109 Matsuki et al. 1999
    Matsuki, N., Nakano, Y., Miyanaga, T., Yokoo, N. and Oka, T.
    Performance of radiant cooling system integrated with ice storage. *Energy and Buildings*, Vol. 30, No. 2, pp. 177-183 (1999)

110 Masoero 1984
    Masoero, M.
    Refrigeration systems based on long-term storage of ice. *International Journal of Refrigeration*, Vol. 7, No. 2, pp. 93-100 (1984)

111 Mei et al. 2002
    Mei, V.C., Gao, Z. and Tomlinson, J.J.
    Frost-less heat pump. *ASHRAE Transactions*, Vol. 108, Part 1, pp. 452-459 (2002)

112 Mettawee and Assassa 2007
    Mettawee, E.B.S. and Assassa, G.M.R.
    Thermal conductivity enhancement in a latent heat storage system. *Solar Energy*, Vol. 81, No. 13, pp. 839-845 (2007)

113 Miller 1984
    Miller, W.A.
    Frosting experiments for a heat pump having a one-row spine-fin outdoor coil. *ASHRAE Transactions*, Vol. 90, Part 1, pp. 1009-1025 (1984)

114 Miller 1987
    Miller, W.A.
    Laboratory examination and seasonal analysis of frosting and defrosting for an air-to-air heat pump. *ASHRAE Transactions*, Vol. 93, Part 1, pp. 1447-1489 (1987)

115 Mills 1995
    Mills, A.F.
    Heat and mass transfer. *Richard D. Irwin Inc*. Homewood, IL. 1995

116 Niederer 1976
Niederer, D.H.
Frost and defrosting effects on coil heat transfer. *ASHRAE Transactions*, Vol. 82, Part 1, pp. 467-473 (1976)

117 Nishimura 2002
Nishimura, T.
"Heat pumps-status and trends" in Asia and the Pacific. *International Journal of Refrigeration*, Vol. 25, No. 4, pp. 405-413 (2002)

118 Nutter et al. 1996
Nutter, D.W., O'Neal, D.L. and Payne, W.V.
Impact of the suction line accumulator on the frost/defrost performance air-source heat pump with a scroll compressor. *ASHRAE Transactions*, Vol. 102, Part 2, pp. 689-698 (1996)

119 O'Neal et al. 1989
O'Neal, D.L., Peterson, K.T., Anand, N.K. and Schliesing, J.S.
Refrigeration system dynamics during the reversing cycle defrost. *ASHRAE Transactions*, Vol. 95, Part 2, pp. 689-698 (1989)

120 O'Neal et al. 1991
O'Neal, D.L., Pterson, K.T. and Anand, N.K.
Effect of short-tube orifice size on the performance of an air source heat pump during the reverse-cycle defrost. *International Journal of Refrigeration*, Vol. 14, No. 1, pp. 52-57 (1991)

121 Padki et al. 1989
Padki, M.M., Sherif, S.A. and Nelson, R.M.
A simple method for modeling the frost formation phenomenon in different geometries. *ASHRAE Transactions*, Vol. 95, Part 2, pp. 1127-1137 (1989)

122 Paone and Rossi 1991
Paone, N. and Rossi, G.
Fiber-optic ice sensors for refrigerators. *Proceedings of SPIE*, Vol. 1511, pp. 129-139 (1991)

123 Paris et al. 1993
Paris, J., Falardeau, M. and Villeneuve, C.
Thermal storage by latent heat: a viable option for energy conservation in buildings. *Energy Sources*, Vol. 15, No. 1, pp. 85-93 (1993)

124 Pasupathy et al. 2008
Pasupathy, A., Velraja, R. and Seeniraj, R.V.
Phase change material-based building architecture for thermal management in residential and commercial establishments. *Renewable and Sustainable Energy Reviews*, Vol. 12, No. 1, pp. 39-64 (2008)

125 Payne and O'Neal 1995
Payne, V. and O'Neal, D.L.
Defrost cycle performance for an air-source heat pump with a scroll and a reciprocating compressor. *International Journal of Refrigeration*, Vol. 18, No. 2, pp. 107-112 (1995)

126 Qi et al. 2008
Qi, Q., Deng, S.M. and Jiang, Y.Q.
A simulation study on a solar heat pump heating system with seasonal latent heat storage. *Solar energy*, Vol. 82, No. 8, pp. 669-675 (2008)

127 Rabin et al. 1995
Rabin,Y., Bar-Niv, I., Korin, E. and Mikic, B.
Integrated solar collector storage system based on a salt hydrate phase change material. *Solar Energy*, Vol. 55, No. 6, pp. 435-444 (1995)

128 Rite and Crawford 1991a
Rite, R.W. and Crawford, R.R.
The effect of frost accumulation on the performance of domestic refrigerator-freezer finned-tube evaporator coils. *ASHRAE Transactions*, Vol. 97, Part 2, pp. 428-437 (1991)

129 Rite and Crawford 1991b
Rite, R.W. and Crawford, R.R.
A parametric study of the factors governing the rate of frost accumulation on domestic refrigerator-freezer finned-tube evaporator coils. *ASHRAE Transactions*, Vol. 97, Part 2, pp. 438-446 (1991)

130 Sanders 1974
Sanders, C.T.
Frost formation: the influence of frost formation and defrosting on the performance of air coolers. PhD. Thesis, Technische Hogeschool, Delft, The Netherlands (1974)

131 Santamouris and Leafs 1988
Santamouris, M.J. and Leafs, C.C.
On the coupling of PCM stores to active solar systems. *International Journal of Energy Research*, Vol. 12, No. 4, pp. 603-610 (1988)

132 Seker et al. 2004a
Seker, D., Kartas, H. and Egrican, N.
Frost formation on fin-and-tube heat exchanges, Part I: Modeling of frost formation on fin-and-tube heat exchangers. *International Journal of Refrigeration*, Vol. 27, No. 4, pp. 367-374 (2004)

133 Seker et al. 2004b
Seker, D., Kartas, H. and Egrican, N.
Frost formation on fin-and-tube heat exchangers, Part II: Experimental investigation of frost formation on fin-tube heat exchangers. *International Journal of Refrigeration*, Vol. 27, No. 4, pp. 375-377 (2004)

134 Shah 1979
Shah, M.M.
A general correlation for heat transfer during film condensation inside pipes. *International Journal of Heat and Mass Transfer*, Vol. 22, No. 4, pp. 547-556 (1979)

135 Sharma and Sagara 2005
Sharma, S.D. and Sagara, K.
Latent heat storage materials and systems: a review. *International Journal of Green Energy*, Vol. 2, No. 1, pp. 1-56 (2005)

136 Sherif and Hertz 1998
Sherif, S.A. and Hertz, M.G.
A semi-empirical model for electric defrosting of a cylindrical coil cooler. *International journal of energy research*, Vol. 22, No. 1, pp. 85-92 (1998)

137 Sherif and Sherif 1992
Sherif, S.A. and Sherif, R.A.
Hot gas defrosting analysis of a flat plate cooler. *Proceedings of the 15th World Energy Engineering Congress and the 1992 World Environmental Engineering Congress*, Atlanta, Georgia, pp. 583-586 (1992)

138 Siegel 1977
Siegel, R.
Solidification of low conductivity material containing dispersed high conductivity particles. *International Journal of Heat and Mass Transfer*, Vol. 20, No. 10, pp. 1087-1089 (1977)

139 Stoecker 1957
Stoecker, W.F.
How frost formation on coils affects refrigeration systems. *Refrigeration Engineering*, Vol. 65, Part 2, pp. 42-46 (1957)

140 Stoecker et al. 1983
Stoeker, W. F., Jr Lux, J. J. and Kooy, R.J.
Energy consideration in hot-gas defrosting of industrial refrigeration coils. *ASHRAE Transactions*, Vol. 89, Part 2, pp. 549-573 (1983)

141 Tanda and Fossa 2006
Tanda, G. and Fossa, M.
Free convection frost growth in a narrow vertical channel. *International Journal of Heat and Mass Transfer*, Vol. 49, No. 11-12, pp. 1946-1957 (2006)

142 Threlkeld 1970
Threlkeld, J.L.
Thermal environmental engineering, 2nd ed. *Englewood cliffs*, N.J.: Prentice-Hall, Inc. 1970

143 Tong et al. 1996

Tong, X., Khan, J. A. and Ruhulamin, M.
Enhancement of heat transfer by inserting a metal matrix into a phase change material. *Numerical Heat Transfer, Part A: Applications*, Vol. 30, No. 2, pp. 125-141 (1996)

144 Tso et al. 2006a
Tso, C.P., Cheng, Y.C. and Lai, A.C.K.
Dynamic behavior of a direct expansion evaporator under frosting condition. Part I: Distributed model. *International Journal of Refrigeration*, Vol. 29, No. 4, pp. 611-623 (2006)

145 Tso et al. 2006b
Tso, C.P., Cheng, Y.C. and Lai, A.C.K.
Dynamic behavior of a direct expansion evaporator under frosting condition, Part II: Field investigation on a shipping container. *International Journal of Refrigeration*, Vol. 29, No. 4, pp. 624-631 (2006)

146 Vakilaltojjar and Saman 2001
Vakilaltojjar, S.M. and Saman, W.
Analysis and modeling of a phase change storage system for air conditioning applications. *Applied Thermal Engineering*, Vol. 21, No. 3, pp. 249-263 (2001)

147 Velraj et al. 1997
Velraj, R., Seeniraj, R.V., Hafner, B., Faber, C. and Schwarzer, K.
Experimental analysis and numerical modeling of inward solidification on a finned vertical tube for a latent heat storage unit. *Solar Energy*, Vol. 60, No. 5, pp. 281-290 (1997)

148 Velraj et al. 1999
Velraj, R., Seeniraj, R.V., Hafner, B., Faber, C. and Schwarzer, K.
Heat transfer enhancement in a latent heat storage system. *Solar Energy*, Vol. 65, No. 3, pp.171-180 (1999)

149 Verma et al. 2002
Verma, P., Carlson, D.M., Wu, Y., Hrnjak, P.S. and Bullard, C.W.
Experimentally validated model for frosting of plain-fin-round-tube heat exchangers, *Proceedings of the 2002 International Conference of New Technologies in Commercial Refrigeration at University of Illinois at Urbana-Champaign*, pp. 152-162 (2002)

150 Vernon 1932
Vernon, H.M.
The globe thermometer. *Proceedings of the Institution of Heating and Ventilating Engineers*, 39:100 (1932)

151 Votsis et al. 1989
Votsis, P.P., Tassou, S.A., Wilson, D.R. and Marquand, C.J.
Investigation of the performance of a heat pump under frosting and defrosting conditions. *Heat Recovery System & CHP*, Vol. 9, No. 5, pp. 399-406 (1989)

152 Wang and Liu 2005
Wang, S.W. and Liu, Z.Y.
A new method for preventing heat pump from frosting. *Renewable Energy*, Vol. 30, No. 5, pp. 753-761 (2005)

153 Wang et al. 2008
Wang, Z.Y., Wang, X.X. and Dong, Z.M.
Defrost improvement by heat pump refrigerant charge compensating. *Applied Energy*, Vol. 85, No. 11, pp. 1050-1059 (2008)

154 Wang et al. 2011
Wang, R.X., Xie, G.Z., Wu, Q.P., Wu, Y.Z. and Yuan, J.W.
An air source heat pump with an advanced cycle for heating buildings in Beijing. *Energy Conversion and Management*, Vol. 52, No. 2, pp. 1493-1500 (2011)

155 Wang et al. 2012
Wang, D., Tao, T., Xu, G., Luo, A. and Kang, S.
Experimental study on frosting suppression for a finned-tube evaporator using ultrasonic vibration. *Experimental Thermal and Fluid Science*, Vol. 36, pp. 1-11 (2012)

156 Watanabe et al. 1993
Watanabe, T., Kikuchi, H. and Kanzawa, A.
Enhancement of charging and discharging rates in latent heat storage system by use of PCM with different melting temperature. *Heat Recovery System and CHP*, Vol. 13, No.1, pp. 57-66 (1993)

157 Watters et al. 2002
Watters, R.J., O'Neal, D.L. and Yang, J.X.
Frost/defrost performance of a three-row fin staged heat pump evaporator. *ASHRAE Transactions*, Vol. 108, Part 2, pp. 318-329 (2002)

158 Wu and Webb 2001
Wu, X.M. and Webb, Ralph.L.
Investigation of the possibility of frost release from a cold surface. *Experimental Thermal and Fluid Science*, Vol. 24, No. 3-4, pp. 151-156 (2001)

159 Yan et al. 2003
Yan, W.M., Li, H.Y., Wu, Y.J., Lin, J.Y. and Chang, W.R.
Performance of finned tube heat exchangers operating under frosting conditions. *International Journal of Heat and Mass Transfer*, Vol. 46, No. 5, pp. 871-877 (2003)

160 Yan et al. 2005
Yan, W.M., Li, H.Y. and Tsay, Y.L.
Thermofluid characteristics of frosted finned-tube heat exchangers. *International Journal of Heat and Mass Transfer*, Vol. 48, No. 15, pp. 3073-3080 (2005)

161   Yang and Su 1997
      Yang, K.H. and Su, C.H.
      An approach to building energy savings using the PMV index. *Building and Environment*, Vol. 32, No. 1, pp. 25-30 (1997)

162   Yang et al. 2006
      Yang, D.K., Lee, K.S. and Song, S.
      Modeling for predicting frosting behavior of a fin–tube heat exchanger. *International Journal Heat Mass Transfer*, Vol. 49, No. 7-8, pp. 1472-1479 (2006)

163   Yao et al. 2004
      Yao, Y., Jiang, Y.Q., Deng, S.M. and Ma, Z.L.
      A study on the performance on the airside heat exchanger under frosting in air-source heat pump water heater/chiller unit. *International Journal of Heat and Mass Transfer*, Vol. 47, No. 17-18, pp. 3745-3756 (2004)

164   Young 1980
      Young, D.J.
      Development of a northern climate residential air-source heat pump. *ASHRAE Transactions*, Vol. 86, Part 1, pp. 671-686 (1980)

165   Yonko et al. 1967
      Yonko, J.D. and Sepsy, C.F.
      An investigation of the thermal conductivity of frost while forming on a flat horizontal plate. *ASHRAE Transactions*, Vol. 73, Part 2, pp. x1.1-x1.10 (1967)

166   Xia et al. 2004
      Xia, Y., Hrnjak, P.S. and Jacobi, A.M.
      An empirical study about frost accumulation effects on louvered-fin micro channel heat exchangers. *Proceedings of International Refrigeration and Air Conditioning Conference*, Purdue, July 12-15 (2004)

167   Xia et al. 2006
      Xia, Y., Zhong, Y. Hrnjak, P.S. and Jacobi, A.M.
      Frost, defrost, and refrost and its impact on the air-side thermal-hydraulic performance of louvered-fin, flat-tube heat exchangers. *International Journal of Refrigeration*, Vol. 29, No. 7, pp. 1066-1079 (2006)

168   Xiao et al. 2010
      Xiao, J., Wang, W., Guo, Q.C. and Zhao, Y.H.
      An experimental study of the correlation for predicting the frost height in applying the photoelectric technology. *International Journal of Refrigeration*, Vol. 33, No. 5, pp. 1006-1014 (2010)

169   Zalba et al. 2003
      Zalba, B., Marin, J., Cabeza, L. and Mehling, H.
      Review on thermal energy storage with phase change: materials, heat transfer analysis and applications. *Applied Thermal Engineering*, Vol. 23, No. 3, pp. 1251-1283 (2003)

170   Zakrzewski 1984
Zakrzewski, B.
Optimal defrost cycle for the air cooler. *International Journal of Refrigeration*, Vol. 7, No. 1, pp. 41-45 (1984)

171   Zukowski 2007
Zukowski, M.
Mathematical modeling and numerical simulation of a short-term thermal energy storage system using phase change material for heating applications. *Energy Conversion and Management*, Vol. 48, No. 1, pp. 155-165 (2007)